The Evaluation of the Corrosion Behaviour of Hercules™ Alloy

Prepared by:

Duduzile Zamavezi Nkomo

Supervisor:

Prof. R.D Knutsen

Centre of Materials Engineering

University of Cape Town

Submitted to the Department of Mechanical Engineering (Centre of Materials Engineering) at the University of Cape Town in partial fulfilment of the academic requirements for a Master of Science degree in Materials Engineering.

Declaration

1. I know that plagiarism is wrong. Plagiarism is to use another's work and pretend that it is one's own.
2. I have used the IEEE convention for citation and referencing. Each contribution to, and quotation in, this project report from the work(s) of other people, has been attributed and has been cited and referenced.
3. This thesis project report is my own work.
4. I have not allowed, and will not allow, anyone to copy my work with the intention of passing it off as their own work or part thereof.

I know the meaning of plagiarism and declare that all the work in the document, save for that which is properly acknowledged, is my own. This thesis/dissertation has been submitted to the Turnitin module (or equivalent similarity and originality checking software) and I confirm that my supervisor has seen my report and any concerns revealed by such have been resolved with my supervisor.

Name: **Duduzile Zamavezi Nkomo**

Signature: Signed by candidate **Date:** 04 August 2017

Signature removed

Terms of Reference

The purpose of this project is to investigate the corrosion behaviour of Hercules™ alloy in different environments in order to evaluate whether or not it can be used as an alternative to conventional austenitic stainless steels.

The following instructions were given:

- Investigate literature survey on work that has been done on corrosion resistance of low Ni austenitic stainless steels (including Hercules™) and Type 304.
- Evaluate the microstructure of Hercules™ and compare it with that of Type 304 using Light Microscope (LM) and Scanning Electron Microscope (SEM).
- Perform electrochemical corrosion tests using corrosion test equipment at Mintek (AMD Corrosion laboratory). The electrochemical tests include using cyclic polarisation technique to evaluate the susceptibility of Hercules™ to pitting and crevice corrosion in comparison with Type 304 and Type 201.
- Perform immersion tests at University of Cape Town Centre of Materials Engineering (CME) corrosion laboratory in order to validate the results obtained from electrochemical tests.
- Provide sensible recommendations for future work that need to be carried out in order to improve the acceptability of Hercules™ in the industry.

The required skills for completion of the project are;

- A researcher has to be familiar with the corrosion and physical metallurgy concepts.
- A researcher has to be able to carry out standard sample preparation using grinding and polishing equipment available at Mintek-Physical metallurgy laboratory or at the University of Cape Town-CME laboratory.
- A researcher has to be able to operate the LM and SEM or learn how to use it with the help of designated instrument operator.
- A researcher must be able to operate the corrosion testing equipment such as potentiostat and be able to interpret the results using Excel or the Origin programme.

Acknowledgements

I would like to acknowledge the following people:

University of Cape Town (Centre of Materials Engineering)

I would like to thank Professor R.D Knutsen for the supervision provided throughout the entire dissertation.

I would also like to thank Miranda Waldron for helping me with operating SEM.

Thank you fellow students for always being there to answer some of my questions.

Mintek-Advanced Materials Division (Physical metallurgy group)

I would like to thank Dr Jones Papo (Manager at AMD) and Mr Joseph Moema (Head of Physical metallurgy group) for seeing the potential in me and giving me the opportunity to further my studies.

I would also like to acknowledge the contribution that was made by Ms Dayanda Masiya and Ms Melannie Smit in helping me with executing electrochemical corrosion tests in the AMD corrosion laboratory. Thank you for your support.

Thank you Mintek for funding my project.

Abstract

Ni contributes about 60% of austenitic stainless steel manufacturing material price. This means that the price of austenitic stainless steel increases with an increase of Ni. Ni price fluctuation has led to major efforts to reduce its content in austenitic steels. Ni has been replaced with readily available, cheap elements such as Mn and N. Hercules™ is a low Ni austenitic stainless steel alloy that was developed at Mintek in the Advanced Materials Division as part of the new development of low Ni austenitic stainless steels. The typical content of Hercules™ comprises of 2 wt.% Ni, 9 wt.% Mn and 2.5 wt.% N.[1]–[3]

When Hercules™ alloy was tested at Mintek for mechanical properties, it was found that it had higher tensile strength than Type 304 in the hot rolled and annealed condition. Therefore, it was concluded that it can be used for structural applications where high strength is required. The target applications for Hercules™ were reinforcement bars and fasteners. There has been work done in order to improve corrosion resistance of Hercules™ in order for it to be used in corrosive environments or for general purposes. A more corrosion resistant Hercules™ alloy with 0.5 wt.% Mo addition was developed.[2]

The current project focused on further characterisation of the corrosion resistance of Hercules™ B (with 0.5 wt.% Mo) and Hercules™ A (without Mo addition) against Type 304 and Type 202. Cyclic polarisation technique was used to test the susceptibility of Hercules™ to pitting, crevice and general corrosion in different solutions. Hercules™ B showed better resistance to pitting in 3.56 wt.% NaCl compared to Hercules™ A and Type 304 but, it showed poor resistance in the presence of an artificial crevice. When the concentration of NaCl was reduced to 1 wt.%, Hercules™ B showed better resistance to crevice corrosion compared to Type 304, while Type 202 consistently showed poor corrosion resistance during each test.

Immersion tests in 6 wt.% $FeCl_3.6H_2O$ were consistent with the results that were obtained from the cyclic polarisation technique. The critical pitting temperature (CPT) test was investigated using 6 wt. % $FeCl_3.6H_2O$ immersion testing. All test alloys started pitting at 25℃, meaning that they all have a CPT value that is less than 25℃.

The results obtained from ten-days immersion and cyclic polarisation test in 5 wt.% H_2SO_4 were also consistent with each other. All test alloys showed good performance in 5 wt.% H_2SO_4 by achieving a corrosion rate that is less than 0.1 mm/y. It was therefore, concluded that Hercules™ B has an overall corrosion resistance that is comparable to that of Type 304 in 5 wt.% H_2SO_4 and 1 wt.% NaCl.

Table of Contents

List of Figures

List of Tables

Abbreviations

Abbreviation	Explanation
ASTM	American society for testing and materials
AISI	American Iron and Steel Institute
LNASS's	Low Nickel Austenitic Stainless steels
PRE_N	Pitting Resistance Equivalence Number
CPT	Critical Pitting Temperature
CCT	Critical Crevice Temperature
WE	Working Electrode
CE	Counter Electrode
RE	Reference Electrode
SCE	Saturated Calomel Electrode
NaCl	Sodium Chloride
$FeCl_3.H_2O$	Anhydrous Ferric Chloride
CCTL	Critical Chloride Threshold Level
H_2SO_4	Sulphuric Acid
CR	Corrosion Rate
EW	Equivalence Weight
HCl	Hydrochloric acid
CCDF	Critical Crevice Damage Factor

Nomenclature

Symbol	Explanation	Unit
ΔT	Thickness reduction	mm
M_{d30}	Transformation temperature	℃
δ	Delta ferrite phase	
γ	Austenite phase	
E_{corr}	Corrosion potential	mV vs. SCE
i_{corr}	Current density	mA/cm^2
E_{pit}	Pitting potential	mV vs. SCE
E_{pro}	Repassivation/protection potential	mV vs. SCE
i_{crit}	Critical-anodic current density	mA/cm^2
K_1	Faraday's corrosion conversion constant	mm g/μA cm yr.
K	Corrosion rate conversion constant	
P	Density	g/cm^3
n	N.o of valence electrons	
W	Atomic weight of elements	
UTS	Upper Tensile Strength	MPa

Chapter 1: Introduction

1.1 Background to the project

Generally austenitic stainless steels require approximately 8 wt.% Ni to maintain the austenitic microstructure at room temperature. Ni however is costly, contributing approximately 60% of the total material cost, and its price suffers from fluctuations, making the cost of austenitic stainless steel unstable and unpredictable. Over the past ten years the price of Ni has decreased from about $55/tonne to $11/tonne according to London Metal Exchange (LME) as shown in Figure 1-1(a) and the price fluctuation can be observed in Figure 1-1(b) within one month.[4], [5]

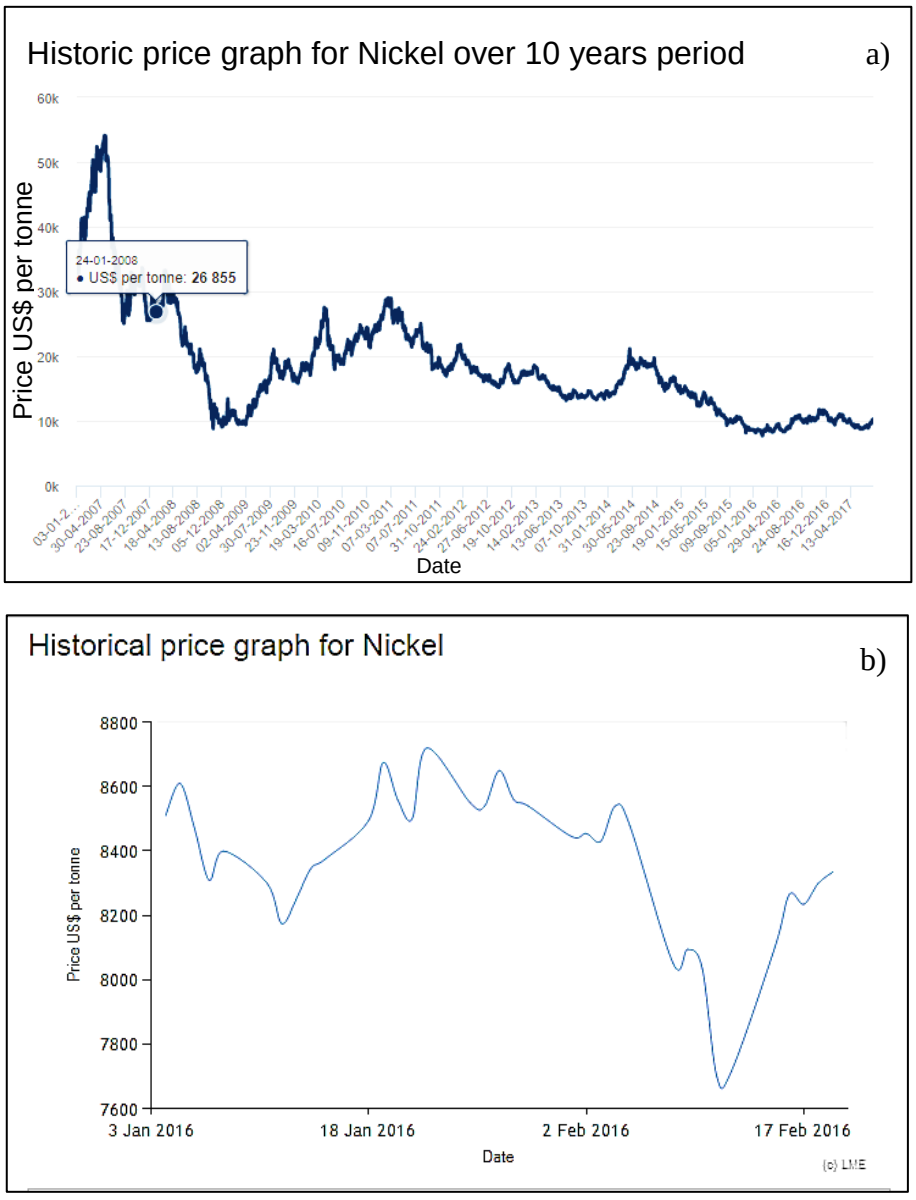

Figure 1-1:Ni price trend[5]

It can be seen that within a month the price of Ni went from approximately being $8600/tonne to $7800/tonne and then went up again to $8300/tonne. The usage of LNASS's has been considered in order to counteract problems associated with Ni price fluctuation. Reducing the Ni content changes the properties of austenitic stainless steel. The Ni content required for austenite stabilisation is substituted by adding a metallurgical calculated amount of Mn and N.[4], [5]

There are LNASS's that have been developed such as the AISI 200 series alloys. These alloys are also called the Cr-Mn-N grades because of their increased Mn and N contents compared to AISI 300 series alloys. These alloys have mostly been studied intensively in India and USA. The most common and commercial Cr-Mn-N grade is Type 201, which has approximately 5 wt.% Ni content. Although this alloy is made following a similar manufacturing route to that of Type 304, it generally does not offer materials cost savings greater than 15% if the Ni price is ≥$6/kg. The price of Ni has remained greater than $6/kg since 2002 and hence the price of austenitic stainless steel has remained high. This does not sufficiently convince consumers to start using Type 201 against the tested and approved alloy such as Type 304.[4]

Due to high and unstable Ni prices, Mintek has also developed a low Ni (≤2 wt.%) austenitic stainless steel alloy called Hercules™. Lower Ni content allows Hercules™ to have a more stable price than Type 304 and Type 201. In fact, the reduction of Ni content in the Hercules™ has resulted in a reduction of the material cost by approximately 25% that of Type 304. This is possible only if the Ni price remains greater than $6/kg and if the processing method is the same as that of Type 304.[2], [4]

The typical chemical composition for Hercules™ is shown in Table 1-1 against that of Type 201 and Type 304. The Ni content in Hercules™ has been substituted by increasing Mn and N contents to ensure an austenitic microstructure at room temperature after processing. Mn and N are readily available in South Africa, therefore using them as substitute for Ni reduces the price of austenitic stainless steel.[2]

Table 1-1: Typical chemical compositions[2]

Alloy	Element (wt.%)					
	C	Si	Ni	Cr	N	Mn
Hercules™	0.05	0.5	2.0	16.5	0.25	9.0
Type 201	0.15	0.5	5.0	17.0	0.15	6.5

Type 304	0.04	0.5	8.5	18.3	0.05	1.5

Although adding Mn and N may be the solution in terms of cost of austenitic stainless steel, mechanical and corrosion properties may be altered. Therefore, in the early stages of Hercules™ research that was done at Mintek, mechanical properties and a number of corrosion tests have been assessed and compared to Type 304 and Type 201 steels.[2]

Tensile properties of 5 kg ingots of Hercules™ that were produced at Mintek-AMD were measured. It was found that it has 0.2% proof stress that lies between 420 and 550 MPa in the hot rolled and annealed condition. The 0.2% proof stress of Type 304 and Type 201 was approximately 265 and 326 MPa, respectively. Hercules™ thus has a higher yield strength-to-cost ratio compared to conventional austenitic stainless steels when the processing cost is kept similar to that of Type 304.[1], [4]

Other Hercules™ ingots were produced at Special Alloys & Metallurgical Services (SAMS). Further processing was done at Mittal Steel in order to test the hot workability of Hercules™ alloy against Type 304 and Type 201. It was then reported that the hot workability for Hercules™ would be good enough to allow it to be forged and hot rolled down during long product manufacturing without cracking. The long product that was produced was the batch of 16 mm and 24 mm diameter round Hercules™ bars.[4]

Produced bars were further characterised at Mintek for validation. Before tensile tests were carried out, bars were annealed at 1100°C for comparison with the laboratory produced alloys. The average Vickers hardness measurements ranged between 232 and 248 HV_{30} for 24 mm diameter bar. The 0.2% proof stress of the hot rolled and annealed bars was statistically measured to be 589 MPa. This made Hercules™ alloy to be more acceptable with regard to tensile properties because it has higher yield strength than Type 304. Reinforcement bars were then recommended as the target market for Hercules™.[4]

The other market target was the manufacturing of fasteners using 16 mm and 24 mm diameter Hercules™ bars. Therefore, some hot rolled bars were sent to SA Bolt (Pty) Ltd for production of fastener prototypes. The M16, M20 and M24 hexagon head bolts were produced and marked accordingly. Six M20 fastener prototypes were further taken for tensile tests with Type 304 fasteners for comparison. The UTS of Hercules™ fasteners was measured to be 732 MPa and 700 MPa for Type 304 fasteners. Therefore, Hercules™ fasteners were also recommended as a potential application because of a comparable UTS.[4]

Apart from chemical composition, metallurgical, mechanical, and other necessary requirements for the reinforcement bar and fasteners, corrosion resistance is also of much importance. Rebars are usually covered with waterproof membranes or electrochemical protection methods to avoid corrosion. Using stainless steels is considered the short cut to achieving a corrosion resistant rebar because they are known for forming a protective passive oxide layer. However, even a stainless steel rebar may corrode due to ingress of chloride ions from the concrete additives such as $CaCl_2$, NaCl or surrounding environment.[4]

Furthermore, corrosion resistance is of importance when manufacturing fasteners because they are exposed to atmosphere and the surrounding environment. The corrosion resistance is of most importance especially if the application of fasteners involves exposure to coastal environments or for roofing. It is therefore, an advantage to use stainless steel fasteners because of the known reputation of corrosion resistance.[2]

Hercules™ was tested for corrosion resistance in order for it to be ranked against the already commonly used Type 304. Laboratory corrosion tests of Hercules™ were performed at Mintek. The general corrosion test was done using the Potentiodynamic polarisation technique in 5 wt.% H_2S0_4 for Hercules™ against Type 304 and Type 201. Hercules™ was measured to have a corrosion rate approximately 23.5 mm/y. Type 304 and Type 201 were measured to have a corrosion rate approximately 3.1 mm/y and 12.65 mm/y, respectively. The results showed that Hercules™ had poorer resistance to general corrosion compared to Type 304 and Type 201.[3], [4]

Hercules™ was also tested for pitting corrosion resistance using cyclic polarisation technique in 1 wt.% NaCl. The measured pitting potential for Hercules™ ranged at 187 and 267 mV vs. SCE. Type 304 and Type 201 had the pitting potential measured at 376 and 331 mV vs. SCE, respectively. The results showed that Hercules™ again had poor pitting resistance compared to Type 304 and Type 201.[3], [4]

Poor corrosion resistance results led to the development of a more corrosion resistant Hercules™ alloy with 0.5 wt.% Mo addition, also called Hercules™ B. The typical composition of Hercules™ B is shown in Table 1-2. The alloy composition of Hercules™ B is similar to that of Hercules™ A with only 0.5 wt.% Mo additions as an exception. The variation in composition of Hercules™ A and Hercules™ B alloy is possible with other alloying elements as long as it is within the expected range of base Hercules™ alloy composition. The corrosion rate of Hercules™ B in 5 wt.% H_2SO_4 was measured to be 0.3 mm/y. Therefore, addition of 0.5 wt.% Mo improved the resistance of Hercules™ to general corrosion.[3]

Table 1-2: Typical composition of Hercules™ B[3]

Alloy	Elements (wt.%)						
	C	Si	Ni	Cr	**Mo**	N	Mn
Hercules™ B	0.05	0.5	2	15.9	**0.52**	0.25	9.0

Hercules™ will soon find its market in the industry because of low cost and superior mechanical properties. Currently the target market for Hercules™ is rebars and roof fasteners. About 240 000 tonnes of fasteners are produced per year globally. South Africa contributes about 35 000 tonnes per year. The trial production of Hercules™ has shown that there are no problems regarding producing fasteners. Therefore, stainless steel fasteners produced per year has a chance to be increased to levels greater than 35 000 tonnes if Hercules™ is accepted to the industry.[3], [6]

1.2 Problem statement

It has already been established that Hercules™ has a potential of having a reduced price compared to Type 304. It also has superior tensile properties compared to Type 304. The combination of low cost and high tensile properties is the advantages of using Hercules™. However, it has also been established that Hercules™ has poor resistance to pitting compared to Type 304.[2]

Columbus Stainless (Pty) Ltd has done corrosion tests on some austenitic and duplex stainless steels. They have ranked alloys based on the theoretical Pitting resistance equivalence number (PRE_N). The PRE_N values of some alloys are shown in Figure 1-2 with their corresponding possible applications. Type 202 and Type 304 alloys are only suitable for use for general purposes based on their estimated pitting corrosion resistance.[7]

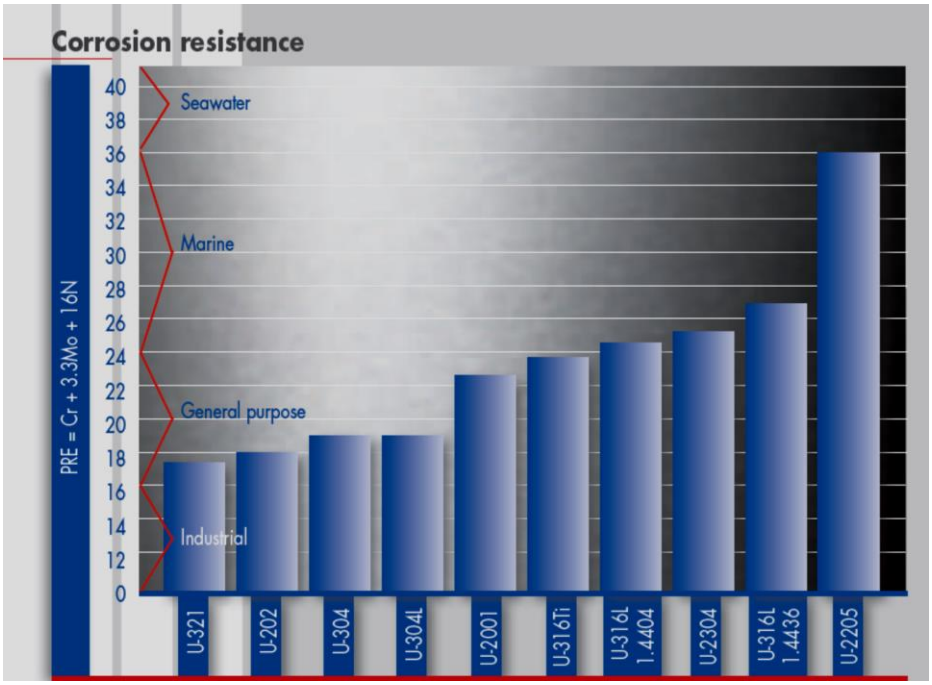

Figure 1-2: Pitting corrosion resistance of austenitic and duplex stainless steels[7]

The current target applications for Hercules™, which are rebars and fasteners suffers from corrosion when in-service. Stainless steel rebars undergo corrosion due to the diffusion of chloride ions through the concrete and hence cause failure of the whole infrastructure. Fasteners also undergo corrosion due to weather and atmospheric exposure. It has been reported that replacing the whole infrastructure is way too costly than just preventing its failure by using a corrosion resistant rebar or fasteners.[6]

Therefore, as part of progressive characterisation, more corrosion tests should be carried out for Hercules™ and also on Type 304 and Type 201 stainless steels for comparison purposes. This will therefore further qualify whether or not Hercules™ can be used as an alternative to Type 304.

1.3 Objectives

The main objective of this research is to determine whether or not the corrosion resistance of Hercules™ alloy is good enough to be used as an alternative for Type 304 (including rebars and fasteners application) in various environments.

The objectives of this project are therefore to:

- Conduct a literature survey on the metallurgy of Low Ni austenitic stainless steels (LNASS's), including the metallurgy of Hercules™.
- Carry out the processing of Hercules™ ingots.

- Conduct a literature survey on corrosion behaviour of LNASS's.
- Carry out relevant corrosion tests in order to understand the corrosion behaviour of Hercules™ A and Hercules™ B in different environments.
- Rank the corrosion resistance of Hercules™ A and Hercules™ B against that of Type 201 and Type 304.
- Make possible recommendations on how to improve corrosion resistance of Hercules™ alloy.
- Make recommendations about other possible applications of Hercules™ alloy based on corrosion resistance.

1.4 Scope of the project

All corrosion tests were done on the laboratory scale and were performed in the Mintek-AMD corrosion laboratory. A number of Mintek-AMD internal reports were used for literature survey on Hercules™. The techniques for corrosion testing were adapted from the ASTM standards, although some had to be modified in order to compare the corrosion behaviour of test alloys. The University of Cape Town, Centre of Materials Engineering laboratory was used for some metallurgical characterisation of test alloys as well as for executing some of the immersion tests.

1.5 Structure of the project

Chapter 2 is a review of work that has been done before that is related to the objectives, experiments and analysis of this project. The first section of chapter 2 is the review on conventional austenitic stainless steel that has long been accepted in the market and work that has been done on Hercules™. The second section is the review on the corrosion mechanisms possible for stainless rebars and fasteners. The third and fourth section consists of review on methods used to carry out corrosion tests for stainless steels. The last section is the review on how to evaluate the microstructure of test alloys.

Chapter 3 explains the processing route of Hercules™. It gives details of chemical composition of test alloys. The last section of Chapter 3 details the general microstructure of Hercules™ alloys, including features that affect their corrosion resistance.

Chapter 4 explains the experimental approach to corrosion tests. The first section explains the cyclic polarisation technique that is used to carry out local corrosion tests such as pitting and crevice corrosion. The second section explains the use of cyclic polarisation technique to evaluate the passivation behaviour of test alloys in H_2SO_4 and details the procedure followed.

The third section of Chapter 4 explains the procedure that was used to carry out immersion tests including critical pitting temperature (CPT) tests. Chapter 5 presents the outcome of corrosion tests that are described in Chapter 4. The remaining chapter 6 and 7 consist of conclusions and recommendations drawn from chapter 5.

Chapter 2: Literature Review

2.1 Stainless steel categories

Stainless steels are categorised according to their microstructure at room temperature. They have different composition and properties. There are five groups of stainless steel namely; ferritic, austenitic, duplex, martensitic and age-hardened stainless steels. There are different products of stainless steels that are used for different applications.[8]

Stainless steel is mostly present in the cold rolled sheet form followed by 20% in the form of bars or wires and only 10% is present in hot rolled plate form. The biggest consumers of stainless steels are food and breweries industries and chemical, oil and gas industry. So far stainless steels are not highly used in construction industry or for structural applications. It has been however used in applications where corrosion resistance and good formability is required.[8]

Ferritic grades are alloyed with 11-19 wt.% Cr with no or less than 0.1 wt.% Ni. As Ni is the most expensive alloying element, the low Ni content in ferritic grades make them more price stable compared to Ni containing grades. They are also magnetic because of ferritic microstructure.[8]

The martensitic group is the smallest group of stainless steels. This is because they are very hard and therefore, have less use. They contain higher C content and sometimes N is added to increase the strength. They have insignificant amount of Ni and Mo. Martensitic grades can be hardenable and are magnetic. Precipitation hardened steels are also hardenable by heat-treating at the region where the precipitates are formed and are also magnetic.[8]

Duplex grades have 50% ferrite and 50% austenite microstructure. They have combined properties that are found in both austenitic and ferritic grades. They have approximately 20-25 wt.% Cr and low Ni content of 1.7-7 wt.% compared to conventional austenitic grades. Mo (0.3-4 wt.%) and N is added to improve corrosion resistance and balance the microstructure. Duplex grades are also magnetic due to presence of ferrite phase.[8]

Austenitic grades are the largest group of stainless steels. They are divided into five subgroups namely; Cr-Mn-N grades, Cr-Ni grades, Cr-Ni-Mo grades, high performance and high temperature austenitic grades. They are non-magnetic in a solution annealed condition because they are likely to have fully austenitic microstructure. They have good weldability, formability and excellent corrosion resistance. The combination of these good properties render them as the

most used grade of stainless steels. About 60% of the consumable stainless steel is austenitic grade.[8]

2.2 Austenitic stainless steel grades

High performance austenitic grades are made for application in damaging environment such as high temperature and highly corrosive. They have higher alloying elements of approximately 17-25 wt.% Cr, 14-25 wt.% Ni and 3-7 wt.% Mo. Some grades are alloyed with N to improve strength and corrosion resistance.[8], [9]

The high temperature grades are used in applications at temperatures that exceed 550°C which is where creep strength is required. The composition is designed to provide a long service life in dry gases at high temperatures. They are characterised by 17-25 wt.% Cr and 8-20 wt.% Ni but without Mo content. Si is added to increase oxidation resistance and N to increase creep strength.[8]

The Cr-Ni (also called 300 series) grades are used for most applications compared to other groups. They have higher corrosion resistance owing to 2-3 wt.% Mo content if Mo is added intentionally. They are occasionally alloyed with N to improve strength. They contain around 18 wt.% Cr and 8 wt.% Ni. Type 304 is an example of an alloy that falls under this grade. It is the most commonly used because it contains the minimum amount of Ni needed to stabilize austenite at room temperature.[8]

Cr-Mn-N (also called 200 series) grades have reduced Ni content of approximately 4.5-6 wt.%. Ni is decreased and the austenitic microstructure is maintained by replacing it with increased amounts of Mn and N. One example of an alloy that falls under this group is Type 201.[8]

Cr plays an important role in corrosion resistance of stainless steel. It gives stainless steel its basic corrosion resistance. All stainless steels have about 10.5 wt.% Cr or more. It also increases oxidation resistance at high temperature. As a result 200 series grades have reduced corrosion resistance compared to 300 series because they have a reduced amount of Cr.[8]

2.3 Mechanical properties and applications of test alloys

2.3.1 Type 304

Type 304 is the most used of the 300 series group of austenitic stainless steels. It contains the minimum amount of Ni content required to obtain austenitic microstructure at room temperature. There are two types of Type 304 designations; Type 304 which has a C content that is greater

than 0.04 wt.% whilst Type 304L has less than 0.03 wt.%. Type 304/304L is non-magnetic in annealed condition, but can be slightly magnetic in cold rolled condition.[8], [10]

Type 304/304L is available in the form of plates, sheets, tubular products, bars, fittings and billets. It is corrosion resistant and has been used for a wide range of general purpose applications. It is resistant to atmospheric corrosion, organic and inorganic chemicals and to foods and beverages. The yield strength of Type 304 is typically around 250 MPa, which is at the low end of strengths for C-Mn structural steels. It is not commonly considered for use for structural applications. An example of the microstructure of hot rolled and annealed Type 304 is shown in Figure 2-1.[4], [8]

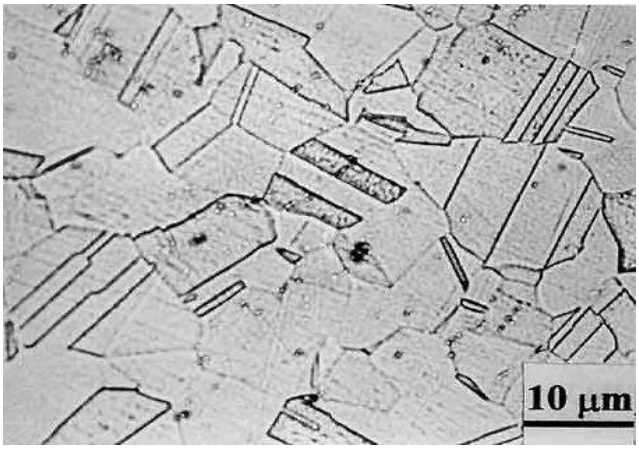

Figure 2-1: Type 304 microstructure in hot rolled and annealed condition[4]

It can be cold rolled through heading, drawing and bending. Cold working operations can increase the strength and hardness of the material. It can also be hot rolled at temperatures between 930℃ and 1200℃. For maximum corrosion resistance, it can be annealed at least at 1050℃ and water quenched. The mechanical properties of Type 304/304L are given in Table 2-1.[10]

Table 2-1: Typical mechanical properties of Type 304[10]

	Type 304	Type 304L
UTS (MPa)	517	482
0.2% Proof strength (MPa)	270	260
Elongation	40%	40%
Density (g/cm^3)	7.94	7.94

The common use of Type 304 is household appliances such as the inside of dish washers, washing machines, tumble drum, kitchen utensils, sinks, ovens, cookers, refrigerators and freezers. Some equipment such as grills that are used outside sometimes may show pitting if not cleaned regularly.[11]

2.3.2 UNS 20100/Type 201

Since the price of Ni has risen from the late 1980's, the price of austenitic stainless steel has also increased. It has been established that the price of austenitic stainless steel can be reduced by switching products made from Type 304 to 200 series grade alloys. Type 201 and Type 202 are most commonly known of 200 series in European countries. The Ni content of Type 201 is almost half that of Type 304. A portion of Ni is replaced by adding 7 wt.% Mn. The general microstructure of Type 201 is shown Figure 2-2.[12], [13]

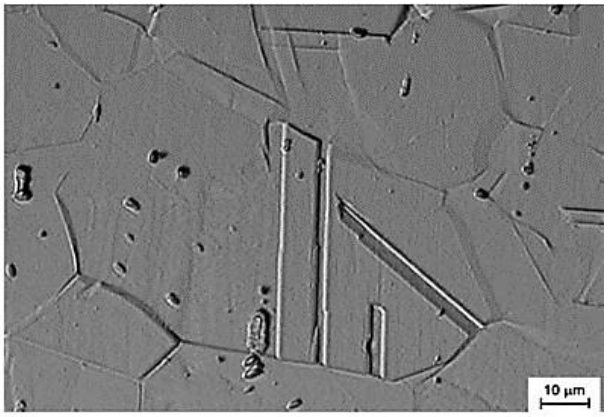

Figure 2-2: The typical microstructure of Type 201[12]

The Cr content has also been reduced slightly to 16 wt.% to ensure that austenite is maintained at room temperature. Variations in composition are often made to enhance some properties such as corrosion and mechanical properties. The typical tensile properties of Type 201 in the annealed condition are shown in Table 2-2.[12]**,** [13]

Table 2-2: Typical mechanical properties of Type 201[13]

UTS (MPa)	724
0.2% Proof strength (MPa)	430
Elongation	58%
Density (g/cm^3)	7.88

Type 201 has higher tensile strength compared to Type 304. This is why it is considered for applications that require higher strength, where Type 304 cannot be used. The formability of Type 201 is less than that of Type 304 because of high work hardening rate. It is therefore limited to normal deep drawing applications as opposed to severe deep drawing.[13]

Since Type 201 is an austenitic stainless steel, it is therefore expected to have good corrosion resistance in some environments. It is however, expected to have lower corrosion resistance compared to Type 304 because of lower Cr content. At least 11 wt.% Cr is required for a Cr oxide passive film to form. Therefore, although Type 201 cannot be used in all environments where Type 304 is used, it can be used in environments where corrosion is not severe.[14]

The combination of strength, formability and corrosion resistance makes Type 201 an alternative choice for some of Type 304 applications. The advantage of using it will be that it is cheaper than Type 304. Taking high strength to advantage, Type 201 has been used for applications such as hose clamps, truck trailer frames and railcars. Examples of some applications of Type 201 are shown in Figure 2-3.[14]

Figure 2-3: Common applications of Type 201[14]

2.3.3 Hercules™

Type 201 is hardly available in South Africa; therefore, Hercules™ could close the gap for applications that require Type 304 properties at a lower price. The cost production of Hercules™ bar is around 25% less than Type 304 using a similar production route. Hercules™ has been proposed for use in structural applications because of its higher strength.[6]

Other possible applications for Hercules™ besides rebars and fasteners are hot rolled channels for construction purposes. Construction industry is likely to benefit from Hercules™ because it has higher strength and reduced cost than Type 304. Other industries will soon find benefit also because it will later be available in flat product such as sheet and coil.[15]

A minimum yield strength required in structural applications is 400 MPa in hot rolled condition. Typical tensile properties for Hercules™ in hot rolled condition are shown in Table 2-3.[4], [15]

Table 2-3: Typical mechanical properties of Hercules™[15]

UTS (MPa)	850
0.2% Proof Strength (MPa)	500
Elongation	50%
Density(g/cm^3)	7.85

Rebar and fasteners prototypes have been manufactured. The fastener market was divided into two types; the large head bolts (M16 and M24) and roof fasteners. The picture of Hercules™ and Type 304 fastener prototypes that were manufactured at SA Bolts is shown in Figure 2-4.[2], [6]

Figure 2-4: Hercules™ and Type 304 head bolts[2]

According to R. White report [6], 240 000 tonnes of fasteners are produced globally per year and South Africa contributes only about 35 000 tonnes per year. Production of corrosion resistant bolts and roof fasteners promises a viable business. New LNASS's fasteners are expected to be resistant to intergranular and stress corrosion cracking. The latter requirement is in response to specific environment such as swimming pool applications, which requires pitting and crevice corrosion resistance.[6]

About 400 000 tonnes of stainless steel rebar is produced per year. South Africa has been using about 95% carbon steel rebars which are cheaper than Type 304. However, there was little

success in marketing of carbon steel rebars because of poor corrosion resistance. Corrosion of rebar is detrimental in that it can cause concrete spalling which leads to infrastructure failure. According to USA reports, an infrastructure repair is more costly than preventing failure. Hence there is a need to use stainless steel rebar in any concrete because they are more corrosion resistant than carbon steel rebar.[6]

2.4 Corrosion of stainless steel fasteners

The biggest users of fasteners are aerospace, oil and gas industries. Large components are assembled and secured by fasteners/bolts. These assembled structures include pipelines, machinery and infrastructure. Joints are the regions where corrosion starts because fasteners are normally smaller than the whole component.[16]

Fasteners fail due to overload, fatigue or corrosion. Therefore, strength, ductility and corrosion resistance are critical factors for selection of fasteners and bolts. Fasteners exposed to different conditions corrode in different forms of corrosion, which are:

- General corrosion
- Pitting corrosion
- Crevice corrosion
- Galvanic corrosion
- Stress corrosion cracking (SCC)
- Hydrogen embrittlement [16], [17]

Some mechanisms listed above are explained in preceding sections. A number of works have been done in order to prevent corrosion of fasteners in-service. Material selection, manufacturing parameters, bolt fabrication, applying coating are all required to ensure long term service performance. External factors such as weather will subsequently determine the service life of the fastener.[17]

Two dissimilar metals joined together causes potential difference in the presence of a conductive solution such as NaCl, H_2SO_4, HCl and HNO_3. If the difference is sufficient enough to cause corrosion, the fastener will act as a sacrificial anode in the system because of its small size. An example of corroded bolts is shown in Figure 2-5. The picture shows the section of a pipe constructed with a combination of low and high-alloy steels in an oil industry, with low-alloy steel used as bolts and nuts.[16]

Figure 2-5: Corrosion of bolts assembling construction pipes in oil industry[16]

Exposure of fasteners to weather is enough to cause corrosion. Acid rain can be the source of a conductive solution. It contains carbon dioxide, which makes it slightly acidic at pH 6.5. This pH is enough to cause potential difference and hence the oxidation of the fastener. Analysis of acid rain has also shown the presence of H_2SO_4 and HNO_3. For the off-shore applications, the environment is expected to have Na and Mn chloride salts. NaCl is not considered alkaline or acidic, but it is electrically conductive. This therefore means that it will participate in the corrosion reaction.[16]

According to U.S Navy, an alloy to be used in marine environments should be immune to crevice corrosion, since previous materials have shown this form of corrosion. The main types of materials used for bolts exposed to marine environment are; high-alloy steel, Cu-based alloys, Ni-based stainless steel and Ti-based alloys. When selecting a material for a certain environment, it is important to consider cost, availability, weight, fatigue and corrosion resistance.[17], [18]

Although fasteners are easy to replace, it is important that their failure in service does not interrupt the whole component that is joined together. It is therefore important to minimise the need for replacement by using a corrosion resistant fastener. One of failures is that experienced by aircrafts. Corrosion of fasteners used in aircraft can be caused by moisture from condensation in a fastener crevice or highly corrosive acidic cargo leak.[19]

Aircrafts are also prone to failure due to tensile stresses exerted by cabin pressurisation and depressurisation as well as manoeuvres and gusts. Under stress a fastener may undergo SCC. The SCC can cause failure quickly without a warning when chloride species are available. This means that the interaction of the electrochemical corrosion and accumulated stress can lead to cracking damage of a metal in service.[19]

Examples of fasteners that fail with SCC are a number of hardened 13-8 stainless steel that were installed on the centre wing of a Navy F-18 aircraft. The fasteners were found to have a crack at the base of the fastener head. It has been reported that cracking of high strength metal is due to hydrogen embrittlement. This cracking mechanism is influenced by adsorption of hydrogen in a pre-existing crack, pit or a notch, which are exerted by stress.[19]

Most stainless steels have been used in fastener manufacturing. Type 304 and Type 316 are the commonly used for general purposes. Type 316 is also used for marine and off-shore industry because it contains Mo. These steels are also susceptible to SCC in chloride containing environments. The tightness of the joints may introduce stresses on bolts and hence SCC might occur if the fastener is exposed to a conductive media.[16]

Type 304 and Type 316 are susceptible to pitting and crevice corrosion when exposed to chloride environment. The intensity of crevice corrosion is high in constant immersion environment. In the study that was carried out by L.Zhengwei [20] it was reported that stainless steel fasteners that were exposed to marine environment for 3 years were found to have undergone localised corrosion. If the corrosion is not prevented or controlled, it can accumulate to potentially unsafe state.[19], [20]

In work done by D.R Jonhs et al. [21], it was also proved that immersion of Type 316 and Type 304 fasteners in 25 wt.% NaCl (pH adjusted to 3 by adding HCl) experienced SCC. Duplex stainless steel that was also immersed did not undergo SCC. It can be added that duplex stainless steel fasteners did not corrode because they contain a certain number of alloying elements that might have prevented corrosion by stabilising the passive layer. Fasteners that were immersed in 3 wt.% NaCl also experienced crevice corrosion at 35℃.[21]

Another example of fastener failure was observed by T. Prosek et al. [22]. Fasteners that were made of 300 series austenitic stainless steel corroded when they were exposed to swimming pool atmosphere. Corrosion is suspected to be due to acidic chloride salts with pH 3-4.[22]

2.5 Corrosion of stainless steel rebars

The use of carbon steel rebars has decreased because they cause premature failure of concrete construction. Carbon steel does not have the ability to form a protective film like stainless steels. Corrosion prevention on carbon steel rebars has become a major focus in order to prevent premature failures.[23], [24]

Cathodic protection, epoxy coating or galvanising rebars have been used as major attempts to prevent corrosion of carbon steel rebars. Galvanising the carbon steel rebar with Zn has shown that although this prolongs the service lifetime of the rebars, corrosion of a rebar may still occur when the hydrogen evolution corrosion reaction occurs. Furthermore, the disadvantages of using coated rebars is the difficulty of handling, transporting and storage to avoid damaging the coating.[24], [25]

Therefore, the use of stainless steel has been the solution because of its better corrosion resistance than carbon steel. Stainless steel rebars offer a cost efficient and long lasting solution. Their corrosion resistance is due to the formation of Cr oxide, self-repairing passive layer (about 10 nm thin). Hence, the need for maintenance for reinforced concrete structures exposed in corrosive environments is minimised by using stainless steel rebars.[11], [26]

There are different kinds of concrete produced worldwide depending on the type of cement that is used.[27] The main components of concrete are cement, aggregate and water. The commonly used cement in South Africa is Portland cement. The cement is made based on the ASTM standard specifications. The main raw materials used to manufacture Portland cement are limestone and shale.[28]

These are processed accordingly to produce powder; i.e. Portland cement, which is further hydrated with water to form the concrete. The hydration process produces two main compounds namely; calcium silicate hydrates and calcium hydroxide. These products provide concrete with its alkalinity state, which has a pH of 13.5 to 13.8.[28], [29]

The steel will be in a passive condition at higher pH unless there are some species that intrude the concrete which may cause passive layer breakdown. It is therefore important to consider the mixing factors when manufacturing the concrete because they determine the diffusion rate of some of these species in the concrete. One of the species that causes passive layer breakdown is chloride ions.[11],[24], [28], [30]

According to British Standard BS 8110 Part 1, the chloride ion content allowed in cement is limited to 0.40 wt.%. While the European standard suggests that the chloride level is limited to

0.15 wt.% of cement. Outokumpu has established the critical chloride threshold level (CCTL) for a given lifetime of a carbon steel rebar. A diffusion profile is developed from a given lifetime and diffusion coefficient of corrosion species and thus the CCTL value at which steel could be used. The CCTL values for carbon steel and Type 304L rebars were measured to be 0.35 and 2.51, respectively at room temperature.[11], [31], [32]

It is also stated in the Outokumpu handbook [11] that a stainless steel exposed to chloride environment of greater than 100 ppm will experience localised corrosion. Chloride ions may be present due to the use of chlorine containing mixing solutions such as brackish water. This will introduce detrimental chlorides inside the concrete construction and hence localised corrosion might occur.[11]

Chloride diffuses through the concrete due to concentration gradients until they reach the rebar and initiate corrosion. Concrete structures close to the sea water, or partially immersed in sea water are susceptible to rebar corrosion. Bridges, roads and car parks where chloride-containing salts are used as an additive are also prone to failure due to rebar corrosion.[11], [24]

Corrosion products formed during corrosion occupy a volume that is several times larger than the original steel rebar. Their formation results in cracking/spalling or delamination of the concrete. The progress of corrosion results in reduced cross section of the steel rebar, which leads to reduced load carrying capacity and causes the structure to collapse. An example of failure of concrete due to rebar corrosion is shown in Figure 2-6.[30], [32], [33]

Figure 2-6: Corroded rebar and damaged concrete[33]

2.6 Pitting corrosion of LNASS's and Type 304

Pitting corrosion is the local discontinuity of a passive film which results in small holes through the material. These holes are referred to as pits. Initiation of pits can be caused by mechanical imperfection such as surface damage or inclusions. The composition of stainless steel may cause formation of inclusions which become nucleation sites for pits at the inclusion-austenite matrix interface.[34]

A.Bautista et al. [14] studied the morphology of pits that were formed on the surface of the test alloys after polarisation. Pits were found to nucleate preferentially at the point of strain and at geometrical irregularities that favoured formation of corrosion cells.[14]

Given the alloy's composition, pitting resistance can be predicted by calculating pitting resistance equivalence number (PRE_N). The PRE_N is defined as %Cr + 3.3% Mo +16% N. Alloys with higher PRE_N are expected to be more resistant to pitting and crevice corrosion than the ones with lower PRE_N. A.Bautista et al. [14] calculated the PRE_N for Type 201 and Type 304 to be 18.4 and 20.4 respectively. However, it was noted that if the solution is too aggressive, the corrosion rate of alloys does not correspond to the calculated PRE_N. It is therefore, important to perform tests in order to validate the usage of an alloy for a particular environment.[14]

The calculation of PRE_N is similar to work that was done by A. Muwila [35]. A similar formula was used to predict the resistance of Hercules™ against that of Type 201 and Type 304. It was calculated that Hercules™ alloy had higher PRE_N of approximately 20 while Type 304 and Type 201 was calculated to be 18 and 16 respectively. The PRE_N was then verified by actual pitting tests.

Actual pitting corrosion tests in 3.56 wt.% NaCl were done following guidelines outlined in ASTM G61. The pitting potential (E_{pit}) for original Hercules™ A was measured to be −295 mV vs SCE, and was lower than what was measured for Type 304 and Type 201. This was contrary to the calculated PRE_N values. This means that PRE_N calculation is not enough to rank the alloy, and actual tests need to be done to confirm the resistance of an alloy to pitting.[3], [35]

The effect of Mo on pitting and crevice corrosion resistance of stainless steels in chloride environments is accounted for in the PRE_N and has been studied by M.Kaneko et al. [36]. The E_{pit} for austenitic stainless steel alloys with 2 wt.% and 5 wt.% Mo contents showed a dramatic increase compared to that of steels without Mo in chloride environment. It is suggested that Mo is adsorbed at the dissolving interfaces of a corroding metal and hence inhibiting dissolution kinetics.[3], [36]

M.Kaneko et al. [36] findings are consistent with the work that was done by A.Pardo et al. [34]. A.Pardo et al. studied the effect of both Mn and Mo in the pitting corrosion resistance of Type 304 and Type 316. Tests were carried out by immersion in 6 wt.% $FeCl_3.H_2O$ and cyclic polarisation technique in 3.5 wt.% NaCl. SEM was used to examine morphology of pits on the surface of corroded coupons. Images of corroded samples of Type 304 that were electrochemically tested in 3.5 wt.% NaCl are shown in Figure 2-7.[34]

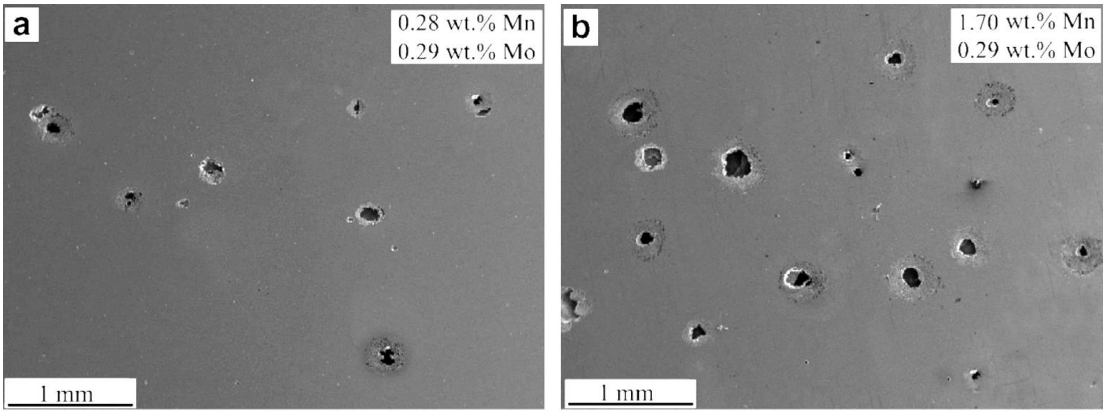

Figure 2-7: Pitting corrosion of Type 304 as a function of Mn[34]

Alloy with high Mn content had larger pores that the one with less. Higher Mn stainless steels experience high pitting because Mn has high affinity for Sulphur and it reacts with it to form inclusions, which in turn are precursors for pit nucleation. When Mo was increased to 2.10 wt.%, pit density decreased and the size of pores evidently decreased as shown in Figure 2-8.[34]

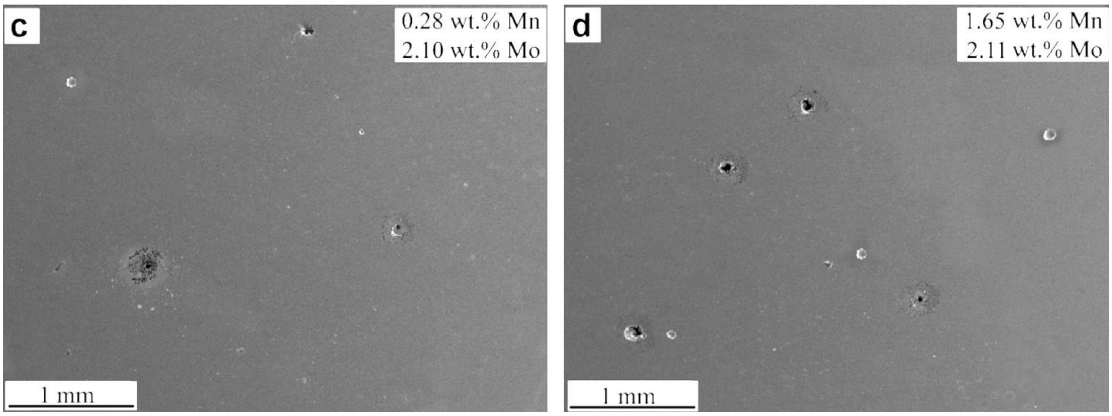

Figure 2-8: Pitting corrosion of Type 304 as a function of Mo[34]

Pit initiation can also be influenced by surrounding conditions such as gaseous environment, temperature and the nature of the electrolyte. Stainless steels tend to form deep pits at specific areas when exposed to environments that contain solutions with chloride, bromide or hypochlorite.[37]

The occurrence of the electrochemical reactions is a result of a potential change created on a conductive metal when exposed to a conductive medium. Electrochemical potential is accompanied by electron movement which leads to electron availability at the metal surface. The electron movement or potential difference can affect the rate of corrosion reactions. Overall, the energy change provides the driving force and control for the spontaneous direction for a chemical reaction. The change in energy can be understood using thermodynamics to show how conditions of the corrosion cell can be adjusted to avoid corrosion.[37]

When a metal is immersed in a conductive solution, a charged surface of an alloy forms a complex interface. The interface is formed when the polar H_2O molecules form an oriented solvent layer. The electric field formed around the solvent layer prevents easy charge transfer, thereby limiting electrochemical reactions at the surface of an alloy.[37]

The positively charged ions such as Fe^{2+} at the anode are transferred to the conductive solution which acts as an electrolyte for the cell. The electrolyte consists of ions that create electrical connectivity with the metal. Oxygen and water act on the cathodic reaction and accept negatively charged ions to form hydroxyl ions (OH^-). Further anodic reactions occur simultaneously with cathodic reaction until rust is formed. Possible anodic reactions are shown in Equation (2-1)-(2-3) and the cathodic reaction in Equation (2-4). These type of corrosion reactions occur when the alternative air exposure and water is present, for example in the sea wave condition.[32]

$$Fe \rightarrow Fe^{2+} + 2e^- \quad (2\text{-}1)$$

$$Fe^{2+} + 2OH^- \rightarrow Fe(OH)_2 \quad (2\text{-}2)$$

$$4Fe(OH)_2 + 2H_2O + O_2 \rightarrow 4Fe(OH)_3 \quad (2\text{-}3)$$

$$4e^- + O_2 + 2H_2O \rightarrow 4OH^- \quad (2\text{-}4)$$

Stainless steels can corrode by pitting mechanism without a significant loss of weight on a structure as a whole being recognised. Chloride induced corrosion of stainless steel rebars in the concrete occur when there exists a difference of electric potential along the rebar. In the presence of chloride ions, the surface of the rebar is activated to act as the anode and the passivated region becomes the cathode. The reactions involved are shown in Equation (2-5) and (2-6)[32]

$$Fe^{2+} + 2Cl^- \rightarrow FeCl_2 \quad (2\text{-}5)$$

$$FeCl_2 + 2H_2O \rightarrow Fe(OH)_2 + 2\,HCl \quad (2\text{-}6)$$

The chloride ions migrate easily towards the interior of the pit and catalyse the hydrolysis reaction. An acidic environment is created in the pit solution as the reaction continues. During corrosion, more than one anodic reaction takes place because of different elements present in the alloy. The electrons produced by these anodic reactions are consumed by the cathodic reactions which includes hydrogen and metal reduction.[38]

Removing the cathodic sites therefore reduces the rate of corrosion. The potential required for corrosion to take place is denoted by E_{corr}. This is the potential at which the total rate of all anodic reactions is equal to the total rate of all cathodic reactions. The current density at E_{corr} is denoted by i_{corr} and it is used to measure corrosion rate of the metal as anionic species are released.[38]

Electrochemical tests can be used to determine i_{corr} and hence the corrosion rate. The corrosion current density can be measured indirectly with the aid of a counter electrode and electronic equipment. This technique uses a potentiostat in conjunction with the reference electrode. Potentiostat is an instrument that applies a potential to a specimen which enables the modification of current flow. The commonly used electrochemical techniques are polarisation resistance technique, electrochemical impedance and Tafel extrapolation. The current can be measured by extrapolation procedure. In this procedure the specimen is initially made to act as a cathode in the electrochemical cell containing the test solution.[38]

Therefore, electrochemical techniques can be used to determine the lifetime of a metal by calculating the sum of the time required for initiation and propagation of corrosion to cause failure. Studies have been done on commercial stainless steels such as Type 304 and Type 316. Pitting or crevice corrosion resistance of these alloys in chloride environments can also be measured by immersion tests in metal-chloride solutions.[39]

B.S Bergstrom et al.[14] followed guidelines outlined on ASTM G48 method A and B to test susceptibility of Type 201 and Type 304 to pitting corrosion. ASTM G48 Method A is the practice for measuring pitting resistance and Method B for crevice corrosion resistance. These two methods included immersion of coupons in 6 wt.% $FeCl_3.6H_2O$ and measuring mass loss due to either pitting or crevice corrosion after 72 hours as shown in Table 2-4.[14]

The results showed that there was no significant difference in the mass loss of Type 201 and Type 304. Therefore, this means that according to B.S Bergstrom et al. [14], there was no difference in the corrosion behaviour of Type 201 and Type 304 in 6 wt.% $FeCl_3.6H_2O$ even in the presence of an artificial crevice.

Table 2-4: Results of ASTM-G48 A and B tests conducted at 22°C[14]

		Type 201	Type 304
ASTM-G48 A	Mass loss	0.0228 g/cm^2	0.0280 g/cm^2
	Max. Pit depth	0.0762 mm	0.0762 mm
ASTM-G48 B	Mass loss	0.0211 g/cm^2	0.0205 g/cm^2

M.C Garcia-Alonso et al.[40] carried out corrosion tests of Type 304 and Type 316 rebars embedded in concrete with different chloride concentrations. Tests were also done for carbon steel and LNASS's for comparison. LNASS's had Ni composition of 0.2 wt.% and 1.5 wt.% respectively, with addition of Mn. The concrete was manufactured with additions of 2 wt.% and 4 wt.% chloride content of cement. Other rebars were also embedded in a portion of concrete without chlorides and immersed into 3.5 wt.% NaCl solution to evaluate the effect of diffusion of chloride ions through the non-chlorinated concrete in the corrosion behaviour of rebars.[40]

The i_{corr} values of carbon steel, Type 304, Type 316 and LNASS's were measured using electrochemical methods. In the absence of chlorides, i_{corr} values for all test alloys were measured to be around 0.1µA/cm^2. The i_{corr} for carbon steel was observed to moderately increase after 300 days of immersion, which is attributed to diffusion of chlorine that reached the surface of the rebar.[40]

The i_{corr} values for alloys that were embedded in concrete with 2 wt.% chlorides were measured to be 3-5 times higher for carbon steel compared to that of LNASS's and Type 316. In the slab with 4 wt.% chlorides, carbon steel was measured to have i_{corr} value 10 times higher than other stainless steels. Type 304 was measured to have an i_{corr} value that is of at least one magnitude lower than other alloys in 4 wt.% chlorides concrete slab.[40]

The response of test alloys towards increased chlorides concentration was due to local breaking of the passive layer or pitting corrosion. LNASS's however showed poorer corrosion resistance than Type 304 irrespective of chlorides content. This is in agreement with preliminary tests that were carried for Hercules™ in 1 wt.% NaCl solution at room temperature. Hercules™ A performed poorer than Type 304 and Type 201.[1], [40]

Furthermore, A.Bautista et al. [39] also carried out corrosion experiments for Type 204Cu in a solution simulating "pore solution" of the concrete. Type 204Cu is considered a LNASS because it contains 1.89 wt.% Ni content and 8.25 wt.% Mn content. Cyclic polarisation technique was

used to test the susceptibility of Type 204Cu cold-rolled rebars towards pitting corrosion. In the tests, Type 204Cu was tested against Type 304 and Type 316. A number of mixtures of saturated calcium hydroxide [$Ca(OH)_2$] concrete solutions were used with different NaCl additions. The E_{pit} values were measured from the cyclic polarisation curves. E_{pit} is a potential measured when the current sharply increases when the working electrode is anodically polarised. No pitting was detected on the media without NaCl addition.[39]

However, pitting was detected for tests done with additions of NaCl. It was reported that the greater the amount of NaCl added for each test, the lower the E_{pit}, which means E_{pit} value was measured to be closer to E_{corr} with addition of NaCl. The presence of chloride ions causes the passive layer to break down at potentials below the transpassive region and results in pitting corrosion. An example of pitting scans showing the effect of addition of NaCl in the corrosion behaviour of Type 204Cu is shown in Figure 2-9.[39]

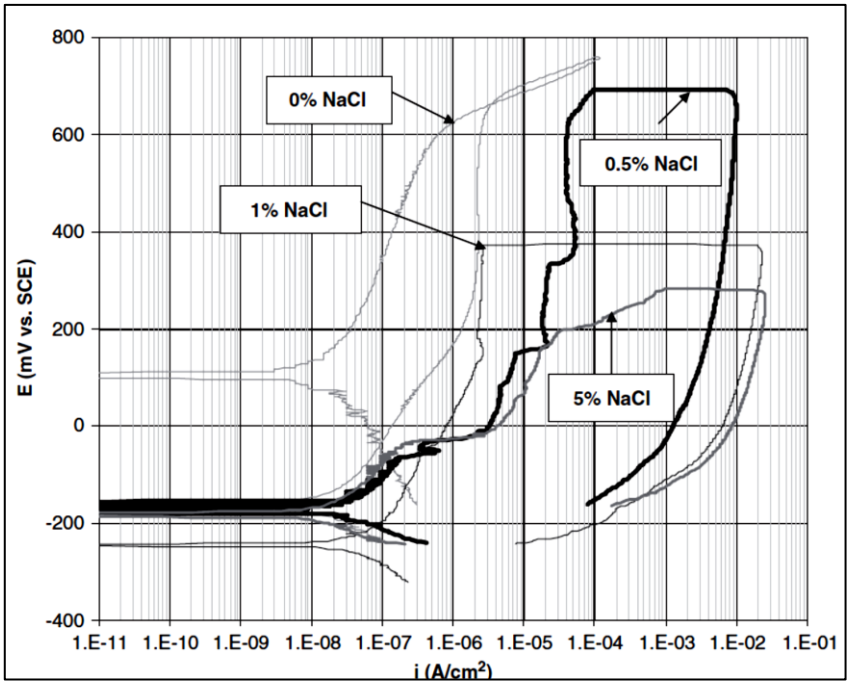

Figure 2-9: Influence of chloride concentration on the pitting of Type 204Cu[39]

The cyclic polarisation curve labelled 0% NaCl illustrates the typical behaviour of stainless steels in the absence of chloride ions. The curve shows passivity until it reaches a potential above 650 mV and evolution of oxygen is observed. The oxygen evolution region is referred to as the transpassive region. The reverse scan for 0% NaCl curve shows current density values that are less than that of the forward scan. This means that in this medium, Type 204Cu is not susceptible to pitting corrosion.[39]

Increasing NaCl concentration reduces the E_{pit} value with a certain significant order and also increases the current density. This therefore means that the presence of chloride ions speeds up the initiation and propagation of pits. Moreover, it was noticed that no repassivation or protection potential (E_{pro}) could be determined on the reverse scans for tests with NaCl additions. Comparison of corrosion behaviour of Type 204Cu with Type 316 and Type 304 in the solution with 0.5 wt.% NaCl is shown in Figure 2-10.[39]

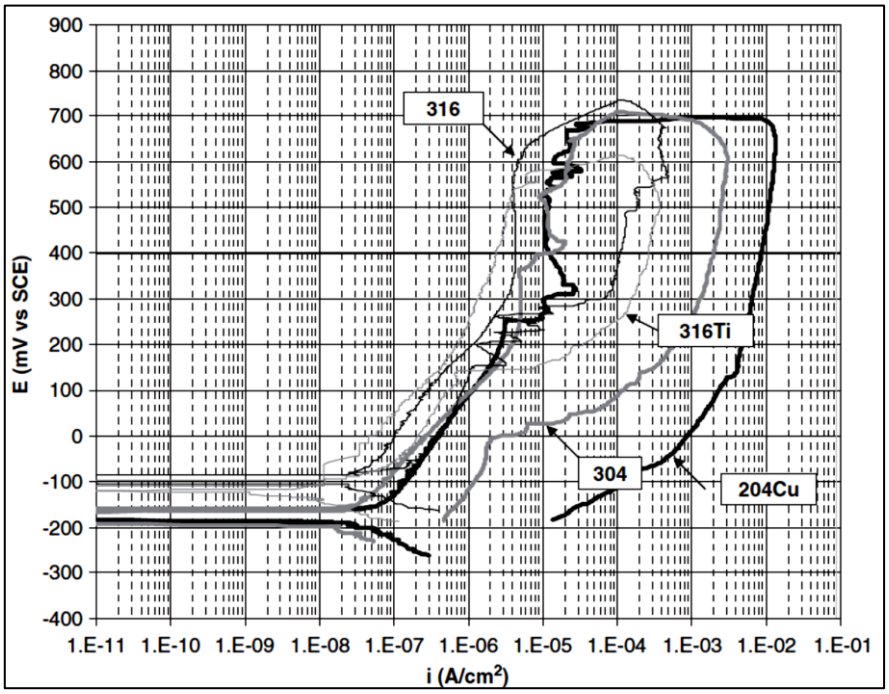

Figure 2-10: Pitting of alloys in non-carbonated [$Ca(OH_2)$] with 0.5 wt.% NaCl[39]

It was observed that E_{pit} for Type 204Cu was measured closer to that of Type 304 and Type 316 around 700 mV vs SCE. Non-carbonated [$Ca(OH)_2$] solution on its own is alkaline with the pH of 12.6 and without NaCl alloys did not experience pitting corrosion. When NaCl was increased to 5 wt.%, it was observed that Type 204Cu has significantly lower E_{pit}. The difference in E_{pit} obtained at different NaCl concentrations is shown in Figure 2-11.[39]

If the E_{pit} value is more noble than E_{corr} of a tested alloy, then pitting will not occur. Thus if the test solution constituents raises the pitting potential above what is estimated by the polarisation curve, that solution will protect the steel from pitting corrosion. Moreover, if the potential of the test solution is below the measured value of E_{pro}, pitting corrosion will not take place. [$Ca(OH)_2$] with 0.5% NaCl as an additive proved to be the safer one to use as an additive to concrete for all alloys that were tested because higher E_{pit} values were obtained compared to solutions with 1 wt.% and 5 wt.% NaCl additive.[39]

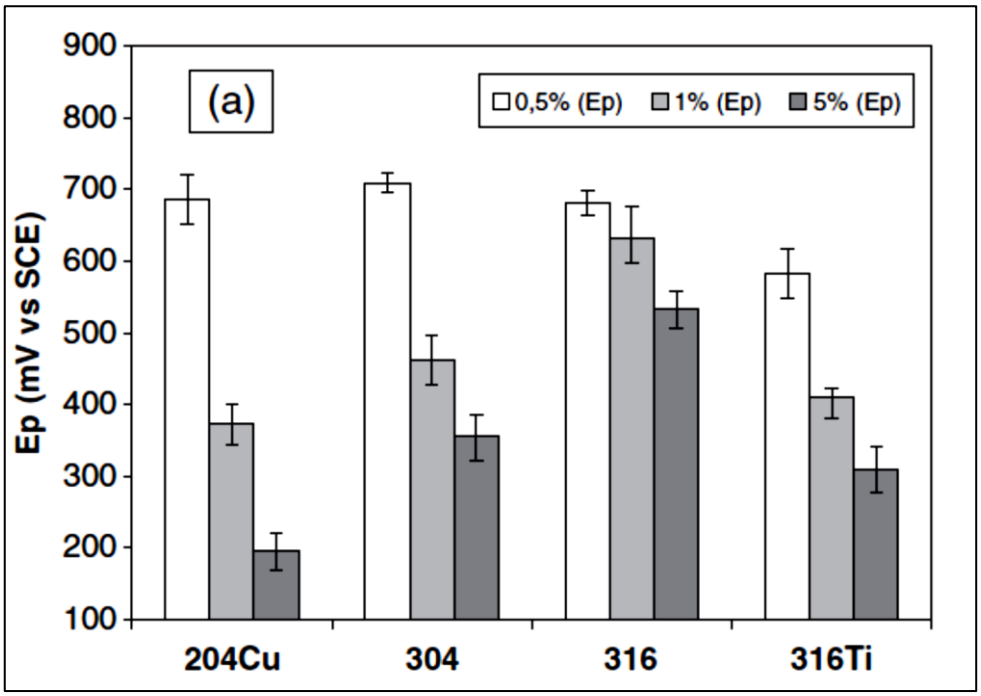

Figure 2-11: Variation of pitting potential with variation of NaCl[39]

A.Bautista et al. [39] work is almost similar to one that was done by N.S Berke [41], where carbon steel rebars were tested in solutions containing different chloride concentrations. It was observed that pit nucleation became more active with increasing chloride content.[41]

It is therefore important to measure the chloride content of the test solution in order to determine if the test alloy will experience corrosion in a certain chloride environment or not. Although the tests were done in the laboratory in the A.Bautista et al. [39] project, the test solution was equivalent to the chloride content in the real life concrete solution.

In order to determine whether certain steel will corrode in a chloride environment, a critical chloride threshold level (CCTL) was calculated. The CCTL is the measure of the chloride level that is enough to cause pitting. According to A.Bautista et al. [39] who used the in-solution method instead of the cast-in method, the CCTL for Type 204Cu was measured to be 1 wt.% chloride and for Type 304 was 5 wt.%.[39]

Outokumpu also ran in-solution tests to determine the CCTL of stainless steels in the concrete solution. The CCTL for carbon steel was measured to be less than 0.35 wt.% chlorides and 2.51 wt.% chlorides for Type 304. M.C Garcia-Alonso et al. measured the CCTL of Type 304 to be 2 wt.% chlorides in similar test conditions.[11], [40]

S. Fajardo et al. [42], [43] also tested LNASS (4.32 wt.% Ni) against Type 304 in a carbonated [$Ca(OH)_2$] solution with different chloride concentrations. The cyclic polarisation curves that were obtained showed that LNASS had almost similar pitting behaviour to that of Type 304,

with Type 304 having a slightly higher pitting potential at all chloride concentrations. The polarisation curves of LNASS and Type 304 that were obtained in carbonated [$Ca(OH)_2$] solution with chloride concentration variation are shown in Figure 2-12.

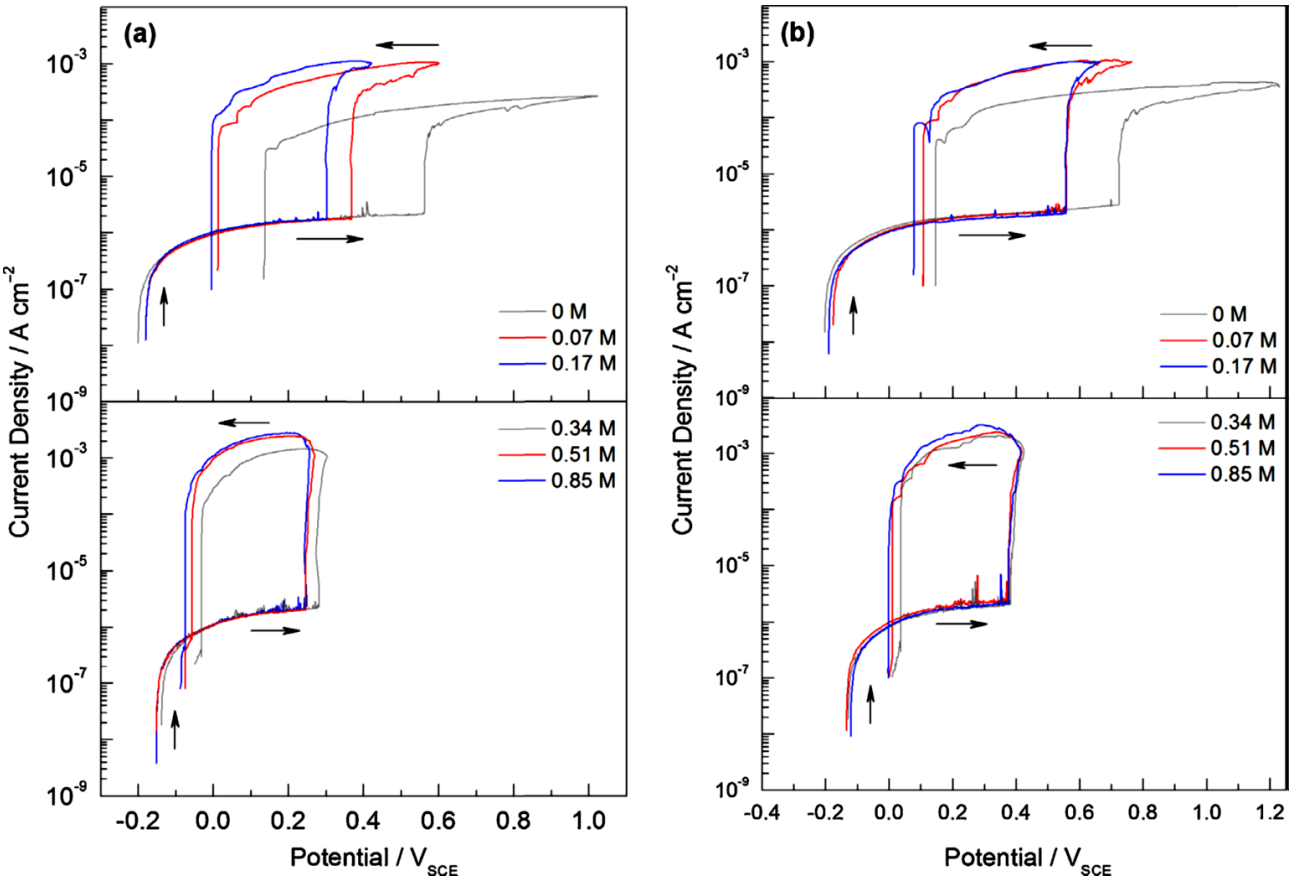

Figure 2-12: Cyclic polarization curves in carbonated solution (pH = 8, 25 ℃) subjected to different chloride concentrations for (a) the low-nickel SS and (b) the Type 304.[42]

The results that were obtained by S. Fajardo et al. [42] were in agreement with the results that have been obtained by other researchers [39]-[41]. LNASS was expected to have pitting potentials that are significantly lower than those of Type 304, but further analysis of corroded samples showed that both LNASS and Type 304 formed passive layers of almost similar thickness. The critical chloride level for LNASS was determined at 0.5 M NaCl and 0.85 M NaCl for Type 304, which is within the range of what other researchers have previously obtained.[43]

2.7 The effect of temperature on the pitting behaviour of stainless steels

The critical pitting temperature (CPT) is the temperature at which stable pits are formed. Generally below the CPT, pits are metastable because the oxide layer formation is more favoured than metal dissolution. Above the CPT, stable pits can form well below the transpassive potentials. The CPT test is performed in order to compare and rank the resistance of different alloys for use in a particular environment.[11], [44]

The stability of pitting is measured by the sudden increase of current density or where the depth of pitting is ≥0.025 mm. Therefore, CPT can be measured where ≥0.025 mm depth pitting occurs, because the depth is an indication of transition from metastable to stable pitting. Furthermore, maximum of 0.2 mg/cm^2 mass loss due to pitting have been commercially set as a limit by certain metal producers and users. CPT tests that were done by Outokumpu for different stainless steel alloys showed that the CPT for Type 316 and Type 304 was measured to be <100℃ and <10℃ respectively, in acidified 6 wt.% $FeCl_3.6H_2O$.[11]

A number of investigations have been done to evaluate the relationship between pitting of austenitic stainless steels and temperature. N.J Laycock et al.[45] observed that the E_{pit} showed a discontinuous variation with temperature. Streicher et. al observed that pit density on Type 304 and Type 316 over 20℃-70℃ increased by a factor of 2-5.[45], [46]

On the other hand, Leckie et al. also studied the dependence of the E_{pit} on temperature. It was observed that at temperatures between 0℃-20℃, the pitting potential of Type 304 decreased sharply, but at 55℃ the decrease of pitting potential was shallower. The steady decrease of pitting potential indicated that temperature does not directly affect pit growth, but there are other factors that are involved.[44]

Wang et al. also tested the dependence of pitting potential on temperature for Type 304. When the testing temperature was increased up to 200℃ in chloride environments, it was observed that E_{pit} decreased by approximately 200 mV between 30℃ and 100℃. However, above 100℃, the rate of decrease of E_{pit} was reduced. Wang et al. then measured the impedance spectra of the surface of corroded Type 304 and concluded that as the temperature is increased above the CPT, the passive film becomes thicker but more porous.[45], [47]

N.J Laycock et al.[44] performed further investigation to evaluate the dependence of pitting potential on temperature for Type 304 and Type 316. It was observed that the E_{pit} for Type 304 and Type 316 decreased gradually with increasing temperature with plot gradients of -2.9 and

-3.8 mV/℃ respectively. He explained the temperature dependence of the pitting potential using factors involved in pit propagation during the pitting process.[44], [46]

The kinetics of pit propagation involves salt concentration of pit solution and bulk solution. The solution provides the pit with polarity which drives pitting. The resistance of the pit solution and bulk solution can be related to the transition potential (E_T) between activation and diffusion controlled pit growth. N. J Laycock et al.[44] used the model in Equation (2-7) to describe the relationship between pit growth kinetics and transition potential.[44], [45]

$$E_T = E_{corr} + b_a \log\left(\frac{i_{lim}}{i_{corr}}\right) + I_{lim}R_s \tag{2-7}$$

Where:

E_{corr} is the corrosion potential inside the pit, i_{lim} is the current density measured when the pit solution reaches saturation, i_{corr} is the current corresponding to E_{corr}, I_{lim} is the anodic limiting current density and R_s is the pit and bulk solution resistance.[44]

The second term on the right of the equation represents activation overpotential and the third term represents the resistance overpotential. According to work that has been done prior to N. J Laycock et al., narrow pits (<10μm) in a solution are less affected by bulk solution resistivity and can be ignored. The implication of narrow pits is that the solution resistance of the pit interior is dominant over the pit exterior. The pit growth is therefore linked to activation potential.[44]

N. J Laycock et al.[44] measured the current during pit growth and it was proven to be dependent on the diffusion of saturated solution (C_{sat}) within the pit. The diffusion of corrosion species inside the pit was also measured to be affected by temperature. For example, the saturation concentration of the metal salt within the pit where ferric chloride was used diffused in the manner that is shown in Figure 2-13. The illustration shows the type of corrosion species that are stable at a given temperature. The solubility of ferric chloride increases with temperature, and so is the diffusion coefficient.[44], [48]

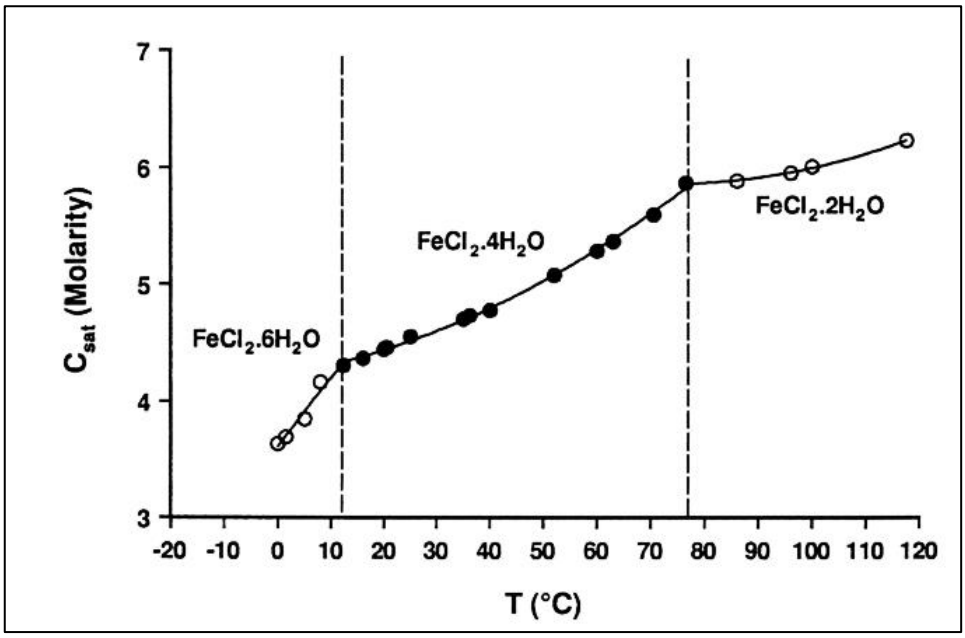

Figure 2-13: Saturation concentration within the pit as a function of temperature[44]

Charges that are transferred during pit growth are recorded as i_{lim} and give rise to E_T. If the current density in the pit is enough to maintain the breakdown of the metal, a stable pit is achieved and an E_{pit} is measured. N. J Laycock et al. results showed that E_{pit} decreased as temperature was increased, owing to increased saturation concentration inside the pit. The relationship between E_{pit} for Type 304 and temperature compared with E_T for Type 302 is shown in Figure 2-14.[44]

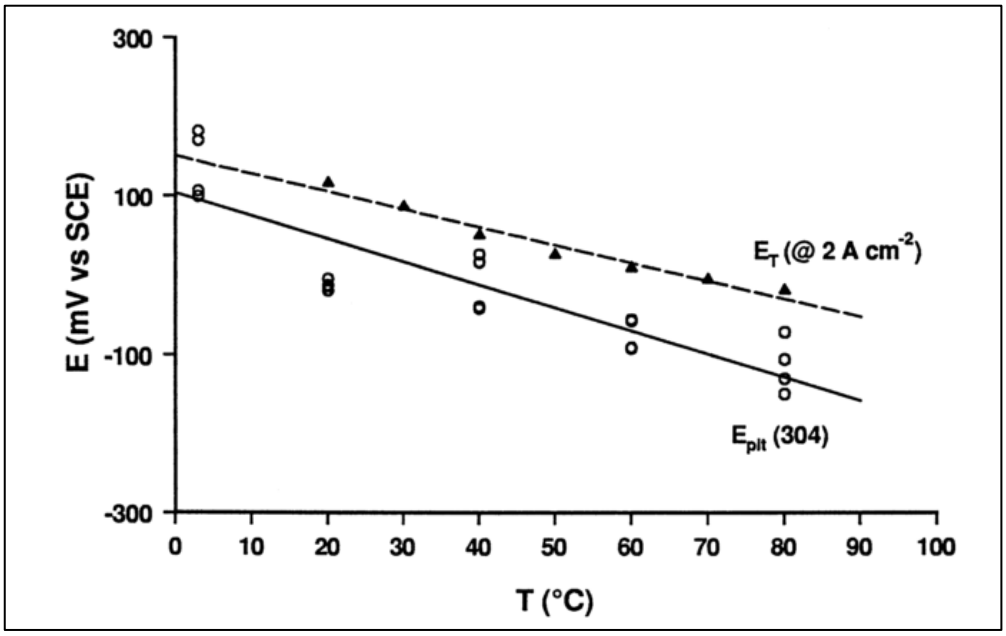

Figure 2-14: Dependence of E_{pit} and E_T on temperature in 1M NaCl[44]

The results shown by N. J Laycock et al. [44]are contrary to the results from other researchers in that, increasing temperature does not always result in reduced measured E_{pit}. The change of concentration of the solution and its resistance to pit propagation also plays a role in pitting.

When the solution resistance (R_s) is considered, increasing temperature does not always result in a linear decrease of E_{pit}, but a shallow decrease with temperature. Figure 2-15 showed the measured values of R_s compared with theoretical solution resistance for 1M NaCl (Bulk solution) and 5M NaCl (artificial pit interior solution). R_s plot showed that there is always a solution gradient inside the pits and it does not directly depend on temperature. Hence sometimes E_{pit} values may vary at different temperatures.[44]

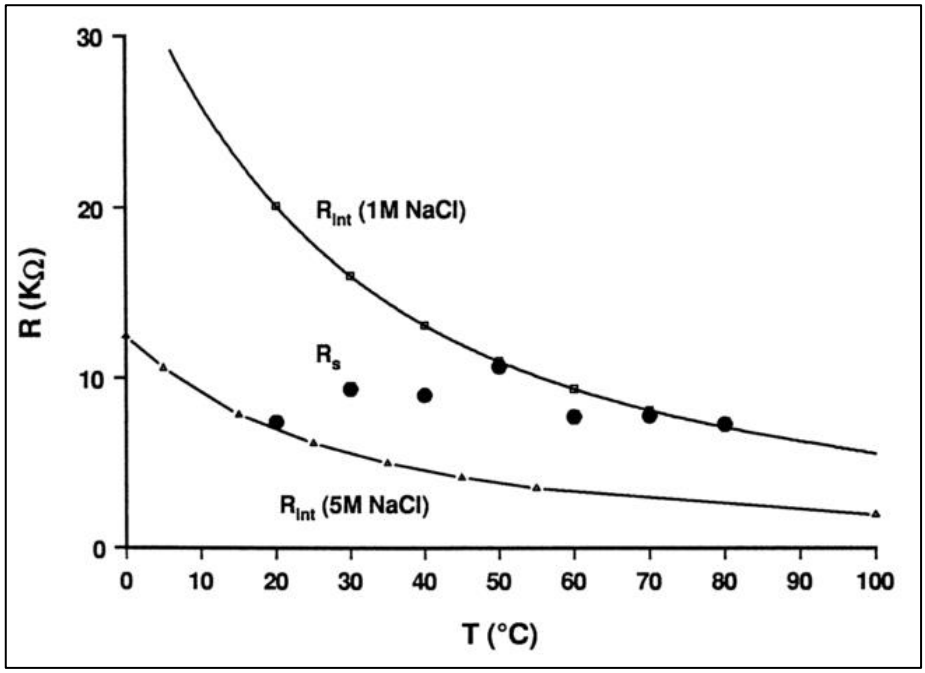

Figure 2-15: Solution resistance as a function of temperature for a 300µm deep pit[44]

J.Brigham [49] also investigated the effect of temperature on different 18 wt.% Cr austenitic stainless steel alloys with varying Mo additions. Coupons were immersed in 10 wt.% $FeCl_3$ for 24 hours at different fixed temperatures. After each test, samples were checked for corrosion attack; if no attack was visually seen, the coupon was further immersed at a temperature increased by 2.5℃.

It was observed that alloys with low (< 3 wt.%) Mo content had a critical crevice temperature (CCT) less than 2.5℃. The results showed consistency with the Outokumpu investigations. Outokumpu investigations involved testing Type 304 in acidified 6 wt.% $FeCl_3$ and the CCT was measured to be less than 0℃.[50], [51]

2.8 Crevice corrosion of LNASS's and Type 304

Crevice corrosion is a severe form of pitting that occurs at any point where a metal is occluded in such a way that a stagnant solution is formed. This type of corrosion is caused by depletion of oxygen at the crevice point. There are numerous interrelated factors that affect initiation and propagation of crevice corrosion. Metal to metal, non-metal to metal and tightness of the crevice are geometrical factors that affect crevice corrosion. Environmental factors include oxygen content, chloride level and temperature. Metallurgical factors include alloy composition, impurities and passive film characteristics.[52]

Crevice corrosion can be observed in passive alloys such as stainless steels, Ti-based alloys and Ni-based alloys when immersed in aerated aqueous environments containing chloride ions. An example of such environments could be seawater or brackish water. An alloy of a given composition can either corrode uniformly or locally underneath the crevice.[52]

Four steps are involved in the mechanism of crevice corrosion. The first step is de-oxygenation, followed by the increase of salt and acid concentration in the crevice, then, thirdly the de-passivation of the protective film. Lastly, if the entire crevice corrosion criterion is met, propagation of already formed crevice corrosion occurs. In the de-oxygenation stage, the solution under the crevice becomes depleted than the surrounding crevice free area.[52]

Oxygen depletion in the crevice causes the shift in the corrosion potential of the alloy from passive to active. This means that the area under the crevice will act as an anode. This provides the initial driving force for crevice corrosion in stainless steels. Areas adjacent to crevice become a cathode. During the second stage, metallic cations such as Fe^{2+}, Cr^{3+}, Al^{3+}, etc. become concentrated in the crevice solution. These cations react with water molecules to generate acidity within the crevice. [19], [52]

The presence of anionic species such as chloride anions will assist in propagation of crevice corrosion. Anion species may be present in the crevice as part of the exposure solution. These anions are mobile and have a small anionic size, therefore are able to move and attach to a highly cation concentrated region within the crevice. Hence, the crevice solution becomes more concentrated with metallic chlorides and lowers the pH of the crevice solution. If the pH is sufficiently low and the concentration of anionic (Cl^-) species is high enough to breakdown the passive film, then the active metallic dissolution will occur.[52]

Crevice corrosion can be characterised by nucleation of pits under a crevice even at small applied potential. A critical potential is reached within the crevice, which causes an increase in

dissolution rate of the alloy. The pits under a crevice are stabilised by formation of metal-anionic species salt films.[52]

The resistance of an alloy to crevice corrosion can be tested using either electrochemical or non-electrochemical techniques. Testing methods involve an introduction of artificial crevice on the surface of the alloy tested. The exposure environment should contain anionic species such as chloride and an oxidising agent such as Fe^{2+} to accelerate initiation of crevice corrosion. Non-electrochemical tests use measured mass loss after duration of test and visual methods.[52]

The most reported failures in sea water applications are due to crevice corrosion. A number of studies have been carried out to determine the susceptibility of new materials to crevice corrosion [11]. J.Dundas et al. [50] conducted non-electrochemical crevice corrosion tests on austenitic stainless steels that were produced for use in seawater. A laboratory test was developed in order to predict the behaviour of stainless steels in the filtered seawater. A test included immersion of ferritic, austenitic and duplex stainless steel coupons in acidified 10 wt.% $FeCl_3$.[50]

An artificial crevice was introduced with two rubber bands around the specimen holding two Teflon cylinders that were placed on both sides of specimen faces. Therefore, four crevice points were created around each test coupon and on the two faces of coupons. The temperature was increased every 24 hours by 2.5℃ until the crevice attack was severe or large enough to not require microscopic observation. It was observed that duplex stainless steel test coupons had little to no crevice attack at all test temperatures up to 85 ℃, which was also the maximum testing temperature. A deep attack was observed in low alloyed austenitic and ferritic coupons at 25℃.[50]

The severe crevice corrosion that was observed in ferritic and austenitic stainless steel alloys was due to a minimised alloying elements that are responsible for inhibiting crevice corrosion. Generally, a minimum of 25 wt.% Cr, 4.6 wt.% Mo and 0.2 wt.% N is required for austenitic stainless steels to be used in chloride environments such as seawater. J.Dundas et al. [50] observed that high-alloyed austenitic stainless steels that contained N, Cr, and Mo did not show crevice corrosion up to the maximum testing temperature. This means that 10 wt.% $FeCl_3.6H_2O$ was not suitable to test high-alloyed austenitic stainless steel, but was also aggressive for low-alloyed austenitic stainless steels.[50]

Similar to Outokumpu investigations, Bergstrom et al. [14] also tested the resistance of Type 304 and Type 201 to crevice corrosion by immersing coupons in 6 wt.% $FeCl_3$ as outlined in ASTM G48B. There was no significant difference in weight loss measurements for both alloys. Similar

weight loss measurements mean that they had the same corrosion rate, which was consistent with the PRE_N that was theoretically obtained, and calculated to be almost the same.[14]

T. Ujiro et al. [9] used a similar procedure to compare corrosion resistance of low-alloyed and high-alloyed austenitic stainless steel alloys for use in off-shore environments. Test specimens were immersed in 6 wt.% $FeCl_3.6H_2O$+0.18 wt.% HCl at 60℃. The crevice was induced on test coupons by introducing a multiple crevice assembly with fasteners. Weight loss was recorded and corrosion rate due to crevice corrosion was calculated. High-alloyed stainless steels were found to have superior corrosion resistance compared to low-alloyed austenitic stainless steels.[9]

T. Ujiro et al. [9] also used electrochemical techniques to measure resistance of austenitic stainless steel alloys to crevice corrosion as a function of Mo content in 3.5 wt.% NaCl solution. E_{pit} values were then determined from cyclic polarisation curves. It was found that austenitic stainless steels with higher Mo content (>4 wt.%) had a reduced anodic current density, but no difference in the rate of increase of current density above E_{pit} with an increase of Mo.[9]

The addition of Cr (>26 wt.%) decreased the rate of current density increase below and above E_{pit} for ferritic stainless steels, but not for austenitic stainless steels. Therefore, this means that Mo is effective in inhibiting the onset of localised corrosion. On the other hand, Cr is responsible for maintaining the passive layer and resisting the propagation of crevice corrosion which is why the rate of increase of current density was reduced.[9]

An example of crevice corrosion is the one that occurs at flap/fastened joints that allow ingress of the environmental species. Failure of fasteners as a result of crevice corrosion has been investigated by D.R Jonhs et al. [21]. Test fasteners (Type 304 and Type 316) were clamped on the flat plates and immersed in 3 wt.% NaCl solution at 35℃, for 6 to 21 months. After 21 days, areas with potential crevice sites on each specimen were examined.[21]

D.R Jonhs et al. [21] used Crevice Corrosion Damage Factor (CCDF), which is a sum of all factors involved in the crevice corrosion propagation. Factors are: the extent of penetration into the crevice gap, proportion of circumference of the crevice gap and the greatest depth of the metal removal. CCDF is determined in terms of range from 0-10, where 0 is no attack observed and 10 represents severe metal attack(>0.5mm). Type 304 nuts were found to have a CCDF of 4.8 in the as-received condition and 4.4 for Type 316. These results are acceptable because Type 316 contains Mo, and therefore has better crevice corrosion resistance than Type 304. Higher CCDF means severe crevice corrosion.

2.9 General corrosion and passivation of LNASS's and Type 304

General corrosion refers to uniform thinning of a material without showing signs of localisation. Most uniform corrosion tests are based on immersion of a sample in H_2SO_4, which is the largest inorganic acid that is used by chemical industries. The resistance of austenitic stainless steels in H_2SO_4 is complex because of active-passive nature of stainless steel alloys. A stable passivity can be achieved at ambient temperatures in low and high concentrations.[53]

Stainless steels can exhibit general corrosion in extreme conditions which involves strong acids and alkalis. B. Jegdic et al. [54] tested pure Cr against Type 304 in deaerated H_2SO_4 solution. The corrosion potentials of Type 304 are mainly due to Ni, Fe and Cr. Therefore, the corrosion potential of Type 304 is within the range of alloying elements corrosion potentials. Cr exhibited two corrosion potentials in deaerated H_2SO_4. The first potential was due to cathodic hydrogen evolution at lower potentials and the second one was at passive potential range.[54]

The E_{corr} value for Type 304 was obtained at approximately −360 mV vs. SCE. Unlike, Cr, Type 304 had one E_{corr} value. On The other hand, Cr and Type 304 electrodes were pre-polarised at −0.9 V for 10 minutes in order to induce the passive layer. Type 304 wasn't affected by polarisation, whilst Cr had lower corrosion potentials ($E_{corr,\ 2,\ Cr}$). The difference in corrosion potentials was thought to be due to diffusion controlled processes that take place during corrosion.[54]

The behaviour of Type 304 was that of Wagner-Traud type, where anodic processes involve anodic dissolution of a metal in the passive state and anodic oxidation of hydrogen through the passive layer. The cathodic reaction involves hydrogen evolution on the passive surface. The peak represented by hydrogen evolution was thought to be related to metal dissolution because a part of evolved hydrogen is absorbed by the alloy. The limiting factor for hydrogen absorption is diffusion through the passive layer; hence different anodic currents can be measured for different alloys.[54],[55]

The resistance of 200 series alloys in 1M H_2SO_4 solution has been studied and it was observed that the increased Mn content decreased the ability for the alloys to passivate [56]. A. Muwila et al. [35] evaluated the corrosion behaviour of Type 201 in 5 wt.% H_2SO_4 and compared it to that of Type 304. It was observed that Type 201 showed an unstable passivity compared to Type 304 as shown in Figure 2-16. A larger i_{crit} was observed in Type 201 than in Type 304.The implications of larger i_{crit} are that the alloy does not easily passivate in a particular solution. Type 304 and Type 201 also showed the behaviour that Cr exhibit in H_2SO_4. The scans showed that

the corrosion potential (E_{corr}) was measured at three different potentials, which is an indication of instability of the passive layer.[54]

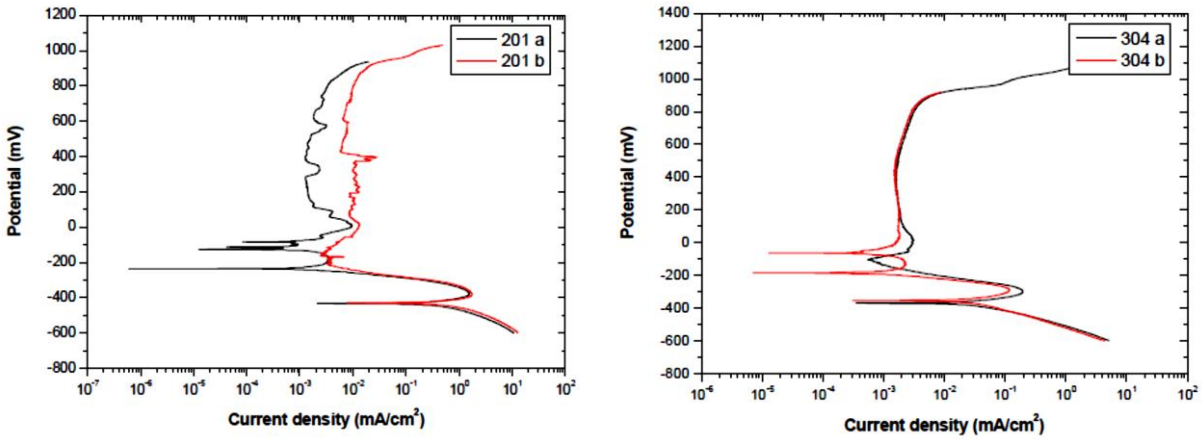

Figure 2-16: Polarisation scan of Type 201 and Type 304 in 5 wt.% H_2SO_4[35]

V.S Rao et al. [56] also studied the corrosion behaviour of LNASS (4.5 wt.% Ni/alloy 1 and 1.7 wt.% Ni/alloy 2) in H_2SO_4. The ASTM G5 standard was used as a guideline to carry out potentiodynamic polarisation tests on the test alloys. The scans were recorded and E_{corr}, i_{corr}, i_{pass} and i_{crit} was measured.

An alloy with 1.7 wt.% Ni contained 8.6 wt.% Mn and the E_{corr} was measured at −335.6 mV vs. SCE and for an alloy with 4.5 wt.% Ni, −263.7 mV vs. SCE. It was also noted that an active-passive transition was observed in alloy 2, and hence it had higher i_{crit} than alloy 1.Higher i_{crit} was linked to Ni content, meaning that Ni helps in lowering the i_{crit} and hence lowers the corrosion rates. The potentiodynamic curves of alloy 1 and alloy 2 are shown in Figure 2-17.[56]

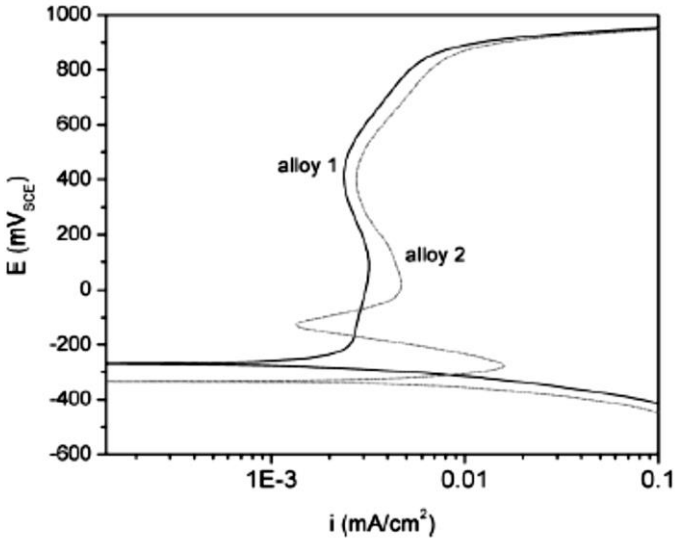

Figure 2-17: Potentiodynamic polarisation curves of alloy 1 (4.5 % Ni) and alloy 2 (1.7 % Ni) in 1M H_2SO_4[56]

2.10 The effect of microstructure on the corrosion behaviour of LNASS's

2.10.1 Effect of carbides

The 300 series group of steels represents modifications of conventional 18-8 stainless steel. Each alloying element added for a certain grade has a specific effect on the microstructure of an alloy. Decreasing Ni content on austenitic stainless steels and replacing it with N and Mn have an effect on the microstructure obtained. Carbon content is also increased in LNASS's as an austenite stabiliser.[38]

The amount of C in stainless steels is approximately between 0 to 1.0 wt.%. The effect of carbon content on the microstructure can be illustrated by a pseudo binary phase diagram for Fe-18Cr-8Ni alloys in Figure 2-18. This group of steels contain a ratio of Ni-Cr content that stabilises the FCC phase at room temperature.[38]

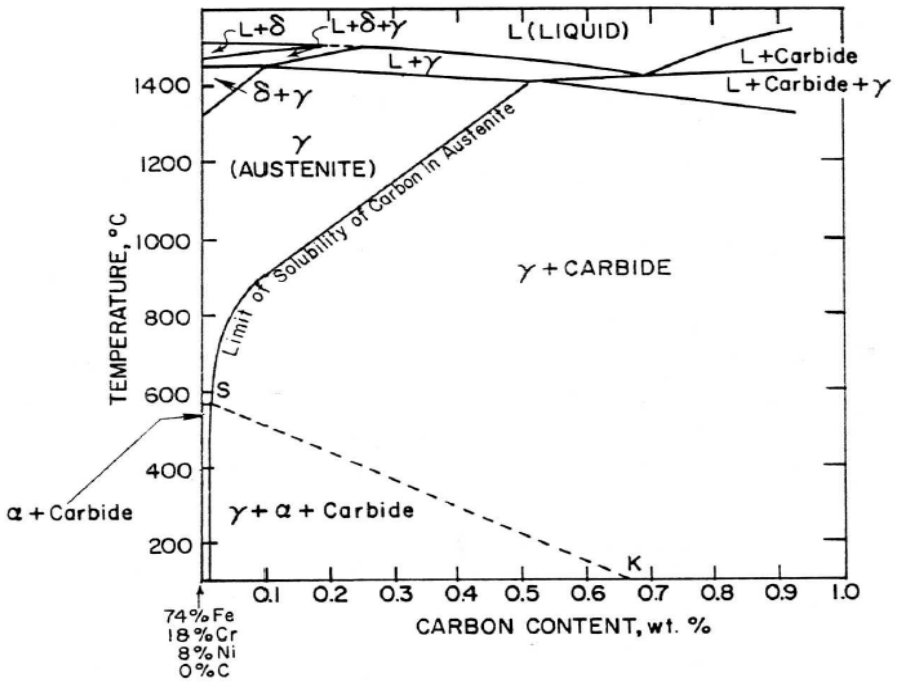

Figure 2-18: Pseudo-binary phase diagram for an 18%Cr-8%Ni alloy[38]

Alloys that contain about 0.003 to 0.7 wt.% C usually have austenite (γ), alpha ferrite (α) and carbides ($M_{23}C_6$) at temperatures below 600℃. The transformation of γ to α and $M_{23}C_6$ in alloys containing various austenite stabilisers is not likely to occur because the stabilisers inhibits dissolution of C from austenite.[57]

Austenitic stainless steels containing less than 0.03 wt.% C are stable up to room temperature because it is the maximum amount of carbon soluble in austenite. Austenitic stainless steels containing more than 0.03 wt.% C are likely to undergo transformation to $M_{23}C_6$ as the

temperature is decreased to room temperature below the C solubility line. However rapid cooling past the solubility line can avoid precipitation of these carbides and hence the alloy will be saturated with C at room temperature.[57]

When austenitic stainless steel containing more than 0.03 wt.% C is annealed at 1050℃ and rapidly cooled to room temperature, it will be supersaturated with C. However, if the cooling rate is not rapid enough, carbides will precipitate. If the supersaturated austenite is reheated at elevated temperatures within the γ and $M_{23}C_6$ field, further precipitation of Cr-rich $M_{23}C_6$ will take place at the grain boundaries. The areas close to carbides become depleted with Cr and hence it will be susceptible to corrosion attack called intergranular corrosion. Steels that experience this kind of corrosion are said to be sensitised.[57]

2.10.2 Effect of delta-ferrite and sigma phase

Delta-ferrite (δ) is a phase that can be formed in austenitic stainless steels as a result of unbalanced Ni-Cr composition and cooling rate during solidification. It is likely to form when an alloy is rich in Cr and other ferrite stabilising elements, but lean in Ni and other austenite stabilising elements.[38]

The amount of delta ferrite can be measured with a ferritescope and its morphology can be studied using the optical microscope. Angelo Fernando et al. [58] in his paper observed that the amount of delta ferrite slightly decreased with the increasing cooling rate for austenitic stainless steels that were examined. This means the liquid metal was cooled quickly to avoid formation of δ-phase.[58]

δ-phase serves as the nucleation site for austenite. If there is high Cr content with respect to Ni, delta ferrite does not completely transform to austenite and hence a large fraction of δ-phase could be detected. The optical microscope can reveal whether the morphology of the delta ferrite phase is a continuous network, semi-continuous network or isolated cores. The morphology of δ-phase in Type 304 stainless steel is shown in Figure 2-19.[58]

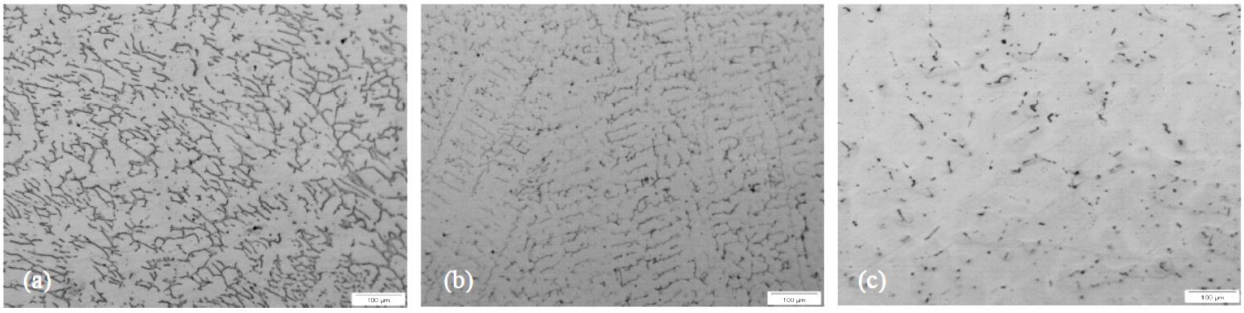

Figure 2-19: Morphology of delta ferrite in Type 304[58]

Formation of δ-phase can have a negative effect on the properties of stainless steel. Long term exposure of δ-phase at elevated temperatures can lead to it transforming to sigma brittle phase that can reduce ductility and toughness. Sigma phase formation is possible between 565℃ and 925℃ in austenitic stainless steels containing more than 16 wt.% Cr and less than 32 wt.% Ni. It is therefore a requirement that austenitic stainless steels contain sufficient amount of Ni or it's equivalents to avoid formation of δ-phase.[38]

The δ-phase is a Cr-rich phase compared to austenite (γ) and it has body centred crystal (BCC) structure. It is difficult to prevent precipitation of sigma phase when the stainless steels contain more than 20 wt.% Cr content because it is a strong ferrite stabilizer. The presence of other strong ferrite stabilisers such as Mo and Si leads to rapid formation of sigma phase. This means that δ-phase readily transforms to sigma phase (δ→σ) in the presence of these alloying elements. Cr and Mo diffuse efficiently in δ-phase and hence accelerate (δ→σ) transformation.[59]

When the alloy is exposed to elevated temperature during processes such as casting, welding, hot-rolling and or aging, sigma phase will be more likely to form. The σ-phase has tetragonal crystal structure. The (δ→σ) transformation precipitate in high Cr regions of δ-phase and is formed directly in δ-phase particles. The Cr and Mo content of δ-phase decreases whilst the Ni content increases simultaneously as the σ-phase precipitates. This then leads to formation of secondary austenite (γ_2) grains which depends on Ni for stabilisation.[59]

The σ-phase is easy to precipitate at the δ-γ interface, at high Cr region. The precipitation of σ-phase reduces corrosion resistance to pitting, crevice and intergranular attack, because of Cr depleted zones where σ-phase has precipitated. Continuous network reduces resistance to intergranular corrosion because when it transforms to sigma brittle phase on exposure to high temperature; it causes embrittlement along the grain boundaries. The σ-phase can be avoided by solution heat treating stainless steels at temperatures above 1050℃. At this temperature σ-phase formed during hot rolling or forging will diffuse into γ-austenite matrix. The dissolution process is called σ→γ phase transformation.[38], [59]

2.10.3 Chi (χ)-phase

The χ-phase is observed in alloys containing substantial additions of Mo. It can also exist as an intermetallic particle with C dissolved in it or as carbide ($M_{18}C$). It has a BCC (α-Mn) crystal structure. The χ-phase nucleates at grain boundaries, then at incoherent twin boundaries, coherent twin boundaries and on dislocation within the matrix. The precipitation range of χ-phase is 550℃-900℃, and it also depends on Mo content of an alloy. It has various shapes from

rod like to globular shape. Increased solution heat treatment does not affect nucleation of χ-phase but its nucleation is accelerated by cold work.[53], [60]

2.10.4 *Laves (η) phase*

The η-phase can also be formed in austenitic stainless steels after long-term high-temperature exposure. It is likely to be observed in alloys containing Mo, Nb and Ti. It is a hexagonal intermetallic compound. Precipitation of this phase occurs at temperatures between 650℃ and 950℃, and has globular shape. It is generally stable below 815℃ depending on Mo, Ti, and Nb content of the steel. The common η-phase are Fe_2Mo, Fe_2Nb and Fe_2Ti or the combination of all, i.e. Fe_2 (Mo, Nb, Ti).The Fe_2Mo can be observed in alloys containing more than 2 wt.% Mo when annealed for a long time.[60]

2.10.5 *Formation of martensite*

Austenitic stainless steels that contain ≤10 wt.% Ni, harden upon plastic deformation as a result of strain hardening and transformation from austenite to martensite. There are two martensitic transformations that take place, which are: austenite to body centred cubic phase (γ to α′) and austenite to hexagonal close packed lattice (γ to ε). The ȧ-phase has the same lattice parameters of ferrite phase.[61]

The transformation is favoured by lower stacking fault energy (SFE) which is influenced by temperature and the chemical composition of the alloy. Ni, Mo and Mn increase the SFE whilst N decreases it. Cr can either decrease or increase the SFE depending on its ratio to Ni. The change in microstructure after rolling was observed by S.Tavares et al. on Type 201 stainless steel as shown in Figure 2-20.[61]

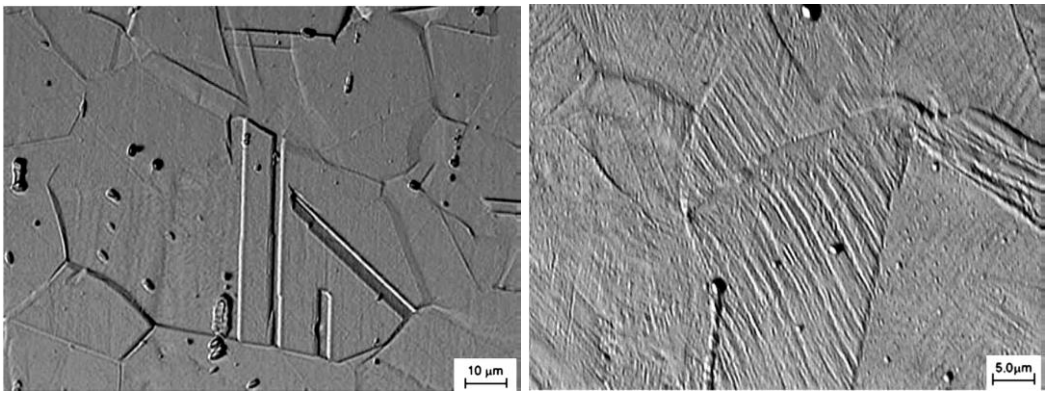

Figure 2-20: Austenite transformation in Type 201 due to strain[61]

Chapter 3: Material Characterisation

3.1 Processing of Hercules™

Hercules™ alloys were received in the as-cast condition from Mintek. The picture of Hercules™ A and Hercules™ B is shown in Figure 3-1. The cut-offs were used to measure the chemical composition before rolling the 5 kg ingots. The composition was confirmed to be within the chemical composition spectra for Hercules™ composition range.

Figure 3-1: Hercules™ alloys ingots

Hot forming parameters that were developed by J.Moema et al. [2] were used to process Hercules™ ingots in this project for comparison sake. Ingots were homogenised at 1200℃ for 4 hours before processing. They were first forged from 40 mm to approximately 30 mm thickness. Then, they were returned to the furnace for 30 mins in order to release stress formed due to forging. Samples were further hot rolled to approximately 12 mm thick plates.

The finishing temperature was measured using the optical AssTech pyrometer with an accuracy of ±25℃. It was important to check the finishing temperature in order to ensure the correct microstructure. The rolling temperature and thickness reduction values are shown in Table 3-1. Rolled out hot strips were quenched in a 1000 litres of water immediately after the 3rd pass.

Austenitic stainless steels have a tendency to transform from austenitic form to martensite during rolling at room temperatures or cooling. Therefore, samples were annealed in the furnace at

1050℃ for 1 hour to remove non-equilibrium phases that might have been formed during quenching.

Table 3-1: Temperature and thickness reduction after each pass

Hot rolling conditions		Hercules™ A	Hercules™ B
Passes	Temperature(℃)	ΔT(mm)	ΔT(mm)
Forging	1155	40.1-30.0	40.5-30.5
1st	1075	30.0-24.7	30.5-21.4
2nd	1058	24.7-17.6	21.4-14.6
3rd	1058	17.6-12.1	14.6-10.6

3.2 Chemical composition

The portion of hot rolled samples was ground and the chemical composition was measured using Spark Emission Spectrometry. The commercial Type 304 and Type 202 were received from Columbus Stainless [Pty] Ltd and also analysed for chemical composition. Type 201 could not be obtained in time, hence Type 202 was used instead. The chemical composition is shown in Table 3-2. The values of alloy composition are within the expected range[1] for Hercules™ alloys, with Mo addition in Hercules™ B.

Table 3-2: Chemical composition of test alloys (wt.%)

No.	C	Si	Mn	Cr	Ni	Mo	N	Cu	Fe
Type 202	0.080	0.38	6.74	16.27	4.61	0.13	0.15	1.95	69.7
Type 304	0.041	0.34	1.33	18.27	8.26	0.07	0.05	0.12	71.3
Hercules™ A	0.065	0.52	9.21	16.60	2.04	0.02	0.111	0.033	71.2
Hercules™ B	0.067	0.52	10.2	16.05	1.61	0.54	0.209	0.039	70.6

[1] See Appendix B for composition range

The composition of Type 202 and Type 304 showed that the alloys are of Type H-grade because they had more than 0.04 wt.% C contents. Therefore, Hercules™ was comparable to Type 304 and Type 202 because of higher C content. Higher C content in Hercules™ is responsible for stabilising austenite since Ni content is reduced.

Alloying elements play a major role in austenite stability. Mn increases the solubility of N in the liquid metal. Addition of 10 wt.% Mn can increase the solubility of N to 0.42 wt.% at 1550℃ [62]. A maximum of 0.25 wt.% N can be absorbed for Hercules™ to maintain austenitic microstructure at room temperature with approximately 5% ferrite.[2]

3.3 Pitting resistance equivalence number

The PRE_N value is the pitting resistance equivalence number that is calculated from the composition of the alloy. This value gives theoretical information about pitting resistance of an alloy. LNASS's such as Hercules™ and Type 202 have high Mn content that has to be accounted for in the PRE_N. Therefore, Equation (3-1) was used to calculate PRE_N [63]. Type 304 had the highest PRE_N value followed by Type 202, and Hercules™ B. Hercules™ A had the lowest PRE_N values and was therefore expected to have lower pitting resistance than the other alloys.

$$\mathrm{PRE_N} - \mathrm{Mn} = \%\mathrm{Cr} + 3.3\%\mathrm{Mo} + 30\%\mathrm{N} - \mathrm{Mn} \quad (3\text{-}1)$$

Table 3-3: PRE_N values for test alloys

Alloy	PRE_N
Type 304	18.684
Type 202	14.459
Hercules™ A	10.780
Hercules™ B	13.902

3.4 Microstructural prediction for Hercules™

Thermo-Calc™ was used to predict the microstructure of Hercules™ alloys. Thermo-Calc™ is a thermodynamics database used to predict the equilibrium phases in multi-component systems. Phase diagrams for Hercules™ A shown in Figure 3-3 and Hercules™ B in Figure 3-3. Given

that alloys were hot rolled and annealed at 1050℃, it was shown from the phase diagram that at equilibrium conditions, both alloys are expected to be fully austenitic at room temperature.

The phase diagrams for both alloys are almost similar besides that the BCC region in Hercules™ A is more extended than in Hercules™ B. This means that a higher volume fraction of delta ferrite would be expected in Hercules™ A if non-equilibrium conditions were considered. Another FCC phase was observed within the hot rolling temperature range of Hercules™ B. The FCC phase present at this temperature was predicted to be carbides. Carbides ($M_{23}C_6$) precipitate from the austenite phase at about 800℃. These carbides are thought to nucleate on stainless steel alloys with C content that is greater than 0.03 wt.%.[59]

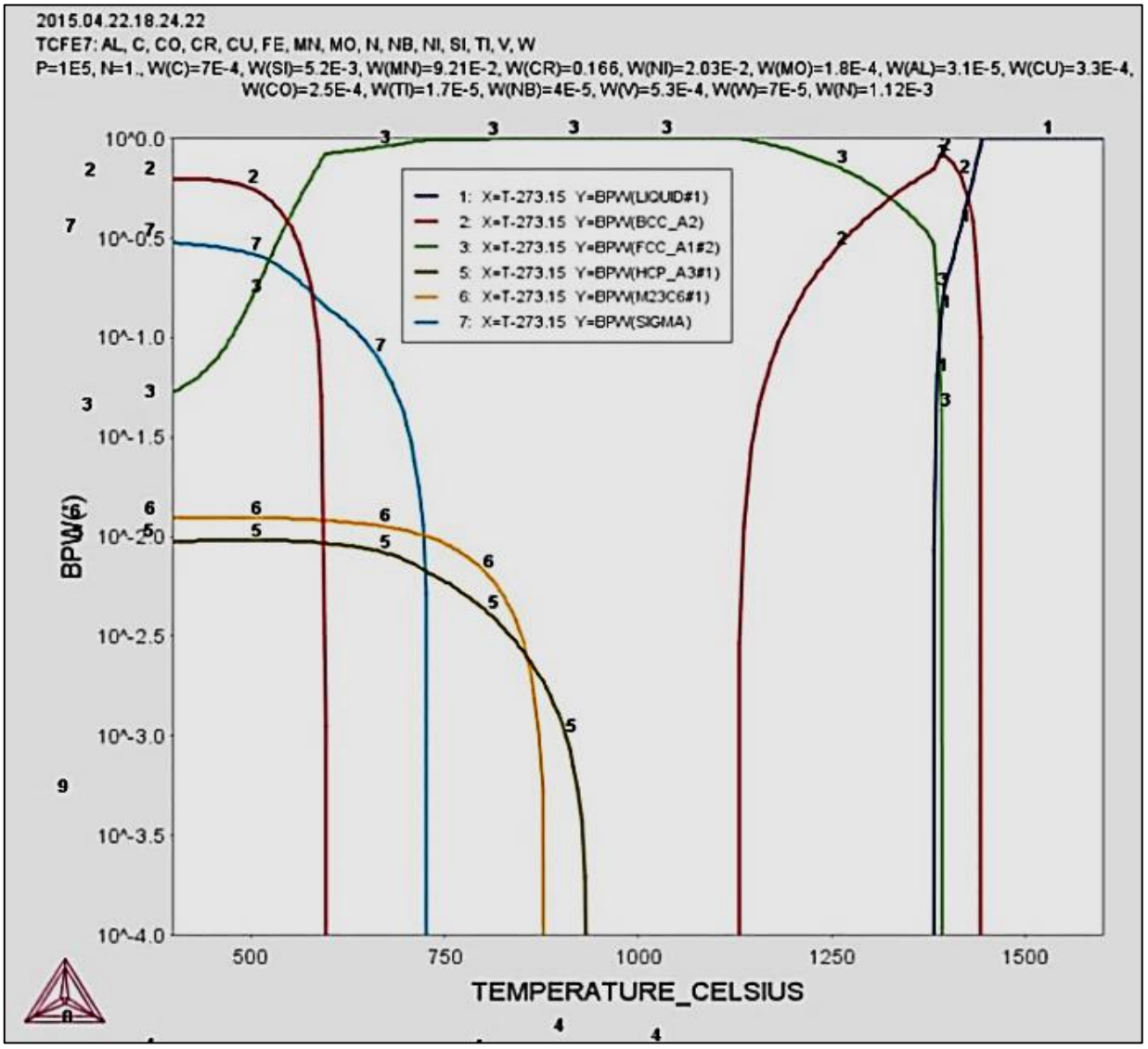

Figure 3-2: Thermo-Calc™ phase diagram for Hercules™ A

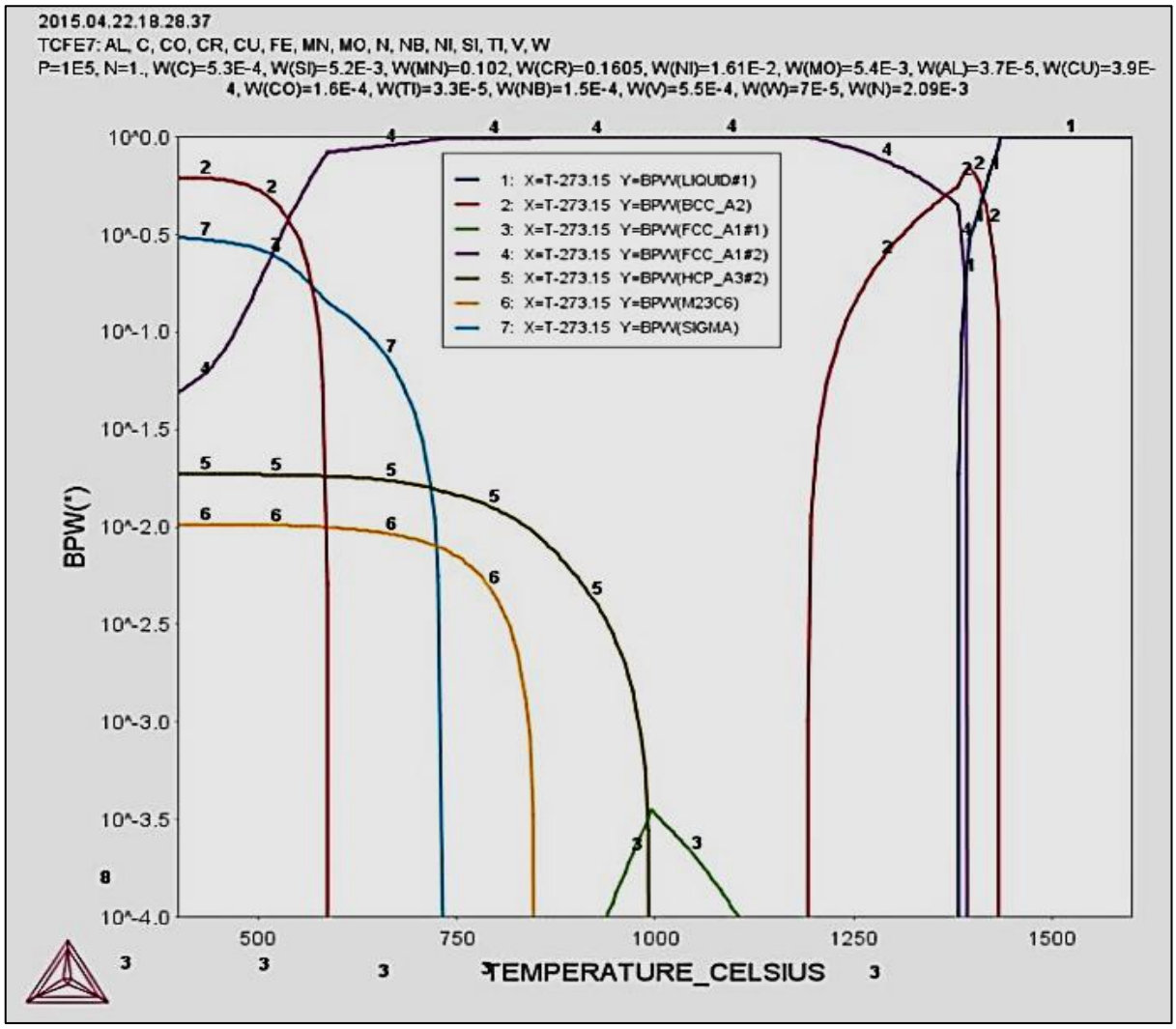

Figure 3-3: Thermo-Calc™ phase diagram for Hercules™ B

3.5 Austenite-Martensite transformation

Besides the predicted phases, other phases may be present in austenitic stainless steels. Austenite has a tendency to transform to martensite during deformation. Therefore, there have been models used to predict the temperature at which the austenite-martensite transformation occurs. One of the models is called Angel's model, which calculates the temperature at which 30% deformation induces 50% transformation (M_{d30}). Angel's model correlates M_{d30} with the composition of the alloy as shown in Equation (3-2).[62]

$$M_{d30} = 413 - 13.7Cr - 9.5Ni - 8.1Mn - 9.2Si - 18.5Mo - 462C - 462N \qquad (3\text{-}2)$$

Transformation may occur because of cooling rate or strain. When an alloy is cooled to room temperature or cryogenic temperatures, it can possibly undergo transformation due to elemental

(Cr, Mn and Ni) depletion at grain boundaries. Grain boundaries favours the nucleation of the martensite.[60] M_{d30} values for test alloys are presented in Table 3-4.

Table 3-4: M_{d30} values for test alloys

Alloy	M_{d30} (℃)
Type 202	−20.45
Type 304	37.20
Hercules™ A	5.13
Hercules™ B	−47.09

An alloy with lower M_{d30} in comparison with other alloys is able to maintain a stable austenite phase. The M_{d30} for Type 304 has been measured to be of 106℃ by A. Dischino et al. [62]. However, since Hercules™ was hot rolled at higher temperatures, deformation induced transformation was not the concern and it was also annealed at 1050℃ for 1 hour to revert back any phase formed during deformation and quenching to austenite.[62]

The deformation induced martensite can be detected using the magnet because its crystal structure. In the internal Mintek report [1] detailing the first tests that were done on Hercules™, martensite and ferrite content was measured using a ferritescope. The samples in the as-cast ingots showed an amount of martensite, but the ones annealed only showed ferrite.[1]

3.6 General microstructure of Hercules™

Samples were ground using SiC paper and then polished using 9µm suspension to 1µm suspension. The micrographs of as-polished samples shown in Figure 3-4 did not show any evidence of martensite, since samples were annealed. The OP-AA suspension slightly revealed austenitic grains with annealing twins in both alloys. No evidence of ferrite phase was observed from the as-polished micrographs.

The microstructure outlining annealing twins and austenitic grains was achievable by colour etching using the method outlined in Table 3-5. The Beraha's tint etchant resolved the austenitic grain boundaries, twin boundaries and the dark spots which may have been attacked by the etchant. The etchant coloured austenite grains brown, while twin boundaries were coloured white. The microstructure of colour etched samples are shown in Figure 3-5. Delta-ferrite was

revealed by electrolytic etching with 20% NaOH. The etchant outlines and colour delta-ferrite tan as shown in Figure 3-6.

Table 3-5: Etchants for general microstructure[64]

Etchant constituents	Name of the etchant	Features revealed
200ml HCl, 1000ml H_2O, 24 g $NH_4F.HF$ Add 1 g of $K_2S_2O_5$.	Beraha's tint etchant	Reveals annealing twins and austenitic grains
20g NaOH, 100 ml H_2O. Electrolytic etch at 20 V dc for 5–20 s	20% NaOH	Outline and colour delta-ferrite(δ) tan

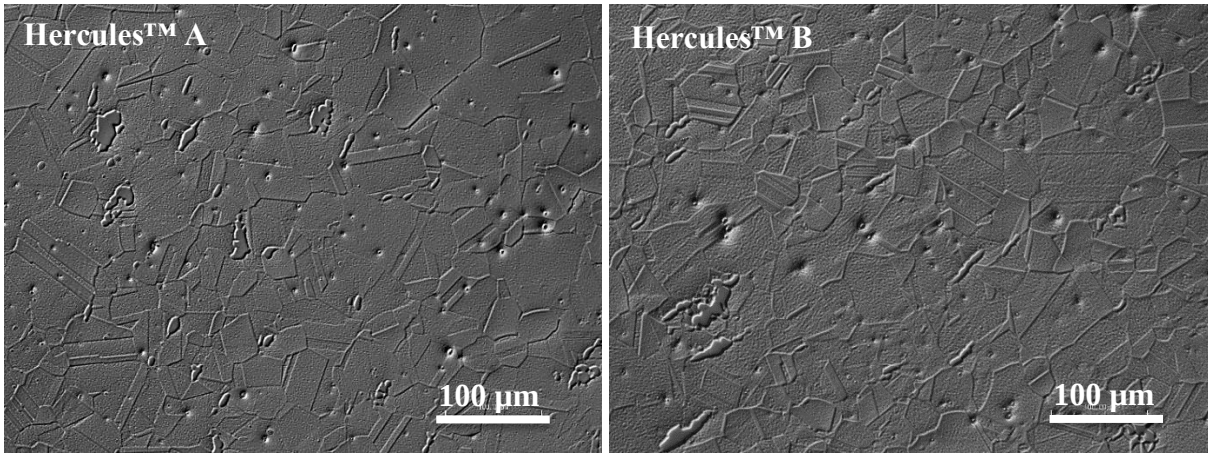

Figure 3-4: As-polished microstructures

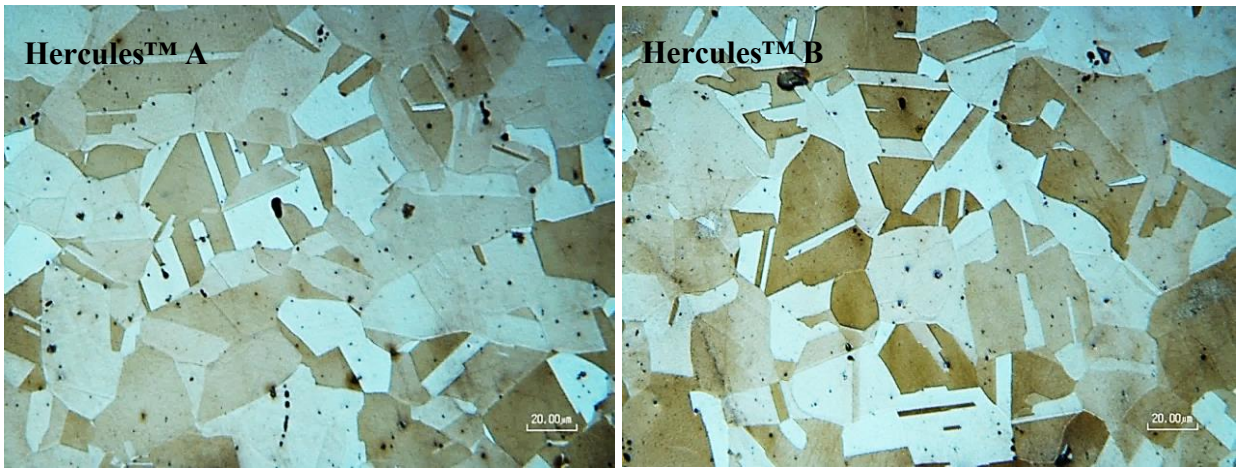

Figure 3-5: Colour-etched with Beraha's tint etchant

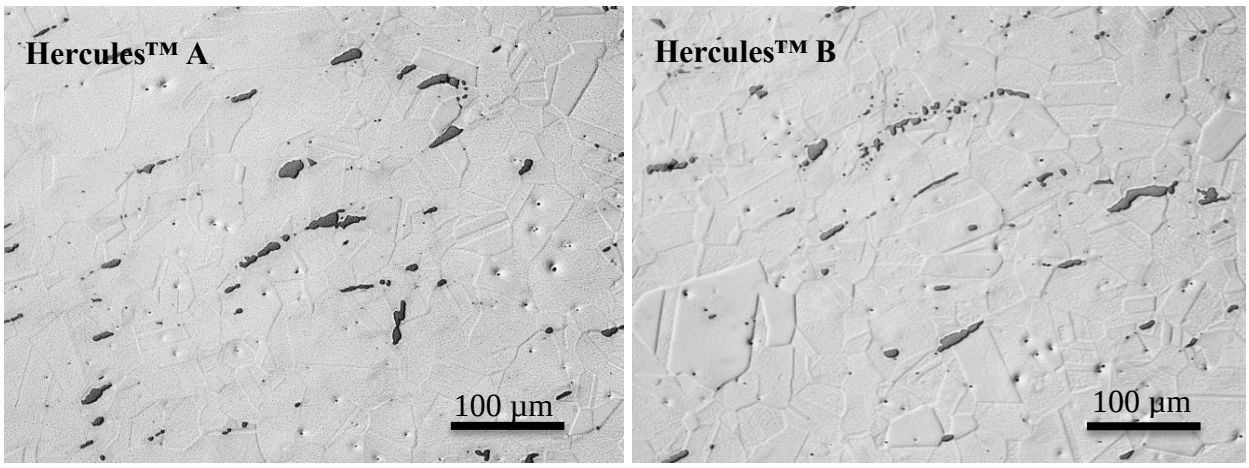

Figure 3-6: Electro-etched with 20% NaOH

Chapter 4: Corrosion Tests Methodology

The following is the Table of summary of all corrosion tests that were carried out:

Table 4-1:The summary of corrosion tests

Test	Corrosion type	Standard	Material	Solution	Conditions
Cyclic polarisation	Pitting	ASTM G61 and ASTM G150	Hercules™ A, Hercules™ B, Type 304	3.56 wt.% NaCl	Room temperature
Cyclic polarisation	Crevice	ASTM G61	Hercules™ A, Hercules™ B, Type 304 and Type 202	3.56 wt.% NaCl and 1 wt.% NaCl	Room temperature
Cyclic polarisation	Uniform	ASTM G5 AND ASTM G61	Hercules™ A, Hercules™ B, Type 304 and Type 202	5 wt.% H_2SO_4	Room temperature
Immersion	Uniform	ASTM G31	Hercules™ A, Hercules™ B, Type 304 and Type 202	5 wt.% H_2SO_4	Room temperature
Immersion	Pitting	ASTM G48 A	Hercules™ A, Hercules™ B, Type 304 and Type 202	6 wt.% $FeCl_3$.6H2O	26℃ ± 2℃
Immersion	Crevice	ASTM G48 B	Hercules™ A, Hercules™ B, Type 304 and Type 202	6 wt.% FeCl3.6H2O	26℃ ± 2℃
Critical pitting temperature	Pitting	ASTM G48 E	Hercules™ A, Hercules™ B, Type 304 and Type 202	6 wt.% FeCl3.6H2O	25℃ ± 1℃ to 50℃ ± 1℃

4.1 Cyclic polarisation technique

Cyclic polarisation technique was used to investigate the susceptibility of test alloys to localised corrosion. This technique is generally used to measure the pitting tendencies of alloys in a given metal-solution system. The experiment starts by applying the potential scan beginning at E_{corr} and continuing in the anodic direction until there is a large increase in current (e.g. a sustained anodic current density $\geq$10 $\mu A/cm^{-2}$).[65]

The resulting graph is a plot of applied potential vs. the logarithm of current density. When the scan reaches the programmed current density limit value, it reverses and begins scanning in the negative direction. The final potential of the reverse scan is called the protection potential (E_{pro}). An example of a typical Cyclic polarisation plot is shown in Figure 4-1.[65], [66]

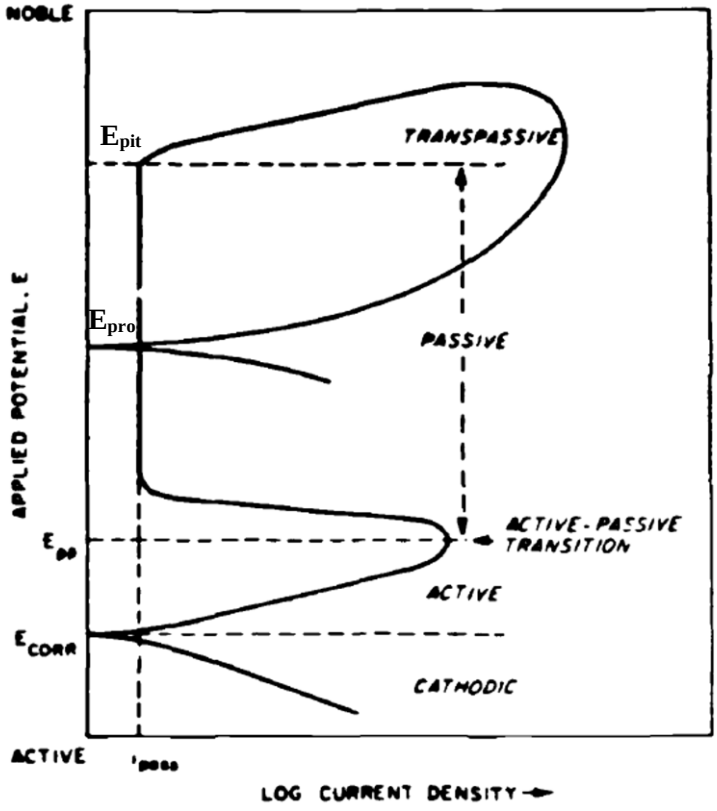

Figure 4-1: A typical Cyclic polarisation plot[66]

The E_{pit} is the potential at which stable pits initiate and propagate as applied potential increases. E_{pro} is the potential below which no initiation of pits will occur. Pits that form above E_{pit} will eventually repassivate below E_{pro} hence the potential is also referred to as the repassivation potential. Both E_{pit} and E_{pro} are used to explain the kinetics of pitting and repassivation.[65]

The direct interpretation of the graph is as follows:[65]

- If the $E_{pro} = E_{pit}$, there will be little tendency for pitting

- If the $E_{pro} > E_{pit}$, there will be no tendency for pitting
- If the $E_{pro} < E_{pit}$, there will be a possibility for pitting

The size of the hysteresis loop can give a rough indication of the extent of propagation of initiated pits. The longer it takes for pits to repassivate, the bigger the hysteresis loop. This may imply that pits that had formed are severe and stable. In some cases, pits show no tendency to repassivate by the hysteresis loop closing at a potential less than E_{corr}.[65]

4.2 Test set-up: Crevice-free cell

The ASTM G61 standard was used as a guide to execute Cyclic polarisation tests. The 50 by 50 mm^2 coupons were cut from each test alloy plate in the hot rolled and annealed condition. Test alloys were then ground to 120 grit SiC paper before the beginning of each scan. Immersion in 10% HNO_3 solution for 10 minutes was performed in order to facilitate passive layer formation.[67]

Test specimens were then washed with tap water and rinsed with ethanol. The Avesta corrosion cell was assembled as shown in Figure 4-2. The cell similar to that used in ASTM G150 for electrochemical critical pitting temperature testing of stainless steels was used.[68]

The advantage of using the Avesta cell is that the edges of the specimen are not involved in the testing and the specimen is not mounted inside the cell. The specimen is placed underneath the cell and a paper crevice washer is put on the surface of the exposed specimen area. Purified water was continuously pumped into the contact area of the cell port and the sample to prevent crevice corrosion. The water flow from the drip bag was set to 5 ml/h.[68]

The reference electrode (RE), working electrode (WE) and counter electrode (CE) were connected as shown in Figure 4-2. E_{corr} was compared to a known standard potential of saturated calomel electrode (SCE), which is +0.244 V. A potentiostat from ACM instruments was used to apply potential on the test specimen and to measure the current flow between the working electrode and the counter electrode.[65]

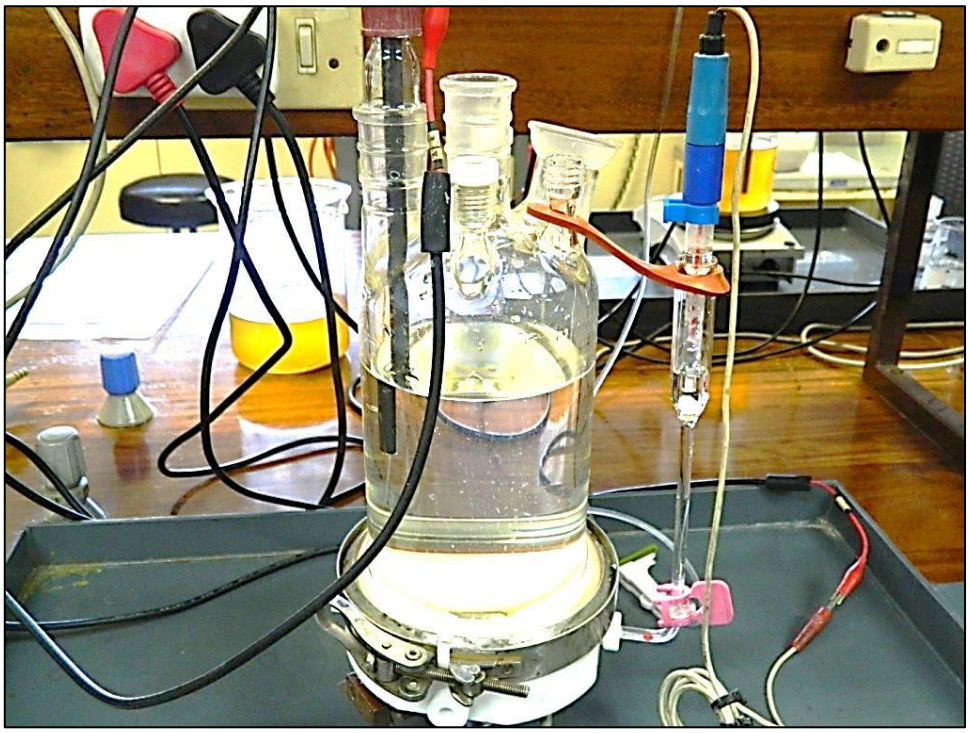

Figure 4-2: Avesta corrosion cell set-up

After pouring the solution into the corrosion vessel, the specimen was left for 60 min to allow it to react in an open circuit without applying external potential. After 60 min, the E_{corr} was recorded and the scan was started from the E_{corr}. The scan was set to increase potential stepwise up to 1200 mV or until the potential at which current density was set to reverse. The test conditions are shown in Table 4-2.

Table 4-2: Test conditions for crevice-free cell

Parameter	Conditions
Temperature	Room temperature
Solution	Deaerated 3.56 wt.% NaCl
Scan rate	10 mV/min
Reverse current density	5 mA/cm^2

Pitting scans were then obtained and the recorded values were transferred to the Origin programme in order to plot the correct potential vs log current density curves. The Tafel extrapolation method was used to measure critical potentials. The optical microscope was used

to capture images of the corroded surface of each test specimen in order to evaluate the morphology and the density of pits.

4.3 Test set-up: Artificial crevice cell

An artificial crevice was introduced on the surface of each sample. Alloys were first tested in 3.56 wt.% NaCl. The Critical chloride threshold level (CCTL) for Type 304 and Type 204Cu have been studied in concrete solution containing different chloride content by [39]. The CCTL for Type 204Cu was measured to be 1 wt.% NaCl.

Outokumpu also measured the CCTL for Type 304 and other steels. It was discovered that the CCTL for Type 304 is 2.5%, while other studies have revealed that CCTL for Type 304 is 2% when it is embedded in concrete. This means that CCTL for Type 304 is higher than that of LNASS's and 3.56 wt.% NaCl is an aggressive solution to test Type 304 and LNASS's. Hence, test alloys were also tested in 1 wt.% NaCl in order to compare the behaviour of alloys in low and high concentration solution.[40], [39], [11]

Disc shape specimens with 12 mm diameter were cut from each test alloy. All specimens were then ground to 120 grit SiC paper and passivated in 10% HNO_3 for 10 minutes. The cell was assembled as shown in Figure 4-3. Then 10 mm diameter O-ring was placed on the surface of each working electrode before mounting it to the sample holder in order to induce an artificial crevice. Test conditions were similar to those presented in Table 4-2.

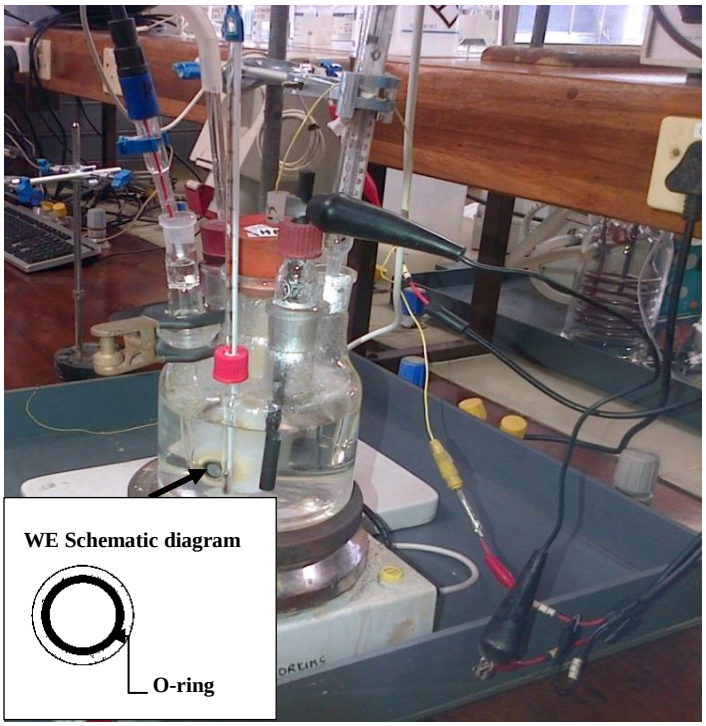

Figure 4-3: Crevice corrosion cell set-up

4.4 Evaluation of passivity behaviour

Temperature and concentration of electrolyte affects the passivation behaviour of an alloy. The ability for test alloys to passivate after activation was investigated using H_2SO_4 in order to rank Hercules™ alloys against Type 304 and Type 202. Outokumpu has done tests on stainless steels using H_2SO_4 at different temperatures. An alloy is considered resistant to uniform corrosion if it has a corrosion rate that is less than 0.1 mm/yr. in any given environment.[11]

H_2SO_4 can be oxidising and reducing at different concentrations. Outokumpu has presented the results in an isocorrosion diagram for different steels. An example of a 0.1 mm/yr. isocorrosion diagram from Outokumpu corrosion handbook is shown in Figure 4-4.

It has been reported that H_2SO_4 is reducing at low and high concentrations, but oxidising at intermediate concentrations (30 wt.% to 80 wt.%) for Type 304/4307. According to isocorrosion diagrams presented by Outokumpu, Type 304 remains passive in H_2SO_4 where the concentration is less than 10% and above 90% wt.%, and at a temperature range of 39℃ to 20℃.[11]

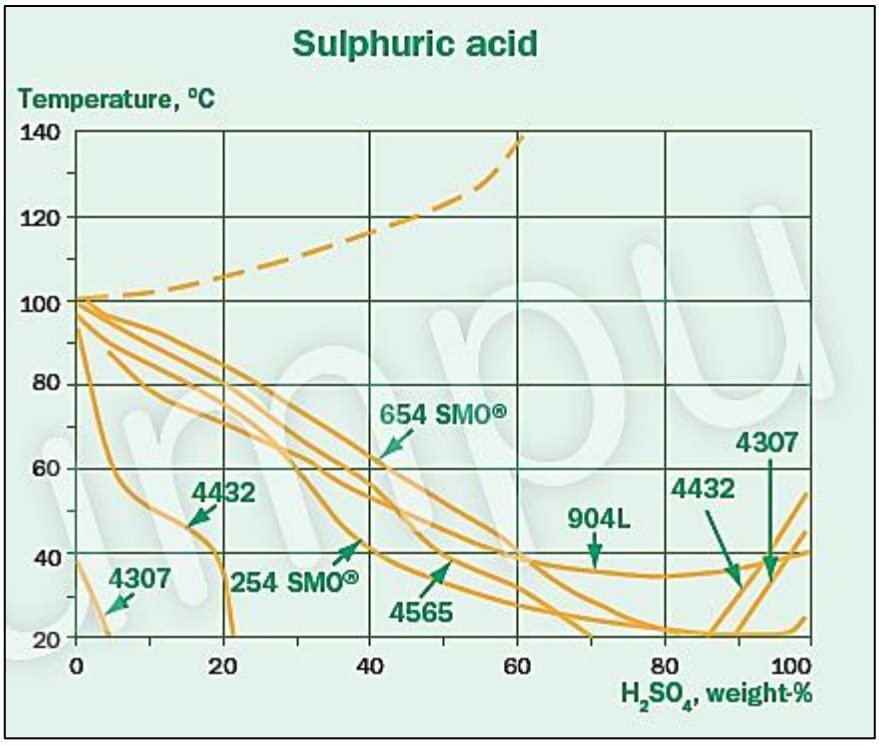

Figure 4-4: Isocorrosion diagram for austenitic stainless steels in H_2SO_4[11]

A. Muwila [35] also tested Hercules™ B against Hercules™ A, Type 304 and Type 201. After a 14-day immersion period, mass loss was measured. Mass loss measurements showed that Hercules™ B and Type 304 remained passive in 5 wt.% H_2SO_4, while Hercules™ A and Type 201 performed badly.[35]

Electrochemical techniques can also be used to investigate passivity of alloys. Cyclic polarisation technique was used to obtain the following information about test alloys behaviour in 5 wt.% H_2SO_4:

- The extent of passivation potential region
- The corrosion rate in the passive region/stability of passive state
- The ability of a material to spontaneously passivate in a given solution system[69]

Before polarisation, specimens were left to passivate for 60 minutes and E_{corr} was measured. Given different reactions taking place on the surface of the specimen during corrosion, there are 6 possible behaviour characteristics that an alloy can display that have been discovered and are presented as shown in Figure 4-5 [66], [69]. These typical illustrations were used to interpret the corrosion behaviour of test alloys that were tested in 5 wt.% H_2SO_4.

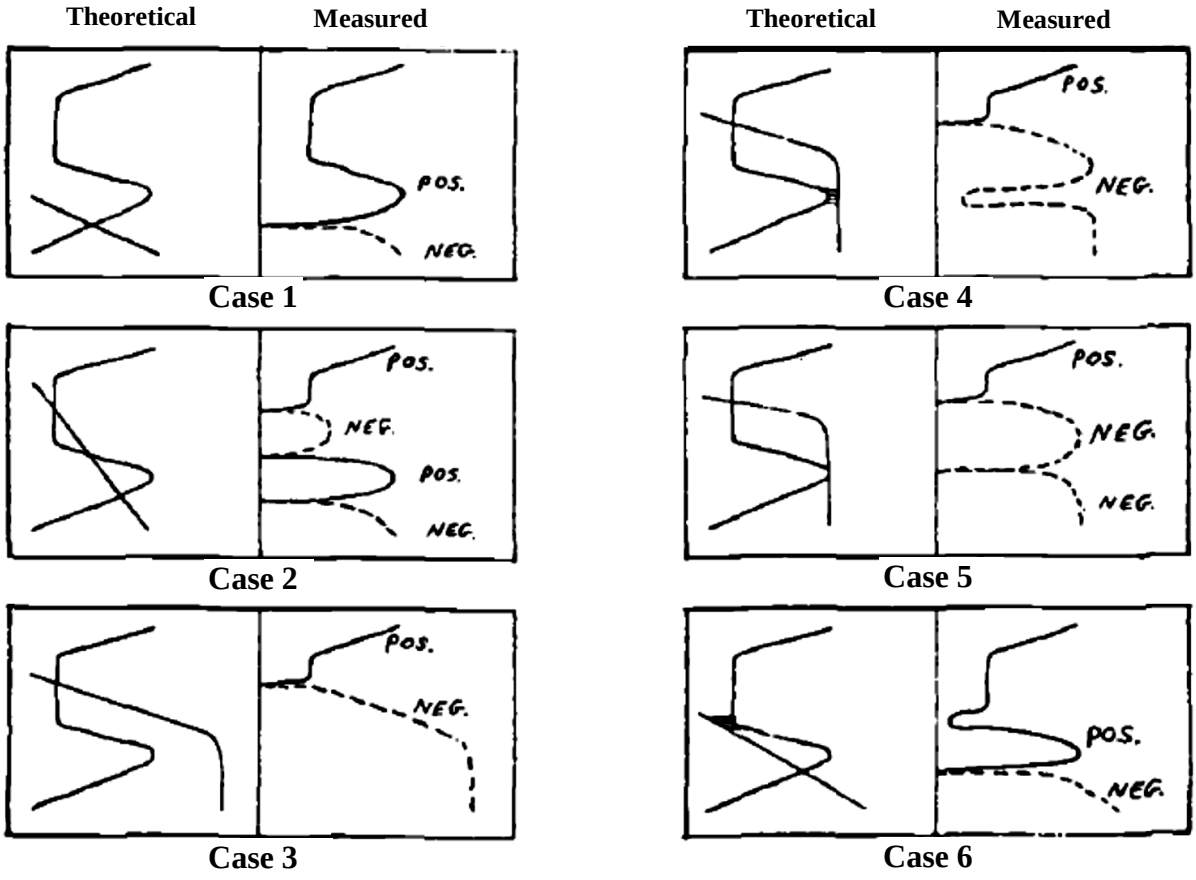

Figure 4-5: Typical active-passive behaviour of particular alloys[69]

Case 1 shows that corrosion potential is obtained in the active region. The specimen will corrode spontaneously in the beginning but is able to passivate in some other experimental conditions. The anodic behaviour of the alloy is the one that dominates, with higher corrosion rates.[66]

In Case 2, the cathodic curve intersects the anodic curve at three potentials and three corrosion potentials can be measured. An alloy with that type of behaviour can exhibit high or low corrosion rates, which is not desirable because the alloy can change from passive to active if a passive layer is slightly disrupted. The alloy that shows that kind of behaviour can either be passive if the passive layer is stable or it can have high corrosion rates when passive layer is disrupted.[66]

In Case 3, the corrosion potential is measured in the stable passive region, meaning that the alloy is able to passivate spontaneously and exhibit low corrosion rates. Most stainless steels exhibit this behaviour if they are tested in acidic solutions that contain sufficient oxidisers such as Fe^{3+} and Cu^{2+}. These oxidisers create higher potentials and cause the alloy to corrode faster and form the passive layer that could be stable for some alloys. It is desirable for a material if it can be kept at i_{crit} that is small enough to avoid intersection with the reduction polarisation curve, and hence lower corrosion rate.[66]

4.5 Calculation of the corrosion rate from polarisation curves

The corrosion rate was calculated using Faraday's equation in Equation (4-1).[70]

$$\mathrm{CR} = \mathrm{k_1}\frac{\mathrm{i_{corr}}}{p}\,\mathrm{EW} = \mathrm{K(i_{corr})} \tag{4-1}$$

Where: $K=k_1 \times EW/p$, CR= corrosion rate in mm/yr., K_1= 3.27x 10^{-3} mm g/μA cm yr., P = density in g/cm^3, i_{corr} = corrosion density in μA/cm^2 and EW =Equivalence weight

K value for Type 304 and 202 is 0.011. For Hercules™ alloys, the K value was calculated. Since there are a number of elements present in an alloy, a sum of EW is required which includes all alloying elements that are active in the corrosion process. The EW of each alloy was calculated from the valence number for each element with a composition >1 wt.%.

Element composition with the participating valence electrons for Hercules™ A and Hercules™ B are shown in Table 4-3. Hence EW for both Hercules™ A and Hercules™ B was calculated to be 0.256. Finally, the K value for both alloys was calculated to be similar, which is 0.0160 for both Hercules™ alloys.[15]

$$\mathrm{K} = \mathrm{k_1} \times \frac{\mathrm{EW}}{p} = \frac{3.27 \times 10^{-3} \times 25.56}{7.85\mathrm{g/cm^3}} = 0.0106 \tag{4-2}$$

The corrosion rates for test alloys was therefore, calculated from the equation:

$$CR = 0.011 \times i_{corr} \times 1000 \text{ (in mm/yr)} \quad (4\text{-}3)$$

Table 4-3: Weight equivalence for Hercules™ A & Hercules™ B

Alloying elements (>1wt.% content)	Hercules™ A		Hercules™ B	
	wt.%	Valence no.	wt.%	Valence no.
Mn^{2+}	9.21	2	10.20	2
Cr^{3+}	16.60	3	16.05	3
Ni^{2+}	2.04	2	1.61	2
Fe^{2+}	71.2	2	70.6	2

The i_{corr} value was calculated by extrapolating the Tafel region. The example of Tafel extrapolation method is shown in Figure 4-6. The data for Tafel extrapolation is obtained from cathodic and anodic regions of the polarisation curve. Anodic region represents the metal dissolution and cathodic represents hydrogen evolution in the acidic electrolyte. It is easier therefore to measure i_{corr} from the cathodic curve because the rate of H_2 evolution is higher because of metal dissolution in acidic solution.[69]

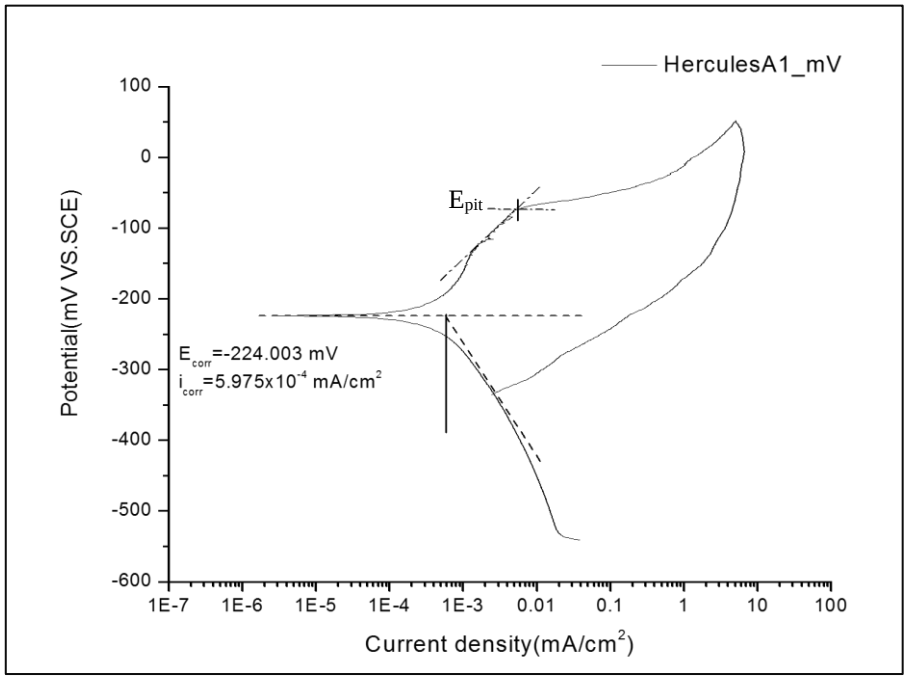

Figure 4-6: Example of Tafel extrapolation[69]

4.6 Immersion tests in 5 wt.% H_2SO_4

Following electrochemical tests for tests alloys in 5 wt.% H_2SO_4, immersion tests were carried out for 10 days. Tests were done following the procedure outlined in ASTM G31[71]. 25 by 50 mm^2 coupons of Hercules™ A, Hercules™ B, Type 304 and Type 202 were ground to 120 grit SiC paper.

Corrosion rates of alloys immersed in the same solution under similar conditions should be within ±10% of each other, when uniform corrosion is observed. However, large differences in the corrosion rate can occur under conditions where an alloy is not given enough time to passivate. Test coupons were therefore left for a minimum of 24 hours to allow them to passivate in air, in order to stabilise the passive layer.[52]

Each coupon was weighed using the Sartorius-research analytical balance. Each specimen was weighed to 3 decimal places. Test coupons were then immersed in a test solution at room temperature; two specimens per 600 ml beaker and closed with a tight plastic wrap. The amount of solution in the beaker was calculated to a ratio: 0.20 ml/mm^2.[71]

After 10 days, samples were taken out of the solution, washed and weighed again. Mass difference was calculated. This is different from what A.Muwila [35] did by weighing specimens every 24 hours for 14 days. This was because a disruption of stainless steel passive layer could lead to extraneous results, since it has already been discussed that Hercules™ behaviour in H_2SO_4 solution can be unpredictable.

After mass loss calculations, the corrosion rate was calculated using Equation (4-4).[71]

$$\text{Corrosion rate} = \frac{K \times W}{A \times T \times D} \tag{4-4}$$

Where:

K = 8.76×10^4 for corrosion rate in millimetres per year (mm/y)

W = mass loss in grams

A = area in cm^2

T = time of exposure in hours

D = density in g/cm^3. Results obtained from this section were used in conjunction with the electrochemical test results calculated from polarisation curves, in order to be able to completely understand the active-passive behaviour of test alloys.

4.7 Immersion tests in 6 wt.% $FeCl_3.6H_2O$

4.7.1 ASTM G48 experimental procedure

ASTM G48 was used to test pitting and crevice corrosion resistance of test alloys. Method A is used to test pitting corrosion and method B for crevice corrosion at room temperature. The temperature was maintained at around 26℃ ± 2℃. ASTM G48: Method E was used as a guideline to test the critical pitting temperature for each test alloy. The information to be obtained from these tests is:

- Detailed corrosion evaluation of Hercules™ against Type 304 and Type 202
- Acceptance of quality assurance of Hercules™ as the new alloy
- Develop a safe window of operation for Hercules™

25 by 50 mm^2 coupons were also prepared the same way as in the H_2SO_4 test for method A and B. Since there was a shortage of material, 20 by 30 mm coupons were used for all test alloys for method E. The summary of the experimental procedure for alloys tested using ASTM G48 is presented in Table 4-4.

Table 4-4: Summary of experiments carried out using ASTM G48 [51]

Method	Solution	Investigation	Sample prep.	Duration	Temperature
A	6 wt.% $FeCl_3.6H_2O$	Pitting corrosion	25 by 50 mm coupons	72 hours	26℃ ± 2℃.
B	6 wt.% $FeCl_3.6H_2O$	Crevice corrosion	25 by 50 mm coupons, TFE blocks fastened with O-rings	72 hours	26℃ ± 2℃.
E	6 wt.% $FeCl_3.6H_2O$	CPT	20 by 30 mm coupons	24hrs/per 5℃ temperature increment	25℃ ± 1℃ to 50℃ ± 1℃

4.7.2 ASTM G48 Method B

An example of a picture of crevice corrosion test specimen before immersion into 6 wt.% $FeCl_3.6H_2O$ is shown in Figure 4-7. TFE-fluorocarbon blocks on each side of the specimen surface were held by 2 elastic bands.

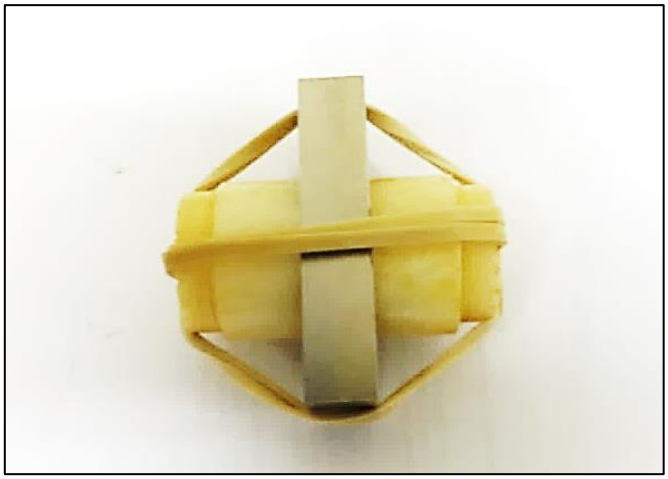

Figure 4-7: Crevice corrosion samples for ASTM-G48: Method B

The severity of crevice corrosion on samples that were exposed according to Method B was measured by calculating the critical crevice damage factor (CCDF) value. Table 4-5 has information outlining the CCDF calculation from the surface examination of each test alloy that corroded by crevice corrosion mechanism.[21]

Table 4-5: Calculation of CCDF[21]

Factors	Penetration/circumference affected	Depth of metal loss	**CCDF (Penetration circumference +depth)**
Scale	1:2:3	1:4	**0:10**
Description	<25% :25%-75%:>75%	Shallow:>0.5 mm	**No visual attack: severe metal loss**

4.7.3 ASTM G48 Method E

On the other hand, the starting test temperature for Method E was estimated using Equation (4-3). Table 4-6 represents the results of calculated starting temperature for Hercules™ alloys and Type 304 and Type 202 according to their alloying element composition.[51]

$$\mathrm{CPT}(℃) = (2.5 \times \%\mathrm{Cr}) + (7.6 \times \%\mathrm{Mo}) + (31.9 \times \%\mathrm{N}) - 41.0 \quad (4\text{-}5)$$

Table 4-6: Calculated initial temperature values for test alloys: ASTM G48E

Alloy type	**Theoretical CPT (**℃)	**Starting temperature** (℃)
Hercules™ A	4.21	10
Hercules™ B	9.90	20
Type 304	7.28	12
Type 202	8.64	13

Normally the test is started at the nearest increment of 5℃ from the calculated theoretical CPT value. A Labotech temperature controlling heater was used to control the temperature of the water bath where samples were immersed. The starting temperature of the heater was limited to room temperature up to a maximum of 100℃. The standard procedure was modified in order to conduct a test using a Labotech heater.

Since Method A and B tests showed that pitting and crevice corrosion was severe even without HCl addition, a non-acidified solution was used starting at 25℃-50℃, with 5℃ and 10℃ increments (within ±1℃). A new coupon was used for each temperature increment. Each test was left to run for 24 hrs at different temperatures. At the end of each test period the coupon was removed and rinsed with water and ethanol. Corroded coupons were then reweighed and examined for pitting corrosion.[51]

According to ASTM G48, CPT is measured as the maximum temperature where pit depth is ≥ 0.025 mm. Therefore, pit depth and density were measured by visual examination of images taken at 10X magnification using the Light microscope.

Chapter 5: Results and Discussions

Table 5-1 represent the summary of results that were obtained form cyclic polarisation tests.

Table 5-1: Summary of test results obtained from cyclic polarisation technique

Cyclic polarisation technique						
Corrosion Type	**Solution**	**Material**	**E_{corr} (mV.SCE)**	**i_{corr} (mA/cm^2)**	**E_{pit} (mV.SCE)**	**Corrosion rate (mm/y)**
Pitting	3.56 wt.% NaCl	Hercules™ A	-156	6.8E-05	-68	0.7E-03
		Hercules™ B	-153	6.9E-05	-70	0.8E-03
		Type 304	-115	5.0E-05	288	0.6E-03
Crevice	3.56 wt.% NaCl	Hercules™ A	-208	4.7E-04	-58	0.5E-2
		Hercules™ B	-192	4.4E-04	-37	0.5E-02
		Type 304	-169	1.6E-04	72	0.2E-02
Crevice	1 wt.% NaCl	Hercules™ A	-205	8.4E-05	219	0.9E-03
		Hercules™ B	-146	4.1E-05	580	0.4E-03
		Type 304	-177	3.1E-05	350	0.4E-03
		Type 202	-130	4.2E-05	188	0.5E-03
Uniform	5 wt.% H_2SO_4	Hercules™ A	-38	9.7E-05	-	0.1E-02
		Hercules™ B	-198	1.5E-03	-	02E-01
		Type 304	-26	1.7E-04	-	0.2E-02
		Type 202	-102	4.5E-04	-	0.5E-02

Table 5-2 represent the summary of test results that were obtained from immersion tests.

Table 5-2: Summary of immersion test results

Immersion tests					
Corrosion Type	**Solution**	**Material**	**Mass loss (g)**	**Corrosion rate (mm/y)**	**CCDF**
Uniform	5 wt.% H_2SO_4	Hercules™ A	0.7010	1.9	-
		Hercules™ B	0.0150	04E-01	-
		Type 304	0.0013	0.3E-02	-
Pitting	6 wt.% $FeCl_3.6H_2O$	Hercules™ A	0.95	11.8	-
		Hercules™ B	1.0182	12.6	-
		Type 304	1.1335	14.0	-
		Type 202	1.4924	18.5	-
Crevice	6 wt.% $FeCl_3.6H_2O$	Hercules™ A	1.0026	12.4	5
		Hercules™ B	1.1937	14.8	3
		Type 304	1.0407	12.9	5
		Type 202	1.3682	16.9	4

Critical pitting temperature tests					
Corroison Type	**Solution**	**Material**	**Maximum Mass loss (g)**	**Pit density (pits/mm^2)**	**CPT (℃)**
Pitting	6 wt.% $FeCl_3.6H_2O$	Hercules™ A	0.487	0.39	< 25
		Hercules™ B	0.185	0.11	< 25
		Type 304	0.211	0.25	< 25
		Type 202	0.232	0.11	< 25

5.1 Pitting corrosion resistance in 3.56 wt.% NaCl solution

The resistance of test alloys to pitting corrosion was tested using the crevice-free Avesta cell. From the pitting scans; E_{pit}, E_{pro}, E_{corr} and i_{corr} values were measured and are presented in Table 5-3. The E_{pit} for Type 304 was measured at 288 mV vs SCE, which is higher than the E_{pit} for Hercules™ A at −63 mV vs SCE and Hercules™ B at −70 mV vs SCE. This means that Type 304 has higher resistance to initiation of pitting than both Hercules™ alloys. The resistance to initiation of pitting corrosion demonstrated by Type 304 over Hercules™ corresponds to the PRE_N values that were calculated in Chapter 3. Type 304 has higher PRE_N of 18, while Hercules™ A and Hercules™ B has PRE_N values of 10 and 13 respectively.

Table 5-3: Critical potentials for pitting corrosion

Sample Identity	Area (cm^2)	i_{corr} (mA/cm^2)	E_{corr} (mV.SCE)	E_{pit} (mV.SCE)	E_{pro} (mV.SCE)	Corrosion rate (mm/y)
Hercules™ A						
1	6,5	6,10E-05	-168	-68	-	6.7E-04
2	6,5	7,40E-05	-144	-57	-122	8.1E-04
Average	**6,5**	**6,75E-05**	**-156**	**-63**	**-122**	**7.4E-04**
Hercules™ B						
2	6,5	6,70E-05	-157	-82	-109	7.4E-04
3	6,5	7,01E-05	-149	-58	0	7.7E-04
Average	**6,5**	**6,86E-05**	**-153**	**-70**	**-55**	**7.5E-04**
Type 304						
1	6,5	3,68E-05	-112	281	-26	4.0E-04
2	6,5	6,36E-05	-119	294	-13	7.0E-04
Average	**6,5**	**5,02E-05**	**-115**	**288**	**-20**	**5.5E-04**

Lower E_{pit} means that addition of Mo in Hercules™ B did not improve the pitting resistance of Hercules™. This is Contrary to A. Muwila [35] pitting corrosion test in 3.56 wt.% NaCl, where E_{pit} values obtained for Hercules™ increased with Mo content. A. Muwila [35] plotted the

relationship between the effect of Mo and N on pitting of Hercules™ alloys as shown in Figure 5-1.[35]. It was noted that Hercules™ alloys with 0.5 wt.% Mo together with 0.18 wt.% N contents will exhibit an E_{pit} value between −25 and 10 mV vs SCE.

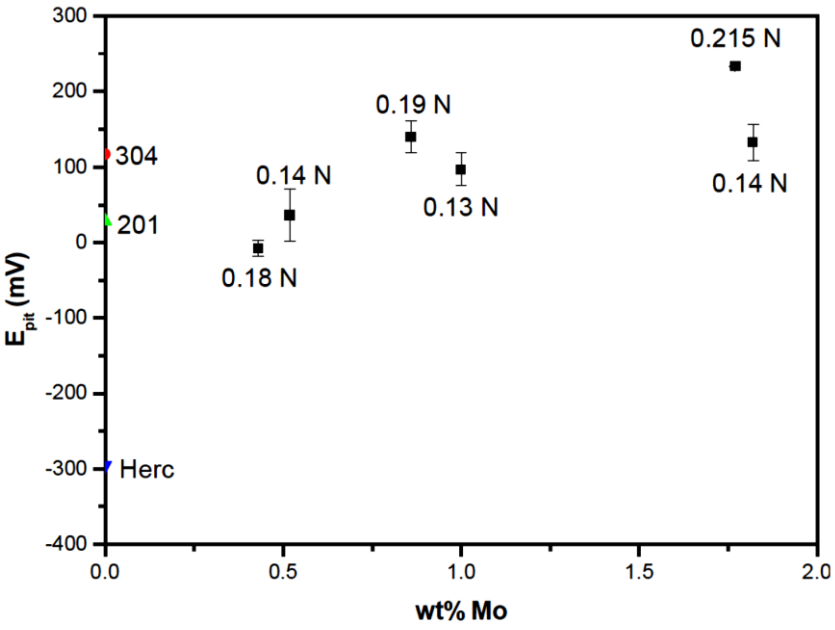

Figure 5-1: Effect of Mo and N in pitting potential of Hercules™[35]

Pitting scans that were obtained are shown in Figure 5-2[2], alongside with a bar graph showing the difference between E_{pro} and E_{pit}. E_{pro} for Type 304 was measured at −20 mV vs SCE and that of Hercules™ B was −55 mV vs SCE. The reverse scan in Hercules™ A closed the forward scan at a potential that is less than E_{corr}, which meant that E_{pro} was not significantly measured for Hercules™ A. The 3.5 wt.% NaCl was aggressive for Hercules™ A to repassivate after the nucleation of pits. Although E_{pit} value for Hercules™ B was measured to be almost close to that of Hercules™ A, the difference is that E_{pro} was measured for Hercules™ B, which makes it a better alloy.

Therefore, the comparison between Type 304 and Hercules™ B is that they both have an ability to repassivate in 3.56 wt.% NaCl. An alloy is considered resistant to pitting in a particular environment if higher E_{pit} and E_{pro} values are measured[66]. Although Type 304 had higher E_{pit} and E_{pro}, the hysteresis loop also shows that the repassivation of pits in Type 304 takes longer than in Hercules™ B. The presence of Mo in Hercules™ B inhibited propagation of pitting, hence a smaller difference in the $|E_{pit} - E_{pro}|$ than Type 304.

[2] More pitting scans are shown in Appendix A

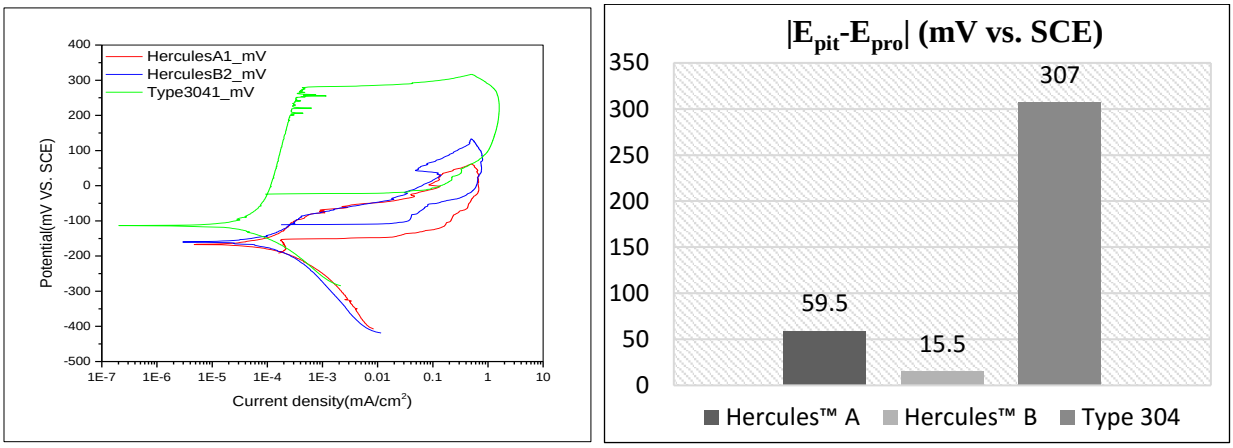

Figure 5-2: Pitting scans and extent of corrosion estimation in 3.56 wt.% NaCl

The extent of pitting was then evaluated by taking micrographs of corroded samples at 10X magnification using the light microscope. The density of pits was also determined by visual examination of the corroded specimen surface as shown in Figure 5-3 (Scale bar = 1mm). All test alloys showed severe pitting in 3.56 wt.% NaCl, with Hercules™ A having higher pit density, but narrow diameter.

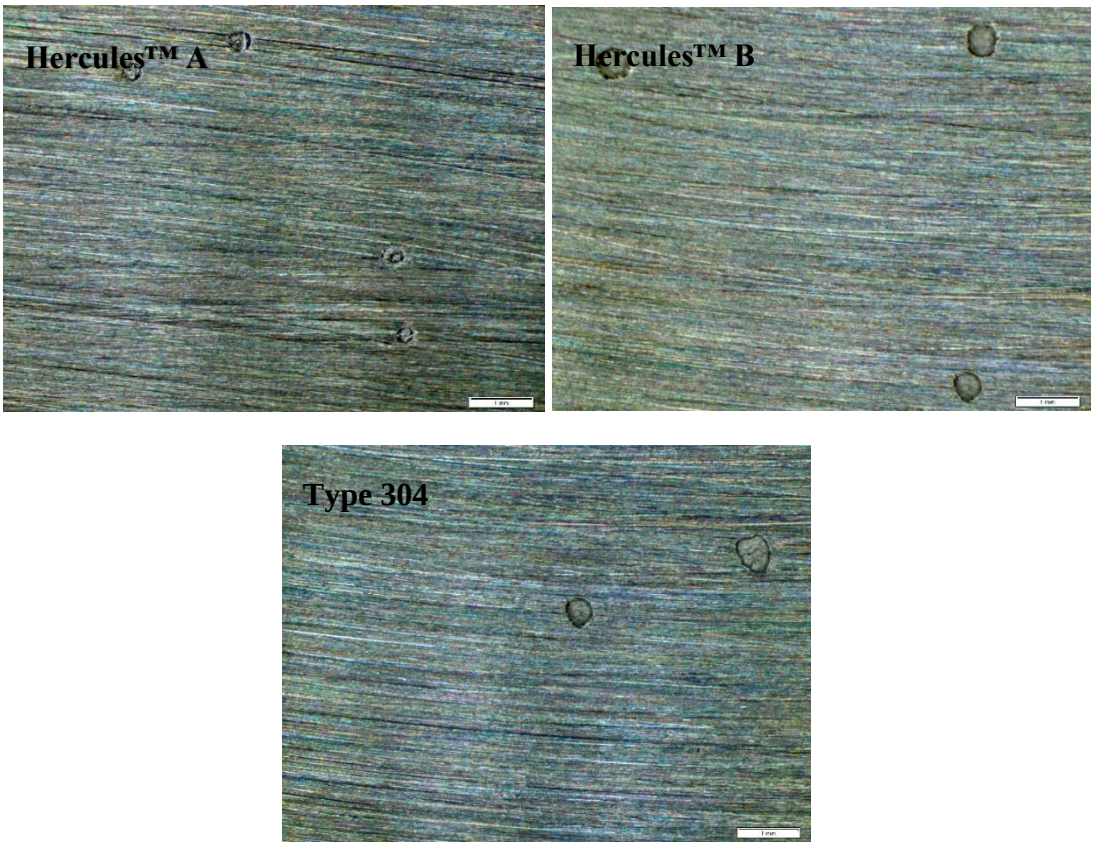

Figure 5-3: Pitting corrosion in 3.56 wt.% NaCl

5.2 Crevice corrosion resistance in 3.56 wt.% NaCl solution

Cyclic polarisation technique was used to test resistance to crevice corrosion of Hercules™ A and Hercules™ B in 3.56 wt.% NaCl against that of Type 304. Pitting scans that were obtained are shown in Figure 5-4 and the critical potentials obtained due to crevice corrosion are summarised in Table 5-4. It was observed that E_{pit} values that were obtained in the presence of an artificial crevice are lower than values that were obtained in the crevice-free cell.

All test alloys performed badly, with just a slightly higher E_{pit} for Type 304 than Hercules™ alloys. The E_{pit} values for Hercules™ A and Hercules™ B were measured to be almost similar, hence their corrosion rates due to crevice corrosion were almost similar.

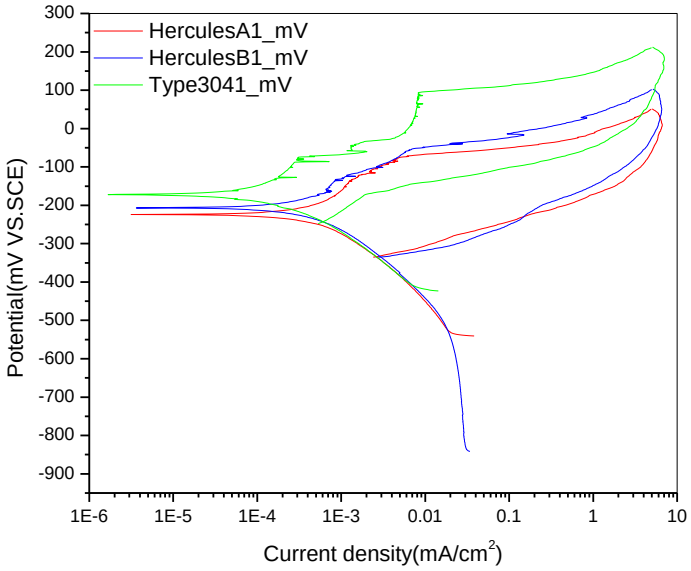

Figure 5-4: Crevice corrosion test scans in 3.56 wt.% NaCl

E_{pro} was measured at potentials below E_{corr} for all test alloys, meaning that in the presence of an artificial crevice, alloys had undergone severe crevice corrosion in 3.56 wt.% NaCl. The test solution contains enough chloride concentration that is required to drive the propagation of crevice corrosion in the area under the crevice. The severity of crevice corrosion was evaluated using the micrographs taken at 5X magnification. The micrographs of corroded specimens are shown in Figure 5-5 (Scale bar = 1mm).

Figure 5-5: Micrographs showing crevice corrosion in 3.56 wt.% NaCl

It is evident from the micrographs that all samples experienced crevice corrosion underneath the plastic O-ring, hence E_{pro} was measured at potentials below E_{corr}. In a crevice metal-solution system, there lies a critical crevice solution, of which a minor shift in potential gradient changes the corrosion behaviour of an alloy from passive to active. The longer it takes for an alloy to reach that critical crevice solution defines the resistance of an alloy to crevice corrosion.[52]

Amongst other factors, critical crevice solution can be affected by alloy composition. The cationic metal species react with water to generate acidity in the crevice region. In stainless steels, the common reaction to take place under a crevice is shown by the chemical Equation (5-1).

$$Fe^{2+} + 2H_2O \rightarrow Fe(OH)_2 + 2H^+ \quad (5\text{-}1)$$

The reaction involves other alloying elements such as Cr, Mn and Mo[52]. Mo was added in Hercules™ B to inhibit the reaction and generation of acidic hydrogen and hence lower the corrosion rate. But, instead the results proved that it reacted as Hercules™ A. Therefore, other factors that affect the corrosion behaviour of test alloys were discussed. Those factors include pH of the test solution and concentration of chlorides.

Metal dissolution occurs when the pH of the crevice solution is sufficiently low and if the concentration of chlorides is high enough to breakdown the passive layer. 3.56 wt.% NaCl is typically neutral and if the composition of Hercules™ only differs by 0.5 wt.% Mo, it can be expected that the generation of acid in the crevice solution is almost similar for both alloys. The only factor that dominates is the chloride concentration, which is the key factor to break the passive layer and cause an active dissolution of an alloy. This can happen faster when the chloride level is increased above critical levels, hence severe form of crevice corrosion was observed.[52]

The CCTL for Type 304 embedded in a chloride containing concrete has been studied by various researchers[11], [40] and it was measured to be between 2% and 5%. M.C Garcia-Alonso et al.[40] measured the CCTL of LNASS Type 204Cu to be less than 1%. Since Type 204Cu has the composition that is almost similar to Hercules™, it is clear that 3.56 wt.% NaCl was too aggressive for testing the crevice corrosion resistance.

Table 5-4: Critical potential values for crevice corrosion tests in 3.56% NaCl solution

Sample	Area (cm^2)	i_{corr} (mA/cm^2)	E_{corr} (mV.SCE)	E_{pit} (mV.SCE)	Corrosion rate (mm/y)
Hercules™ A					
1	0,79	5,98E-04	-224	-75	6.6E-03
2	0,79	3,32E-04	-193	-41	3.6E-03
Average		**4,65E-04**	**-208**	**-58**	**5.1E-03**
Hercules™ B					
1	0,79	4,09E-04	-207	-43	4.5E-03
2	0,79	4,72E-04	-177	-32	5.2E-03
Average		**4,40E-04**	**-192**	**-37**	**4.8E-03**
Type 304					
1	0,79	1,89E-04	-173	96	2.1E-03
2	0,79	1,35E-04	-165	48	1.5E-03
Average		**1,62E-04**	**-169**	**72**	**1.8E-03**

5.3 Crevice corrosion resistance in 1 wt.% NaCl solution

Pitting scans that were obtained from 1 wt.% NaCl solution test are shown in Figure 5-6. The E_{pit} was measured at 219 mV vs SCE for Hercules™ A, which is more positive than the one obtained from 3.56 wt.% NaCl test. The E_{pit} for Hercules™ B was measured at 579 mV vs SCE. The critical potentials are summarised in Table 5-5. There was a noticeable difference in E_{pit} values that were obtained for each alloy because the concentration of NaCl had been reduced. Hercules™ B had higher E_{pit} than all test alloys.

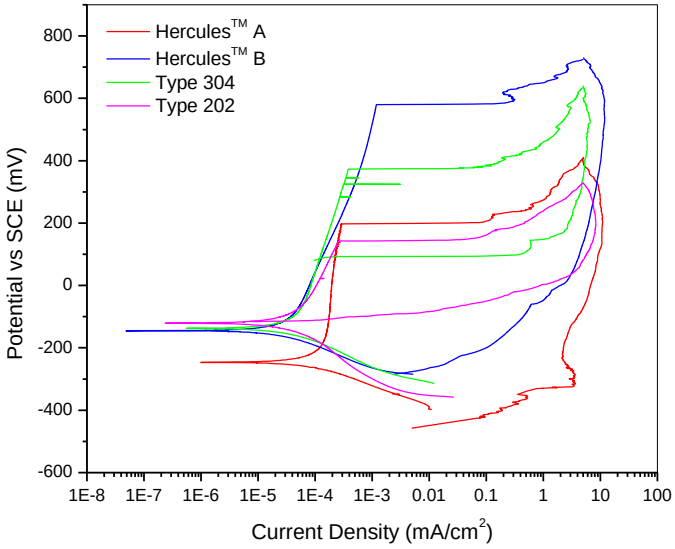

Figure 5-6: Pitting scans in 1 wt.% NaCl solution

E_{pro} value for Type 304 was measured to be 48 mV vs SCE. Type 202 had the E_{pro} at E_{corr} value. E_{pro} was measured below E_{corr} for Hercules™ A and Hercules™ B, although Hercules™ B had higher E_{pit} than other test alloys. Factors that affect the pitting behaviour of alloys are discussed below.

Firstly, the effects of Cr since Hercules™ B had lower Cr content than Type 304. T.Ujiro et al. [9] has studied the effect of Cr additions in the corrosion behaviour of austenitic stainless steels in NaCl solution. It was noted that increasing Cr reduced the rate of increase of current density above E_{pit}; that is, the size of hysteresis loop was decreased. Secondly, T.Ujiro et al. [9] studied the effect of Mo in the corrosion behaviour of austenitic stainless steel alloys with 26 wt.% Cr and varying Mo contents from 0-4 wt.% Mo. It was observed that addition of Mo decreased the anodic current density; that is, the current measured before E_{pit} or before the onset of pitting.[9]

The same behaviour was observed in Hercules™ B pitting scans. Extended passive region was evident in Hercules™ B compared to Hercules™ A, Type 304 and Type 202. However, both

Hercules™ A and Hercules™ B show similar hysteresis loop behaviour. The hysteresis loop closes at potentials lower than E_{corr}. This means that Mo had no effect on the corrosion behaviour of Hercules™ B after the onset of pitting; hence, a larger hysteresis loop was measured.

In addition to that, T.Ujiro et al. [9] explained that crevice corrosion can occur either by depassivation or pitting. Depassivation type occurs by depassivation of surface under the crevice, due to pH drop and extensive destruction of the passive film under artificial crevice. Pitting type occurs by pitting inside the crevice area as a result of chloride concentration increase in the inner solution. The micrographs were taken in order to evaluate corrosion type as shown in Figure 5-7 (Scale bar=1mm).

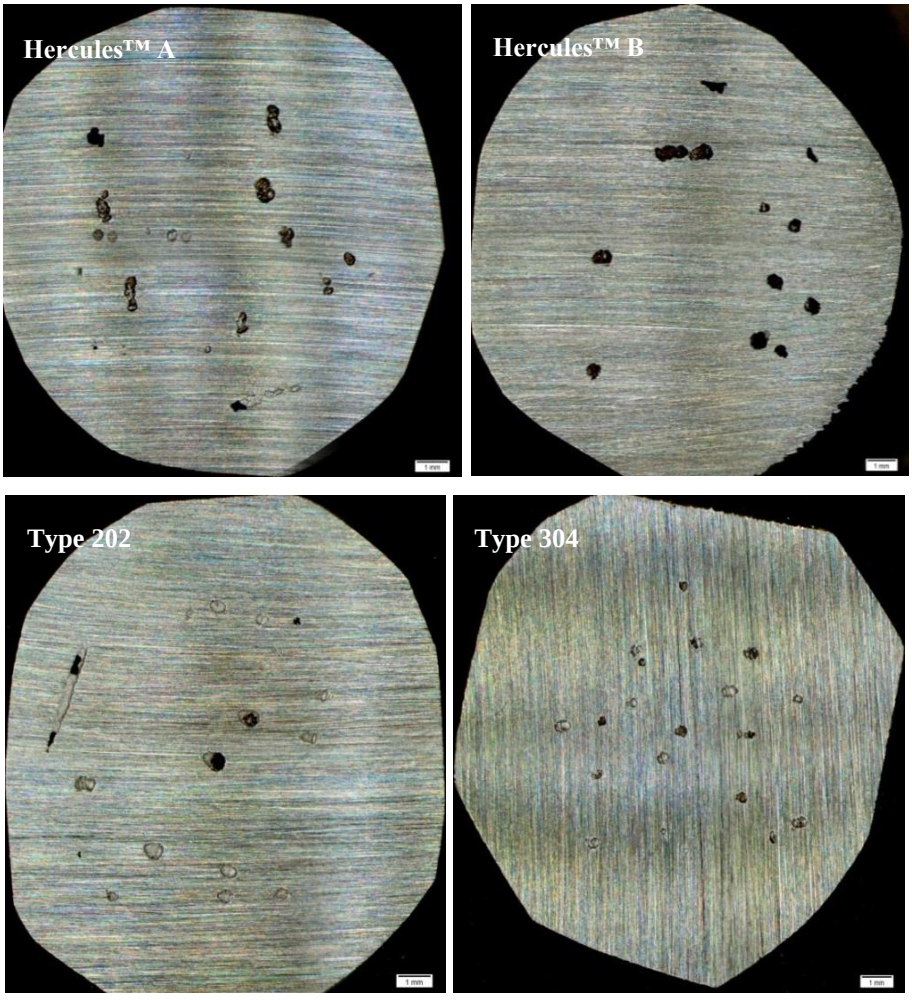

Figure 5-7: Micrographs of test alloys after polarisation in 1 wt.% NaCl solution

A schematic illustration shown in Figure 5-8 was then used to interpret the pitting scans that were obtained from 1 wt.% NaCl test in correlation with the visual examination of corroded specimens. The illustartion shows the expected behaviour of low-alloyed austenitic(A, A$^{'}$- pitting corrosion curve) and ferritic(F, F$^{'}$-pitting corrosion curve) stainless steels. Cathodic reaction is

represented by C-curves. C-curve is for high potential oxidants such as Fe^{3+} and C' represents low potential oxidants such as H^+ and H_2O.[9]

The behaviour of test alloys in the current project resembles the one showed by C-curve and A'. The E_{pit} for austenitic stainless steels is higher when an alloy corrodes by pitting instead of depassivation. It can be seen from the illustration that crevice corrosion by depassivation type occurs at lower potentials than corrosion by pitting corrosion or crevice-induced pitting corrosion.[9]

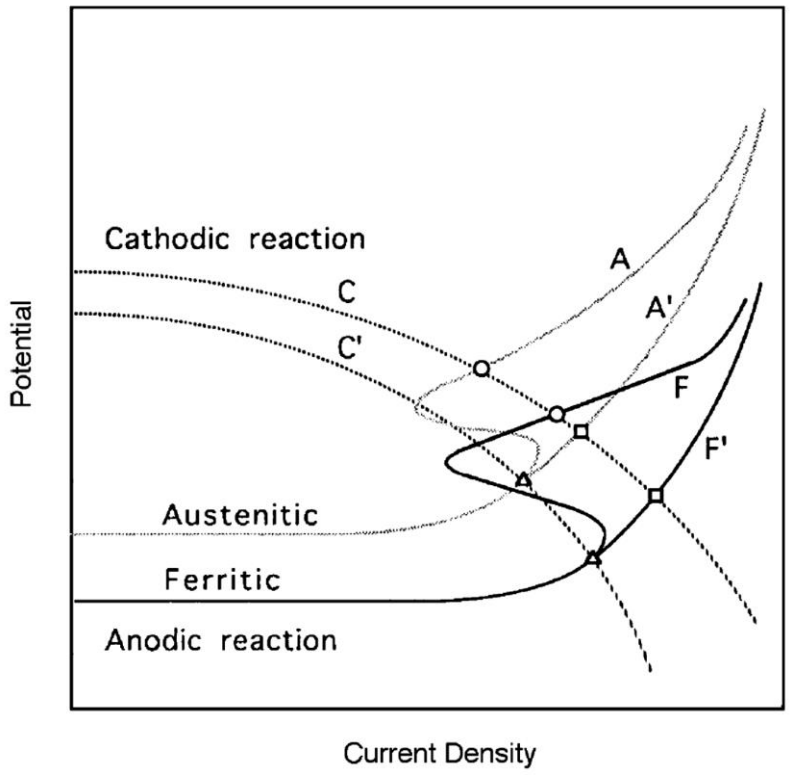

Figure 5-8: Schematic anodic and cathodic polarisation curves for low-alloyed steels[9]

Δ	Crevice corrosion: depassivation type
□	Pitting corrosion
○	Crevice corrosion: pitting type

T.Ujiro et al. [9] also investigated the relationship between the type of corrosion and the E_{corr}. It was observed that ferritic alloys which corroded by depassivation had lower E_{corr} than the ones that corroded by pitting. Crevice corrosion by depassivation is related to E_{corr} because it involves an intensive metal dissolution at lower potentials. Similar to the current project, the E_{corr} values obtained from 1 wt.% NaCl were measured to be higher than the ones obtained from 3.56 wt.%

NaCl. This means that 1 wt.% NaCl did not contain chloride concentration required to reach critical crevice solution. Hence, instead of depassivation, pitting corrosion was observed.

According to the schematic presentation shown above, the solution in the pit is more aggressive once pitting has started as shown by an increase of current density. In some alloys, once pitting initiates, propagation is faster and it becomes difficult for an alloy to repassivate as shown for Hercules™ B. However, the onset of pitting was delayed for Hercules™ B, meaning that it had more extended passive region than the other test alloys. Alloys that delay the onset of corrosion are more desirable because crevice corrosion occurs at lower potentials and can be more detrimental than pitting, which occurs at higher potentials.[9] The graph comparing the difference in measured E_{pit} from different NaCl solutions is shown in Figure 5-9.

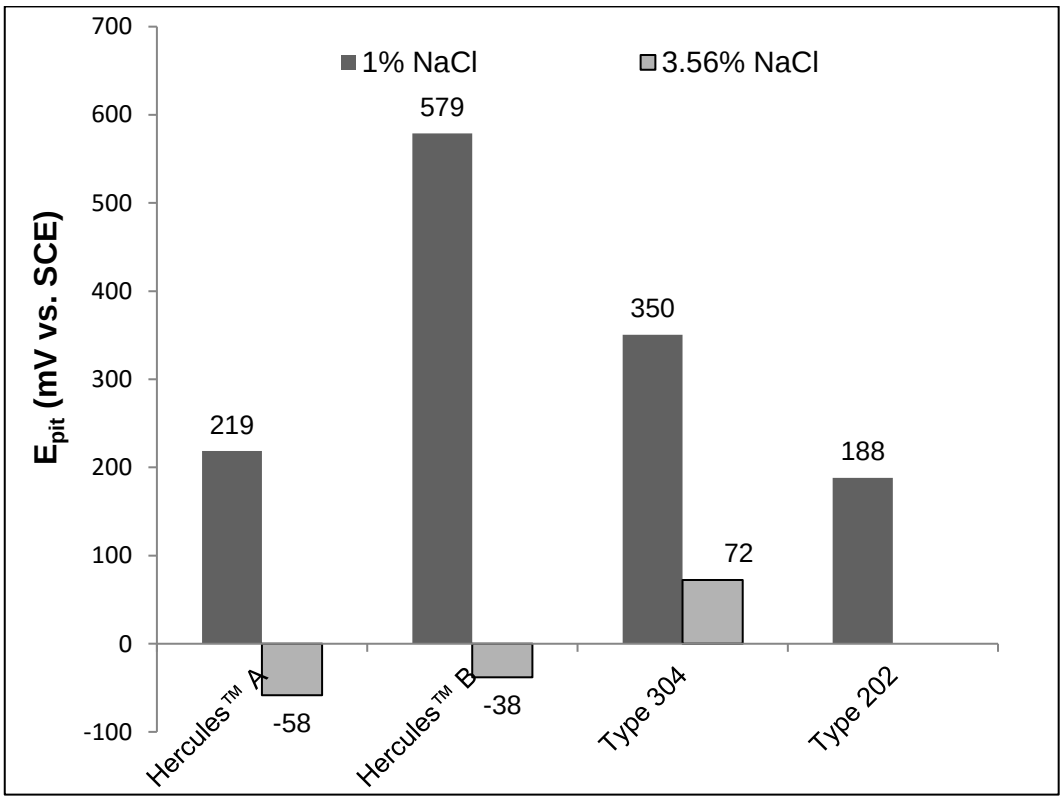

Figure 5-9: E_{pit} at different NaCl concentrations

Table 5-5: Critical potentials for crevice corrosion in 1 wt.% NaCl

Sample Identity	Area (cm^2)	i_{corr} (mA/cm^2)	E_{corr} (mV.SCE)	E_{pit} (mV.SCE)	E_{prot} (mV.SCE)	Corrosion rate (mm/y)
Hercules™ A						
1	0,79	3,88E-05	-161	240	_	4.3E-04
2	0,79	1,29E-04	-249	197	_	1.4E-03
Average		**8,39E-05**	**-205**	**219**	**_**	**9.2E-04**
Hercules™ B						
1	0,79	5,04E-05	-146	578	_	5.5E-04
2	0,79	3,21E-05	-146	580	_	3.5E-04
Average		**4,12E-05**	**-146**	**579**	**_**	**4.5E-04**
Type 304						
1	0,79	4,26E-05	-136	377	92	4.7E-04
2	0,79	2,74E-05	-97	324	6	3.0E-04
Average		**3,50E-05**	**-117**	**351**	**49**	**3.9E-04**
Type 202						
1	0,79	4,72E-05	-139	234	_	5.2E-04
2	0,79	3,66E-05	-121	142	_	4.0E-04
Average		**4,19E-05**	**-130**	**188**	**_**	**4.6E-04**

5.4 Active-passive behaviour in 5 wt.% H_2SO_4 solution

According to Outokumpu [11], an alloy is considered to be resistant to uniform corrosion in a particular environment if the corrosion rate does not exceed 0.1 mm/y. All test alloys demonstrated resistance in 5 wt.% H_2SO_4 as shown by pitting scans in Figure 5-10. The corrosion rate of test alloys due to uniform corrosion is summarised in Table 5-6.

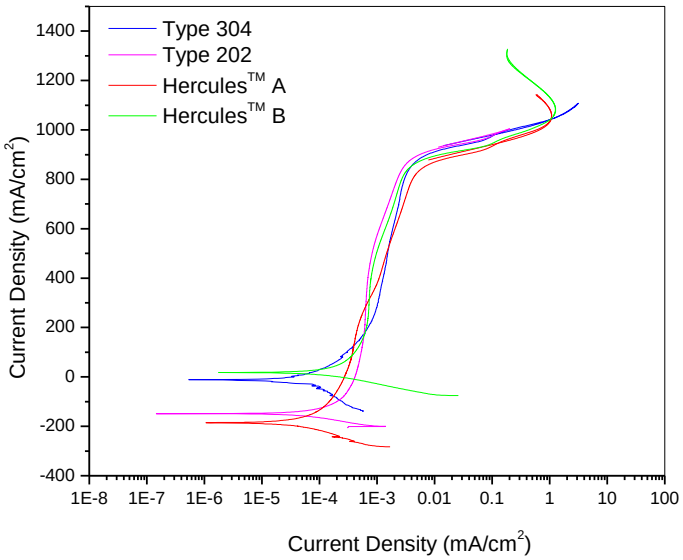

Figure 5-10: Cyclic polarisation scans for test alloys in 5% H_2SO_4

The passivity behaviour of each alloy was studied from the shape of the cyclic polarisation curve and the illustration in Figure 4-5 was used for interpretation. Figure 4-5 shows the possible schematic active-passive behaviour of alloys in a particular solution. All alloys displayed the condition shown by Case 3. Case 3 illustrates a behaviour of an alloy that has an ability to passivate spontaneously in a reducing environment such as 5 wt.% H_2SO_4.

The exception was observed in pitting scans for Hercules™ A and Hercules™ B as shown in Figure 5-11. One of duplicate samples of Hercules™ B showed the behaviour represented by Case 1. This means that Hercules™ B is capable of either spontaneously passivating or corroding rapidly. Alloys that show a behaviour similar to Hercules™ B can be used in environments that are monitored such that the cathodic reaction curves do not intersect the anodic curves at an active region. If the environment is not monitored, then an alloy will corrode at lower potentials. The longer it takes for an alloy to passivate, the higher the corrosion rates obtained, therefore, alloys that have the anodic current peak are not desirable.

Hercules™ A had a number of scans that displayed a behaviour represented by Case 2. Three E_{corr} values were measured for Hercules™ A. The behaviour that was displayed by Hercules™ A meant that its passivity is unstable and unpredictable. That type of an alloy is not desirable because it implies that an alloy will either corrode aggressively or passivate in a given environment. A minor disruption of the passive layer results in an alloy transferring from passive-active and hence unexpected metal loss.

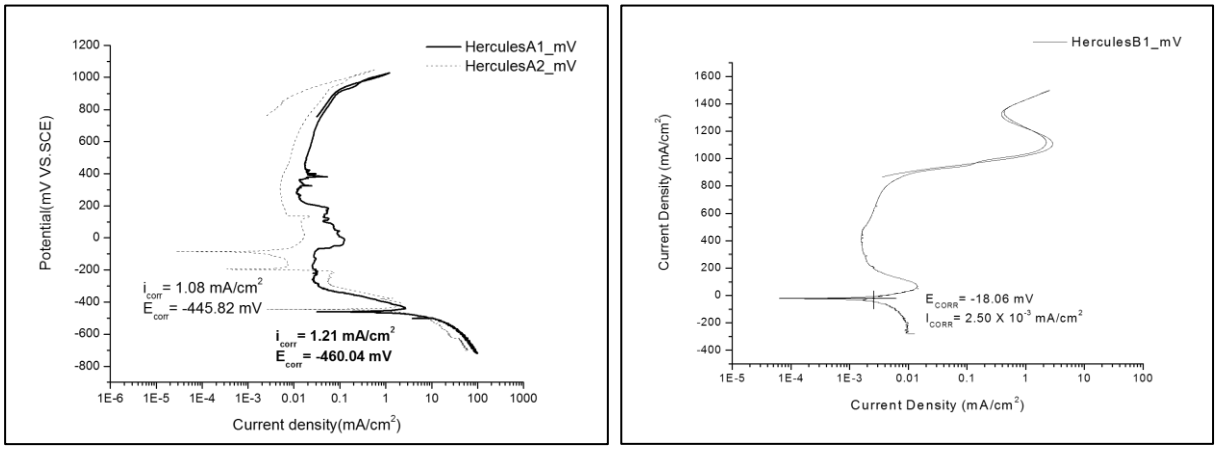

Figure 5-11: Hercules™ A and Hercules™ B behaviour in 5 wt.% H_2SO_4

The behaviour of Hercules™ A is similar to the observations that were made by A. Muwila [35] as shown in Figure 5-12. The scans also show that Hercules™ A had three different E_{corr} values when it was tested in deaerated 5 wt.% H_2SO_4. This is also in agreement with the work that was done by R. Paton et al. [1]. On the report it was shown that Hercules™ A had a tendency to undergo transformation from passive-active state in deaerated 5 wt.% H_2SO_4. R. Paton et al. [1] also calculated the corrosion rate for Hercules™ A to be 35 mm/y. This proves that Hercules™ A does not exhibit stable passivity characteristics.[35]

Furthermore, the absence of a hysteresis loop is an indication that tested alloys did not undergo any type of localised corrosion even though an artificial crevice was introduced in each sample. The presence of an artificial crevice creates passivation current (i_{pass}) that is higher than i_{corr}. However, the conditions were not enough to the activate sample surface for formation of pits or cause crevice corrosion since the test solution did not contain chlorides.[54]

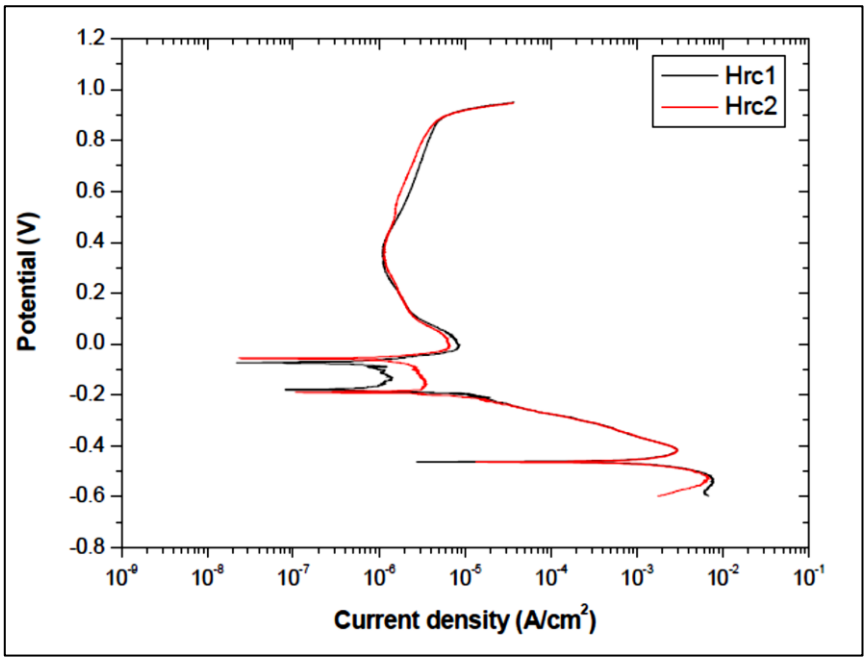

Figure 5-12: Passive-active behaviour in of Hercules™ A[35]

The corrosion rate of test alloys in 5 wt.% H_2SO_4 was calculated to be higher in the immersion tests. The mass loss that was measured is summarised in Table 5-7. The corrosion rate of Hercules™ A was measured to be 1.9 mm/y. Hercules™ B, Type 304 and Type 202 had the corrosion rate that was less than 0.1 mm/y, with Type 304 having the lowest. The immersion test results were therefore consistent with the corrosion rates that were calculated from cyclic polarisation tests since Type 304 had lower corrosion rates than Hercules™ B. These results were contradictory to corrosion rates that were obtained at Mintek as outlined in the Hercules™ data sheet [15], where Hercules™ B was observed to have lower corrosion rate than Type 304.

Furthermore, the immersion tests results obtained in the current project are different from what A. Muwila [35] and A. Muwila et al. [3] obtained. The corrosion rate of Hercules™ A was measured to be 29 mm/y, 0.03 mm/y for Type 304 and 0.001 mm/y for Hercules™ B alloy. In the current project samples were immersed for 10 days with no interval removal, whilst on previous work [35] they were immersed for 14 days with periodical removal. Periodic removal of Hercules™ A may have resulted in the passive film being disrupted and hence higher corrosion rates were obtained by A. Muwila, given that Hercules™ A has an unpredictable active-passive behaviour nature.

It is often assumed that corrosion rate of stainless steels is linear with the function of time, but this is sometimes not true for some stainless steels immersed for a longer time. This was observed by A. Muwila [35] for Hercules™ A, Hercules™ B, Type 304 and Type 201. Hercules™ A was observed to react aggressively for the first 24 hours at a higher corrosion rate

but decreased as a period of 14 days progressed. Type 201 showed low corrosion rate in the beginning and then went up after a few days and went down towards the end of the test, as shown in Figure 5-13. Hercules™ B did not react aggressively in the beginning and had low corrosion rates throughout the entire exposure time.[35]

Based on observations that were made in the current project, the solution in which the Hercules™ A was immersed had a dark bluish deposit after a few hours of immersion and the reaction was more aggressive than Hercules™ B. The solution with Hercules™ B, Type 304 and Type 202 did not show any change of colour and the reaction was less aggressive. Therefore, the corrosion rates for Hercules™ B, Type 304 and Type 202 were comparable.

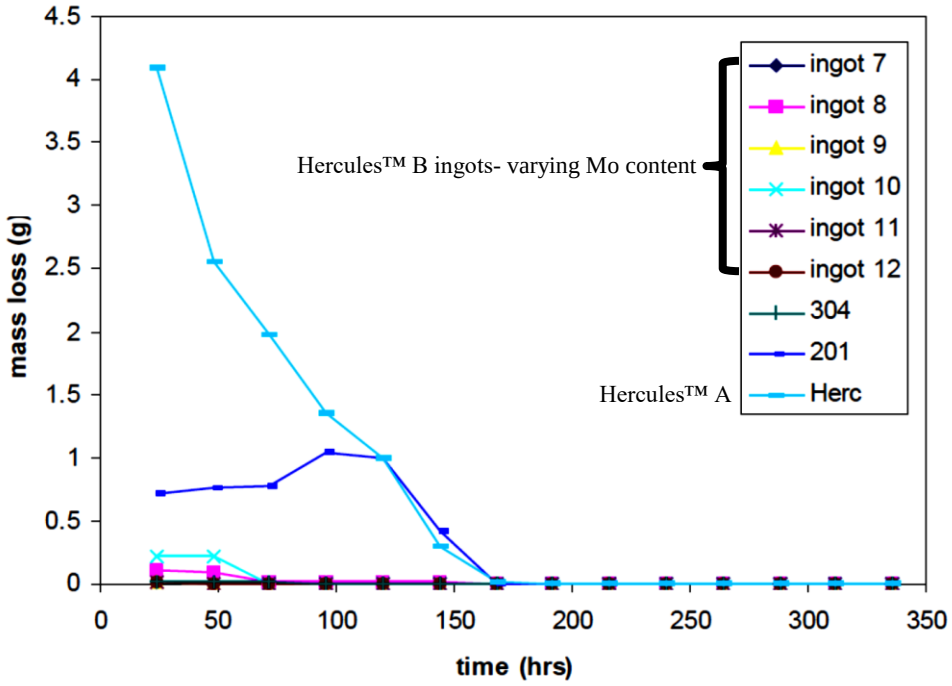

Figure 5-13: Mass loss vs. time graph for alloys immersed in 5% H_2SO_4[35]

It has been established that passive films formed by stainless steels may be broken down in a prolonged exposure period and hence higher corrosion rates are obtained in immersion tests than electrochemical tests. Although mass loss is negligible after a certain period it can still add up to the final mass loss measurement. Electrochemical tests took less than 4 hours to obtain a complete scan. Therefore, the corrosion rate measured is less than that obtained from immersion tests.[52]

Table 5-6: Corrosion rates in 5 wt.% H_2SO_4 from polarisation curves

Sample Identity	Area (cm^2)	i_{corr} (mA/cm^2)	E_{corr} (mV.SCE)	Corrosion rate (mm/y)
Hercules™ A				
1	0.79	6.47E-05	110	7.1E-04
2	0.79	1.30E-04	-186	1.4E-03
Average		**9.74E-05**	**-38**	**1.1E-03**
Hercules™ B				
1	0.79	2.50E-03	-18	2.7E-02
2	0.79	5.23E-04	14	5.8E-03
Average		**1.51E-03**	**-2**	**1.7E-02**
Type 304				
1	0.79	1.25E-04	-11	1.3E-03
2	0.79	2.10E-04	-41	2.3E-03
Average		**1.68E-04**	**-26**	**1.8E-03**
Type 202				
1	0.79	2.78E-04	-155	3.1E-03
2	0.79	6.12E-04	-49	6.7E-03
Average		**4.45E-04**	**-102**	**4.9E-03**

Table 5-7: Mass loss measurements due to uniform corrosion from immersion tests

Sample Identity	Initial mass(g)	Final mass(g)	Mass loss(g)	Area (cm^2)	Corrosion rate(mm/y)
Hercules™ A					
Sample 1	97.6500	96.9360	0.7140	12.5	1.9
Sample 2	97.6650	96.9770	0.6880	12.5	1.8
Average	**97.6575**	**96.9565**	**0.7010**	**12.5**	**1.9**
Hercules™ B					
Sample 1	77.9580	77.9440	0.0140	11.5	3.7E-02
Sample 2	78.1000	78.0840	0.0160	11.5	4.3E-02
Average	**78.0290**	**78.0140**	**0.0150**	**11.5**	**4.0E-02**
Type 304					
Sample 1	82.4032	82.4022	0.0010	12.5	2.7E-03
Sample 2	75.3328	75.3313	0.0015	12.5	4.0E-03
Average	**78.8680**	**78.8668**	**0.0013**	**12.5**	**3.3E-03**

5.5 Pitting corrosion resistance in 6 wt.% $FeCl_3.6H_2O$

The mass loss of test alloys was measured and the corrosion rate due to pitting was calculated. **Error! Reference source not found.** shows the mass loss measurements and corrosion rate for each alloy. There was no significant difference in the measured mass loss of all test alloys. This behaviour is similar to the results that were obtained by B.S Bergstrom et al. [14] when Type 201 and Type 304 were tested in 6 wt.% $FeCl_3$ for 72 hours. Both alloys showed a corrosion rate of 0.0228 g/cm^2 and similar pit depth of 0.0762 mm.[14]

The 6 wt.% $FeCl_3.6H_2O$ solution is generally used as a test for localised corrosion for accelerated tests. Therefore, test alloys were immersed in the solution for 72 hours as suggested in the ASTM G84 standard. This test solution is used to simulate a very rough composition of environment within a localised corrosion site in a stainless steel. However, 6 wt.% $FeCl_3.6H_2O$ solution can be very aggressive for low-alloyed steels such as Type 304 and Type 202. This was proven by the tests that were carried out by T. Ujiro et al. [9] in 6 wt.% $FeCl_3.6H_2O$. Alloys with higher Mo and Cr contents (above 26% Cr and 4% Mo) showed more corrosion resistance than the one with the composition similar to that of Type 304.[9]

Furthermore, 6 wt.% $FeCl_3.6H_2O$ serves as a chemical potentiostat by forming the Fe^{3+}/Fe^{2+} redox couple which has an approximate potential of 450 mV in an acidic and high chloride concentration. For the current experiment, the solution was not acidified with HCl, but the pH was still measured to be 1.44, which is acidic enough to create a large current without a need to polarise the specimen as in the electrochemical tests [52]. From the electrochemical tests, it was already established that chloride concentration from neutral 1 wt.% NaCl was enough to cause an E_{pit} that is less than 450 mV. The 6 wt.% $FeCl_3.6H_2O$ solution has higher chloride concentration than NaCl, hence Hercules™, Type 304 and Type 202 corroded aggressively.

Furthermore, the high potential of the test solution almost guarantees that the pitting potential of each alloy was exceeded. The acidic nature of 6 wt.% $FeCl_3.6H_2O$ also inhibits repassivation and lowers passive film strength by cathodic reactions that occur on the surface of the sample via Fe^{3+}/Fe^{2+} ions.[52]

Surface examination was carried out by taking micrographs of corroded samples using a light microscope at 10× magnification as shown in Figure 5-14(Scale bar = 1mm). The individual pit morphology was evaluated. Hercules™ A had irregular shaped pits which are wide, whilst Hercules™ B had wide and round shallow pits. This means that pitting propagated quicker in Hercules™ A than in Hercules™ B.

Table 5-8: Mass loss measurements due to pitting corrosion

Sample Identity	Initial mass(g)	Final mass(g)	Mass loss(g)	Area (cm^2)	Corrosion rate(mm/y)
Hercules™ A					
Sample 1	96.6787	95.7471	0.9316	12.5	11.5
Sample 2	92.1524	91.1757	0.9767	12.5	12.1
Average	**94.4156**	**93.4614**	**0.95415**	**12.5**	**11.8**
Hercules™ B					
Sample 1	103.1339	102.1123	1.0216	12.5	12.7
Sample 2	101.4412	100.4264	1.0148	12.5	12.6
Average	**102.2876**	**101.2694**	**1.0182**	**12.5**	**12.6**
Type 304					
Sample 1	34.2966	33.1688	1.1278	12.5	14.0
Sample 2	35.1042	33.9650	1.1392	12.5	14.1
Average	**34.7004**	**33.5669**	**1.1335**	**12.5**	**14.1**
Type 202					
Sample 1	45.7252	44.2627	1.4625	12.5	18.1
Sample 2	43.4613	41.9390	1.5223	12.5	18.9
Average	**44.5933**	**43.1009**	**1.4924**	**12.5**	**18.5**

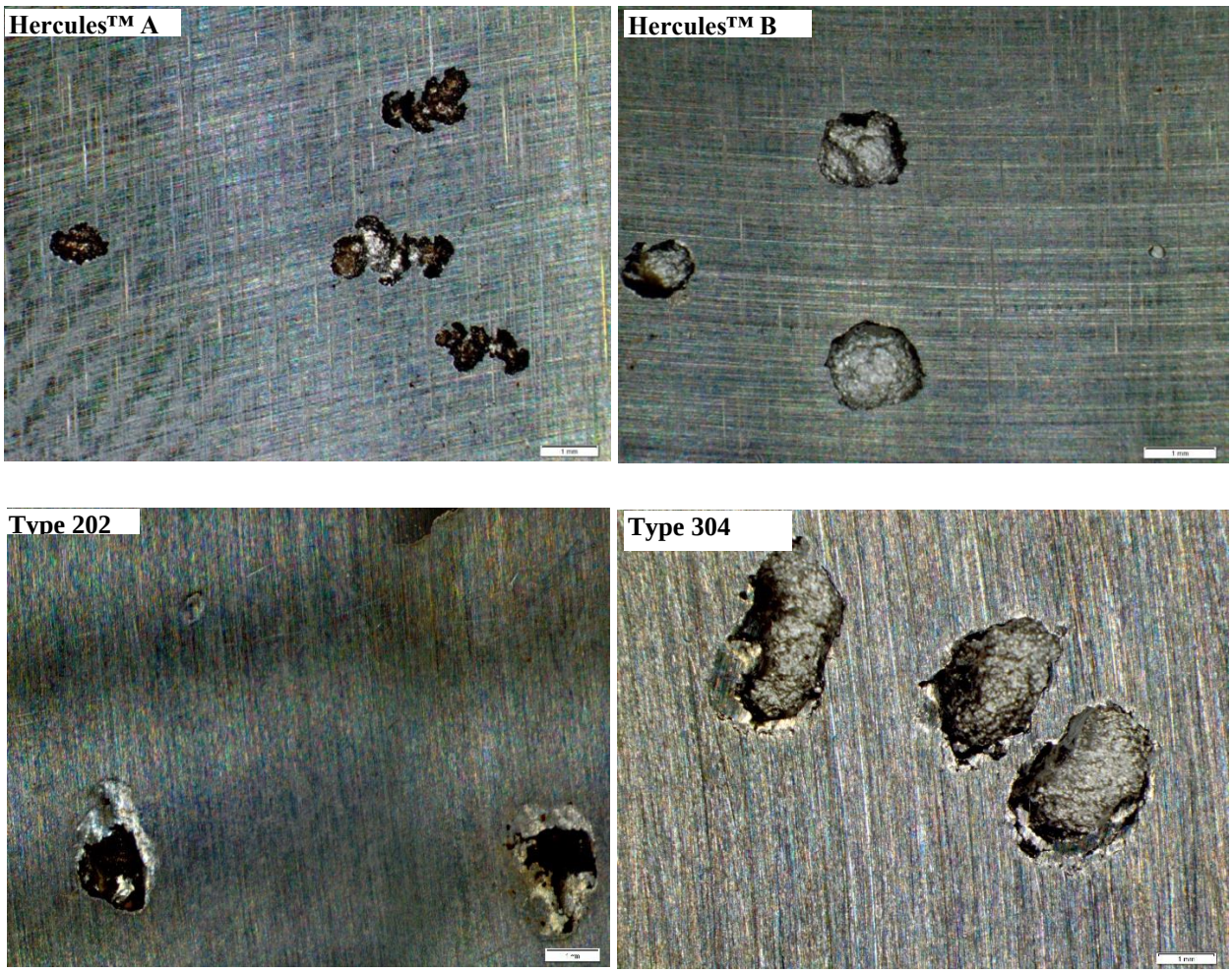

Figure 5-14: Test alloys after immersion in 6 wt.% $FeCl_3.H_2O$

The extent of pitting was evaluated using the SDX510 Light Microscope(10× magnification) at Mintek. The opening width and depth of pits for samples that showed maximum pitting were measured and the values are shown in Table 5-9. The width was measured from the top surface of each pit.

Table 5-9: The extent of pitting for test alloys after 72 hours immersion in $FeCl_3.6H_2O$

	Top opening of the pit		
Sample Identity	**Width(µm)**	**Length(µm)**	**Depth(µm)**
Hercules™ A	1563	1607	129
Hercules™ B	1259	1289	275
Type 202	1676	1684	305
Type 304	1388	1394	374

Figure 5-15 shows the representative pit that was observed in Hercules™ A after 72 hours of immersion in $FeCl_3.6H_20$. Although pit density of all test alloys was almost similar, Hercules™ A showed severe pitting because of larger pit opening.

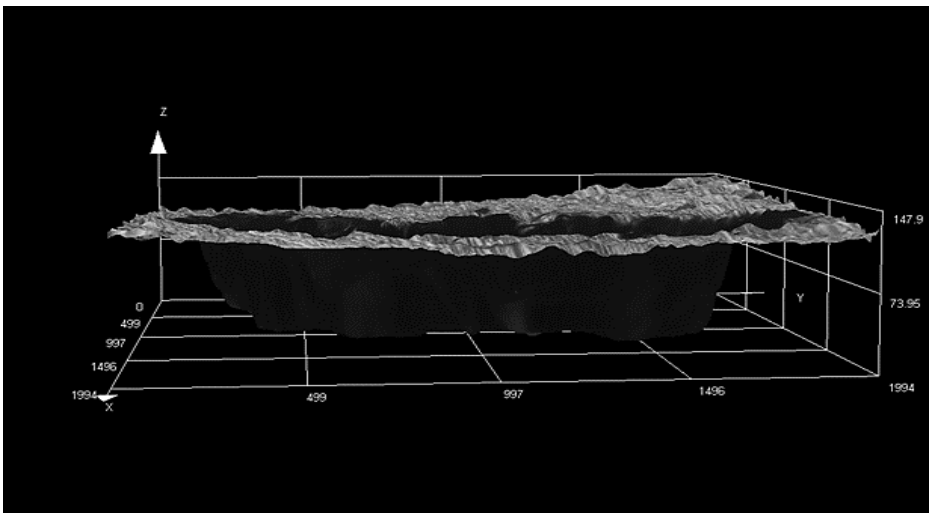

Figure 5-15: Pitting extent of Hercules™ A in $FeCl_3.H_2O$

Figure 5-16 shows that a the size of pit opening that was observed in Hercules™ B is smaller than that of Hercules™ B. However, the pit depth for Hercules™ B was measured to be higher than that of Hercules™ A. Therefore, the corrosion of Hercules™ A was more uniform but deeper, which can be more associated with depassivation that is observed in samples that undergo crevice corrosion. This further proves that in comparison to other alloys, Hercules™ A is not suitable for use in aggressive chloride environments represented by $FeCl_3.H_2O$ in the current project.

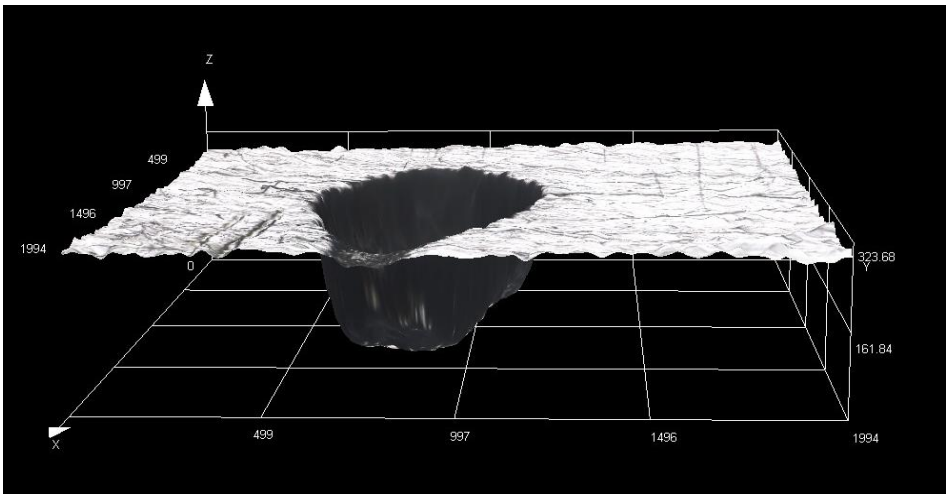

Figure 5-16: Pitting extent of Hercules™ B in $FeCl_3.H_2O$

Figure 5-17 and Figure 5-18 show the extent of pitting that was observed for Type 202 and Type 304, respectively. Overall, the whole evaluation proves that $FeCl_3.H_2O$ is an aggressive solution for testing such stainless steel alloys. Even addition of Mo for Hercules™ B is not enough for it to be used for applications in aggressive environments, however it can be used as an alternative for Type 304 applications.

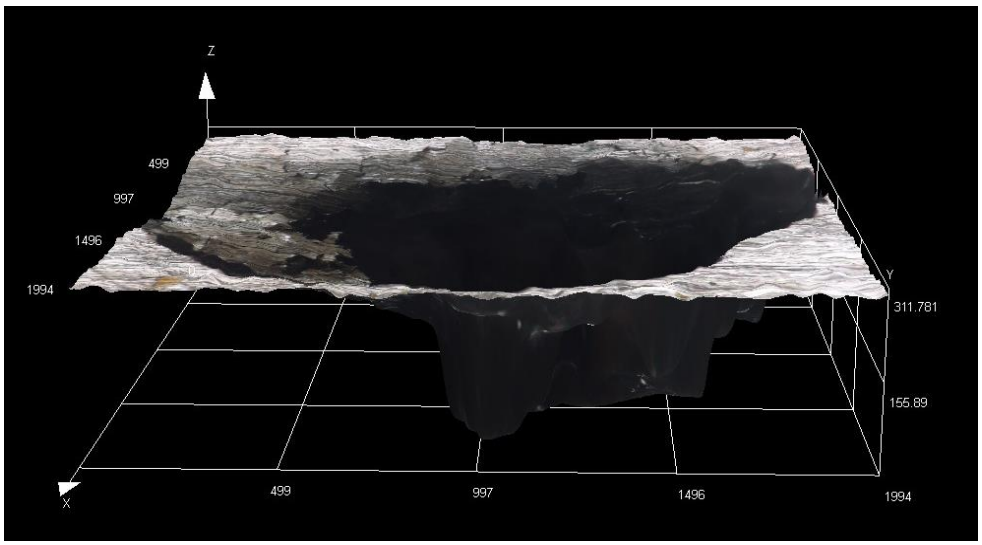

Figure 5-17: Pitting extent of Type 202 in $FeCl_3.H_2O$

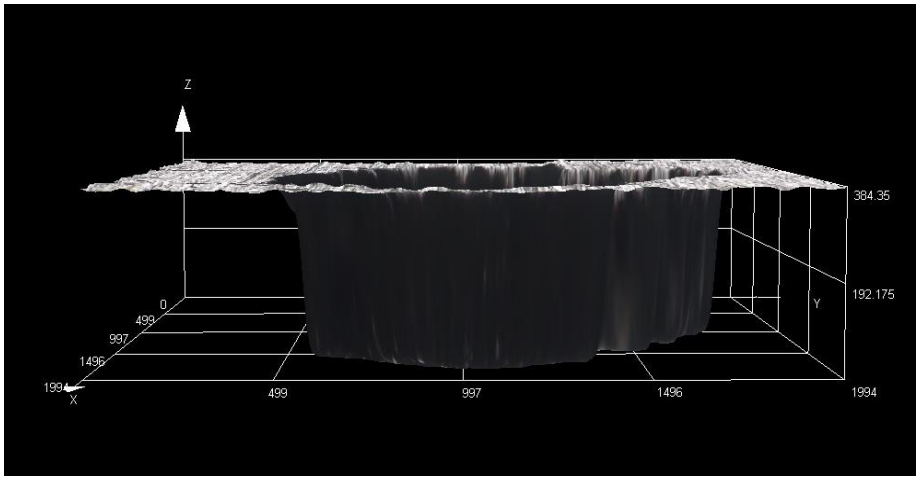

Figure 5-18: Pitting extent of Type 304 in $FeCl_3.H_2O$

The pit opening shapes of pits were interpreted using Figure 5-19Error! Reference source not found. from ASTM G46 standard.[72] Micrographs showed that Hercules™ B resembled the pit shape (b) when viewed in the cross section, while Hercules™ A resembled pit shape (c). This means that pitting was severe for all test alloys and they can not be used for applications where corrosion of concern.

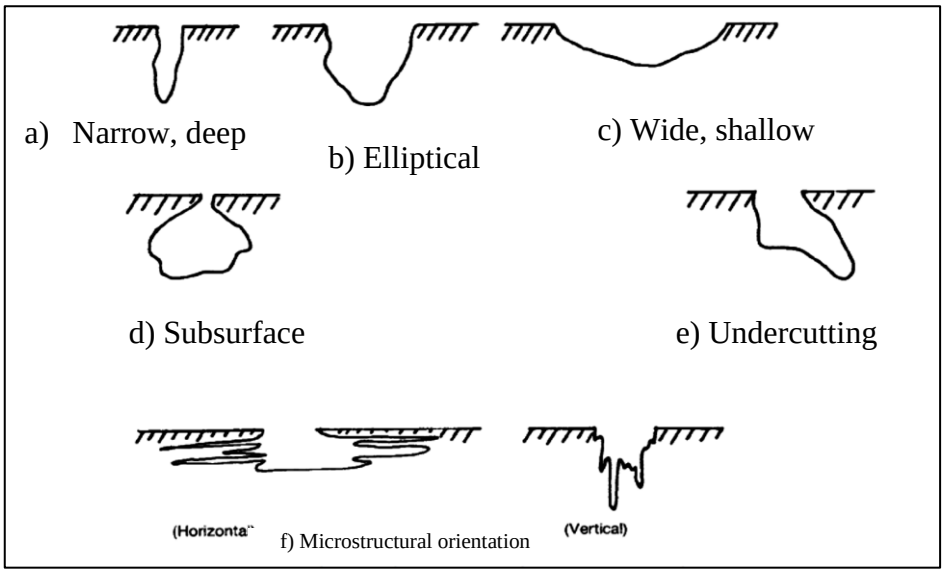

Figure 5-19: various shapes of pits in cross-section view[72]

5.6 Crevice corrosion resistance in 6 wt.% $FeCl_3.6H_2O$

The results that were obtained from the crevice corrosion test of test alloys are shown in Table 5-11. Similar to the pitting corrosion test, there was no significant difference in mass loss of test alloys. Corrosion rate in the presence of a crevice was measured to be slightly higher than corrosion rate from pitting corrosion tests.

According to Outokumpu regulations, the acceptable mass loss due to crevice corrosion is ≤ 0.038 mg/cm^2 for any alloy. The mass loss ≥ 0.07 g/cm^2 was measured for test alloys in the current project, meaning that the solution was sufficiently aggressive to cause a larger mass loss for test alloys. On the other hand, B.S Bergstrom et al. [14] also noted that mass loss for Type 304 and Type 201 was 0.0211 mg/cm^2 for both alloys, which substantiate the assumption that 6 wt.% $FeCl_3.6H_2O$ was aggressive for testing crevice corrosion for low-alloyed stainless steels.

T. Ujiro et al. [9], observed that high-alloyed stainless steels such as 26 wt.% Cr-4 wt.% Mo had superior resistance to crevice corrosion compared to low-alloyed stainless steels. In addition, J. Dundas et al. [50] tested low and high-alloyed stainless steels in 10 wt.% $FeCl_3$. High alloyed steels showed resistance in this solution; whilst for low-alloyed stainless steels (including Type 304) crevice corrosion was observed. Similar to the current project, severe crevice corrosion was observed in Hercules™ A, Hercules™ B, Type 304 and Type 202.

The corrosion rate calculated is based on the whole area of the coupon, while the affected region is the one beneath the crevice. It could therefore be misleading to use the corrosion rate to rank the alloys where crevice corrosion is concerned. Furthermore, mass loss measurements include corrosion at the edges which is supposed to be ignored because it is not due crevices.[11]

The picture of corroded samples was taken and is shown in Figure 5-20. The images of corroded samples were further visually analysed in order to evaluate the extent of damage.

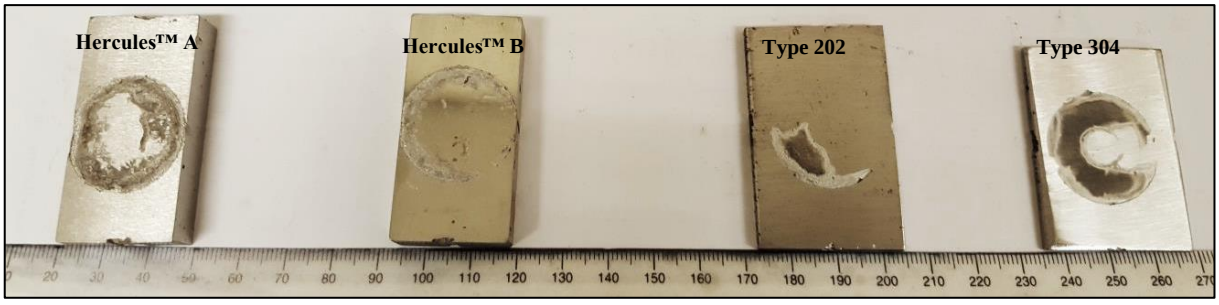

Figure 5-20: Crevice corrosion test samples after immersion in 6 wt.% $FeCl_3.6H_2O$

Four different corrosion locations were observed in each coupon. These locations are; both face sides of the coupon where TFE-fluorocarbon blocks were placed and the two edges where the

rubber bands were in contact with the coupons. The corrosion rate calculated was therefore based on all four crevice locations. Type 202 had the highest corrosion rate of all test alloys followed by Hercules™ B, while Type 304 and Hercules™ A had almost similar corrosion rates.

Corroded samples were further analysed using the crevice corrosion damage factor (CCDF) method that was developed by D.R Johns et al. [21]. The CCDF summarises the extent of damage caused by crevice corrosion by summing the percentage of penetration, circumference affected and depth of the pit. The proportion of circumference affected was rated on a scale of 1-3, where 1: >25%, 2: 25%-75% and 3: >75%. The depth of metal loss was rated on a scale of 1-4, where 1-shallow etching, 2-discernible depth, 3-significant metal dissolution and 4- severe metal loss (> 0.5mm)[21].Using Figure 5-20 above, Table 5-10 shows estimated CCDF values calculated from the area that was occluded by TFE-fluorocarbon blocks

Table 5-10: CCDF values for test alloys

Alloy	circumference affected	Depth of metal loss	**CCDF (Penetration circumference + depth of attack)**
Hercules™ A	3	2	**5**
Hercules™ B	2	1	**3**
Type 202	1	4	**5**
Type 304	2	2	**4**

Hercules™ A and Type 202 were measured to have similar CCDF values, which is in agreement with their corrosion rates. This means that although the proportion of circumference affected in Hercules™ A was 100%, this does not mean the depth of attack was more severe than that of Type 202. Although the circumference affected in Hercules™ B was also 75%, the depth of attack was not severe, hence the lower CCDF than other tested alloys. The CCDF of Hercules™ B and Type 304 were comparable, with Type 304 being slightly higher because of deeper metal loss.

Table 5-11: Mass loss measurements due to crevice corrosion

Sample identity	Initial mass(g)	Final mass(g)	Mass loss(g)	Area (cm^2)	Corrosion rate(mm/y)	corrosion rate (g/cm^2)
Hercules™ A						
Sample 1	96.5488	95.5256	1.0232	12.5	12.7	0.1
Sample 2	97.2153	96.2334	0.9819	12.5	12.2	0.1
Average	**96.8821**	**95.8795**	**1.0026**	**12.5**	**12.4**	**0.1**
Hercules™ B						
Sample 1	103.8139	102.8085	1.0054	12.5	12.5	0.1
Sample 2	102.4521	101.0701	1.3820	12.5	17.1	0.1
Average	**103.1330**	**101.9393**	**1.1937**	**12.5**	**14.8**	**0.1**
Type 304						
Sample 1	32.8465	31.7930	1.0535	14.4	13.1	0.1
Sample 2	32.4981	31.4702	1.0279	14.4	12.7	0.1
Average	**32.6723**	**31.6316**	**1.0407**	**14.4**	**12.9**	**0.1**
Type 202						
Sample 1	42.8305	41.4437	1.3868	16.5	18.0	0.1
Sample 2	41.7555	40.4060	1.3495	16.5	16.7	0.1
Average	**42.2930**	**40.9249**	**1.3682**	**16.5**	**17.0**	**0.1**

5.7 Critical pitting temperature

5.7.1 Mass loss at different temperatures

The mass loss measurements for test alloys at different temperatures are presented in Table 5-12. It was observed that mass loss varied with temperature increase for Hercules™ A, Type 202 and Hercules™ B. A constant increase of mass loss due to pitting corrosion with an increase of temperature was observed in Type 304. Hercules™ B and Type 304 showed comparable mass loss almost at all testing temperatures, except at 30℃. The variation of mass loss at different temperatures indicated that mass loss is not directly affected by temperature.

Table 5-12: Mass loss at different temperatures

Temperature (℃)	**25**	**30**	**40**	**50**
Alloy	**Mass loss (g)**			
Hercules™ A	0.171	0.209	0.487	0.359
Hercules™ B	0.160	0.1075	0.185	0.193
Type 202	0.149	0.152	0.232	0.143
Type 304	0.133	0.154	0.177	0.211

Other researchers [45]–[48] have discovered that as temperature is increased, E_{pit} become less dependent on temperature because of factors such as the chemistry of the passive layer and the concentration of the pit solution. N.J Laycock et al. [44] evaluated the dependence of E_{pit} on temperature and observed that it gradually decreased with temperature but, in some instances E_{pit} varied as temperature was increased.

N.J Laycock et. al [44], [45] described the reduced dependence of E_{pit} to temperature by considering solution resistance inside the pits. As the temperature is increased, the concentration of saturated solution (C_{sat}) within the pit is changed according to the alloy composition and the electrolyte. The change of C_{sat} affects the resistivity of the pit solution (R_{int}) and the diffusion of corrosion species and hence a variation in E_{pit} can be observed.

This therefore justifies the variation in measured mass loss with temperature increase that was observed in the current project. The measured mass loss was also consistent with the observed pit density. Hercules™ B had lower pit density than Hercules™ A, Type 304 and Type 202 in

correspondence with lower mass loss at all testing temperatures. At 50℃ Hercules™ A mass loss was measured to be higher than other test alloys and therefore the higher pit density was observed. The variation in mass loss as temperature was increased indicated that the rate at which pitting was occurring decreased with temperature increase.

5.7.2 Pit density at different temperatures

Micrographs of corroded samples that were taken in order to determine the morphology and density of pits are shown in Figure 5-21(scale bar = 1mm). Pits with larger diameter were observed in Hercules™ A compared to Hercules™ B. Pitting was observed for all after immersion of test samples at 25℃, but more localised pitting was observed for Hercules™ B and Type 304. Hercules™ B pit density increased with temperature up to the maximum testing temperature at 50℃, but pits were more localised and of smaller diameter. Therefore, in a given chloride environment Hercules™ A will experience pitting corrosion quicker than other tested alloys because severe pits were observed at room temperature.

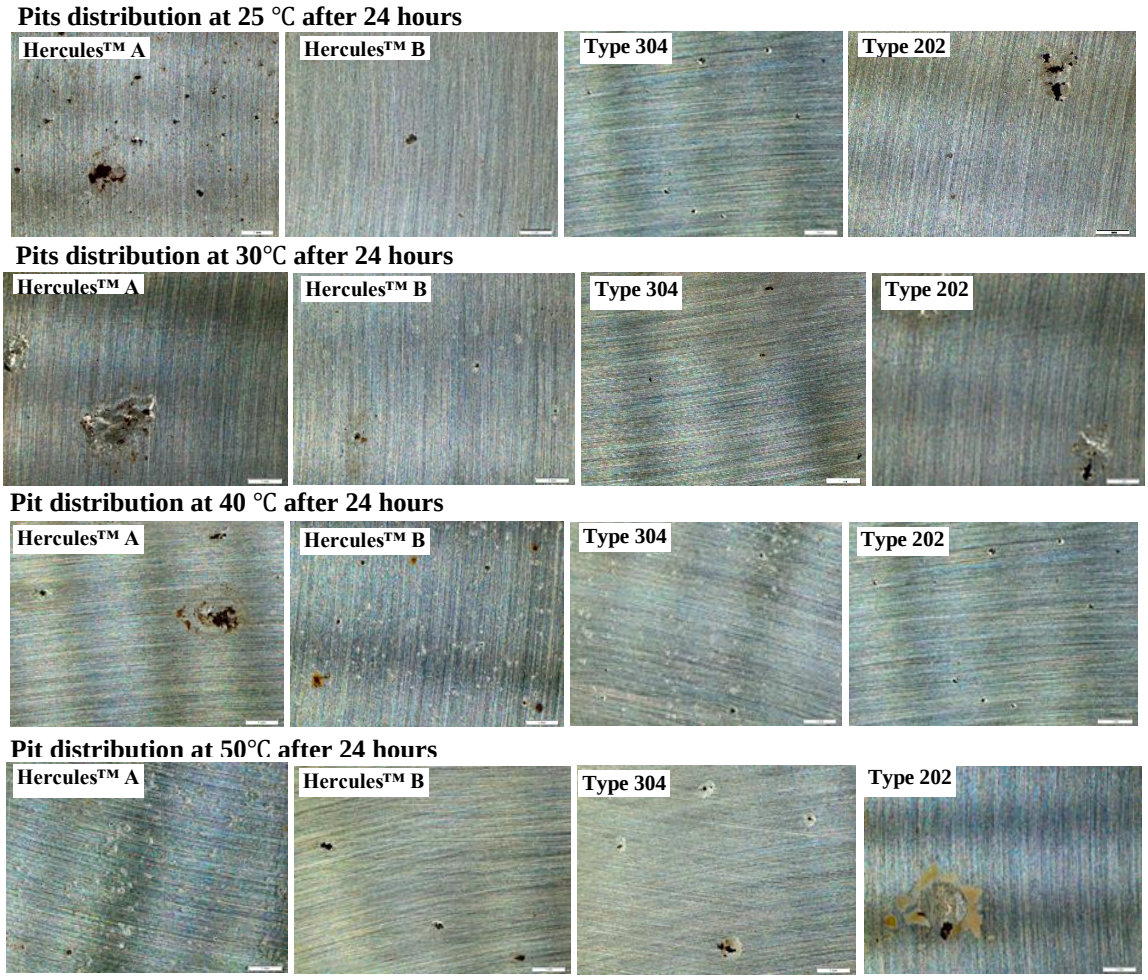

Figure 5-21: Pitting of test alloys at different temperatures

Chapter 6: Conclusions

The aim of the project was to evaluate the corrosion behaviour of Hercules™ and suggest whether or not it can be used as an alternative to some of Type 304 applications (including rebar and fastener industry). The cyclic polarisation technique was used to evaluate pitting and crevice corrosion resistance of Hercules™ against the already accepted Type 304 and Type 202. Immersion tests were also conducted in order to validate the results that were obtained from the cyclic polarisation technique. Based on results and discussions, the following conclusions were therefore drawn regarding Hercules™ alloy:

6.1 Hercules™ B and Type 304 have comparable pitting behaviour

The results obtained from crevice-free tests using 3.56 wt.% NaCl indicated that Hercules™ B has better pitting resistance than Type 304 and Hercules™ A. The $|E_{pit}-E_{pro}|$ value for Type 304 showed that although initiation of pitting is delayed, repassivation is also difficult to achieve. Hercules™ B is desirable because of its ability to show repassivation quicker than Type 304 and Hercules™ A.

Immersion tests in 6 wt.% $FeCl_3.6H_2O$ also proved that Hercules™ B has better pitting resistance compared to Hercules™ A, Type 304 and Type 202. Although there was no significant difference in mass loss and corrosion rate of test alloys, the visual examination of corroded samples showed that Hercules™ B had a smaller sized pitting than other test alloys.

The CPT tests showed that all alloys started pitting after 24 hours of immersion at 25 ℃. Therefore, although a few localised pits were formed at 25℃ for Hercules™ B, pit density was comparable to Type 304 and Type 202 at 50℃. This means that the pitting behaviour of Hercules™ B is similar to that of Type 304. Furthermore, it means that all test alloys have CPT values that are less than 25℃. This lowers the chances for Hercules™ alloy to be used in more corrosive chloride environments.

6.2 Crevice corrosion inhibited in 1 wt.% NaCl

Poor resistance to crevice corrosion was observed for Hercules™ A and Hercules™ B in 3.56 wt.% NaCl. In the presence of an artificial crevice former, Hercules™ alloys corroded rapidly at lower potentials in the same way as Type 304 and Type 202. Hercules™ B showed improved resistance to crevice corrosion compared to other test alloys when the concentration of NaCl solution was reduced to 1 wt.%.

Therefore, Hercules™ B can be safely used to manufacture products for applications in environments containing <1 wt.% chloride at room temperature, even when there are potential crevices.

Furthermore, the crevice corrosion test in 6 wt.% $FeCl_3.6H_2O$ showed that Hercules™ B is more resistant to crevice corrosion. Visual examination and calculation of CCDF of test alloys showed that all test alloys experienced crevice corrosion, but the metal penetration in Hercules™ B was shallower than other tested alloys. Both electrochemical and immersion tests showed that Hercules™ B can be used as an alternative to Type 304. This is because even in aggressive solutions it displayed better resistance compared to other test alloys.

6.3 Complex active-passive behaviour for Hercules™

All test alloys could easily passivate in 5 wt.% H_2SO_4, since the corrosion rate measured in electrochemical tests was less than 0.1 mm/y. However, the undesirable active-anode behaviour was observed for Hercules™ A, with more than one E_{corr}. Therefore, Hercules™ A can only be used in much less hostile environments because it displayed poor passivation properties and had a corrosion rate of 1.9 mm/y, which is equivalent to serious corrosion.

Type 304 showed better resistance to uniform corrosion than Hercules™ A and Hercules™ B from the results that were obtained from electrochemical and immersion tests. However, since the corrosion rate of Hercules™ B was less than 0.1 mm/y in immersion tests, it can therefore be used as an alternative to Type 304 to mitigate the onset of corrosion.

Chapter 7: Future Work Suggestions

The proposed applications for Hercules™ are stainless steel rebars and fasteners. Hercules™ A has been recommended in the previous research because of its higher strength than the conventional Type 304. It has already been established that the reduction of Ni content in Hercules™ could potentially provide a reduced price for austenitic stainless steel. Hercules™ B was also developed to address the corrosion resistance.

From the conclusions, it can be deduced that addition of Mo has improved the corrosion resistance of Hercules™ for applications where pitting or crevice corrosion may be of concern. The combination of good corrosion resistance, higher strength and reduced price compared to Type 304 increases the acceptance of Hercules™.

The following recommendations for further work were therefore made:

- To further increase the acceptance of Hercules™ alloy for use to manufacture rebars and fasteners, perform an in-service corrosion testing and compare them with the laboratory tests. This will help in determining the true limiting threshold parameters such as chloride level, temperature and crevices.
- Carry out stress corrosion cracking tests in order for Hercules™ alloy to be further accepted in the fastener industry.
- Consider using Hercules™ B as an alternative for Type 304, which means include it for general purposes that Type 304 has been used for, such as washing machines, tumble drum, kitchen utensils, sinks, ovens, cookers, refrigerators and freezers.
- Use Hercules™ alloy within suggested safety window that has been discussed in the current project for where corrosion is concerned.
- Mo is not readily available in South Africa; therefore, it is difficult to predict its price[3] in the future. The solution may be to conduct research looking into other elements that might be cheaper or readily available to improve the corrosion resistance of Hercules™ against Type 304 and Type 202.

[3] Current price trends of metals are shown in Appendix C

Chapter 8: List of References

[1] J. Kerr, J. Moema, P. Scheers, and R. Paton, "Main technical Reports on new generation low-nickel(< 2%) austenitic stainless steels for structural applications-Report C4105M," 2004.

[2] J. S. Moema, R. Paton, and M. J. Papo, "On the Development of a New Low-Nickel Stainless Steel for Structural and Long Product Applications," 2005.

[3] A. Muwila and M. J. Papo, "A more corrosion resistant Hercules ™ alloy," *South. African Inst. Min. Metall.*, vol. 107, pp. 155–157, 2007.

[4] J. Kerr and R. Paton, "Preliminary Investigations of Low-Nickel Stainless Steels for Structural Applications," in *Tenth International Ferroalloys Congress*, 2004, pp. 757–765.

[5] LME, "Historical price graph for Nickel," *http://www.lme.com/metals/non-ferrous/nickel/*, 2016. .

[6] R. T White, "New generation low-nickel(<2%) austenitic stainless steels for structural applications," 2005.

[7] Columbus Metals Pty Ltd, "Cr-(Mn)-N 304 Austenitic Stainless Steel Technical Brochure," *Cr-Mn-Ni Austenitic Stainl. Steel*.

[8] Outokumpu, *Handbook of Stainless Steel*. 2013.

[9] T. Ujiro, K. Yoshioka, and R. W. Staehle, "Differences in Corrosion Behavior of Ferritic and Austenitic Stainless Steels," *Corrosion*, vol. 50, no. 12, pp. 953–962, 1994.

[10] Outokumpu high perfomance stainless steel, "Type 304 Data sheet," 2014.

[11] Outokumpu, *Corrosion Handbook 11th edition*. 2015.

[12] J. Charles *et al.*, "A new European 200 Series Standard to Substitute 304 Austenitics," *Rev. Métallurgie*, vol. 106, no. 2, pp. 90–98, 2009.

[13] BSSA Stainless steel industry, "200 Series Stainless Steels an overview," 2006.

[14] D. S. Bergstrom and C. A. Botti, "AL 201HP TM (UNS S20100) alloy : alternative to 300 series alloys," 2005.

[15] Mintek, "Technical Data Sheet Stainless steel: Chromium-Nickel-Manganese Hercules(TM)."

[16] B. T. Davison, “Stopping Rust in Bolted Systems,” 2016.

[17] K. P. Fischer, “A review of offshore experiences with bolts and fasteners,” *Corros. 2003.NACE Int.*, vol. 1, pp. 1–13, 2003.

[18] D. C. Agarwal and R. Behrens, “Results of various corrosion and mechanical tests on cold reduced bars of alloy 59, UNS N06059, for fastener applications,” *Corros. 2005.NACE Int.*, pp. 1–7, 2005.

[19] J. . De Luccia, “The corrosion of aging aircraft and its consequences,” 1991.

[20] Branz, “Corrosion of fasteners,” 2011.

[21] D. R. Johns and K. Shemwell, “The crevice corrosion and stress corrosion cracking resistance of austenitic and duplex stainless steel fasteners,” *Corros. Sci.*, vol. 39, no. 3, pp. 473–481, 1997.

[22] T. Prosek, A. Iversen, C. Taxén, and D. Thierry, “Low-Temperature Stress Corrosion Cracking of Stainless Steels in the Atmosphere in the Presence of Chloride Deposits,” vol. 65, no. 2, pp. 105–117, 2009.

[23] A. Poursaee, “Temperature dependence of the formation of the passivation layer on carbon steel in high alkaline environment of concrete pore solution,” *Electrochem. commun.*, vol. 73, pp. 24–28, 2016.

[24] J. O. Rivera-Corral, G. Fajardo, G. Arliguie, R. Orozco-Cruz, F. Deby, and P. Valdez, “Corrosion behavior of steel reinforcement bars embedded in concrete exposed to chlorides: Effect of surface finish,” *Constr. Build. Mater.*, vol. 147, pp. 815–826, 2017.

[25] R. Pernicova, D. Dobias, and P. Pokorny, “Problems Connected with use of Hot-dip Galvanized Reinforcement in Concrete Elements,” *Procedia Eng.*, vol. 172, pp. 859–866, 2017.

[26] L. Bertolini, M. Gastaldi, M. Pedeferri, and P. Pedeferri, “Effects of galvanic coupling between carbon steel and stainless steel reinforcement in concrete,” *International Conference on Corrosion and Rehabilitation of Reinforced Concrete Structures*. 1998.

[27] B. Pradhan, “Corrosion behavior of steel reinforcement in concrete exposed to composite chloride-sulfate environment,” *Constr. Build. Mater.*, vol. 72, pp. 398–410, 2014.

[28] C. . Locke, “Corrosion of Steel in Portland Cement Concrete:Fundamental Studies,” 1986.

[29] P. Garcés, L. Ga Andión, I. De la Varga, G. Catalá, and E. Zornoza, “Corrosion of steel

reinforcement in structural concrete with carbon material addition," *Corros. Sci.*, vol. 49, no. 6, pp. 2557–2566, 2007.

[30] D. Boubitsas and L. Tang, "The influence of reinforcement steel surface condition on initiation of chloride induced corrosion," *Mater. Struct.*, vol. 48, pp. 2641–2658, 2014.

[31] M. M. Ibrahim, S. S. Abd El Rehim, and M. M. Hamza, "Corrosion behavior of some austenitic stainless steels in chloride environments," *Mater. Chem. Phys.*, vol. 115, no. 1, pp. 80–85, 2009.

[32] A. Neville, "Chloride attack of reinforced concrete : an overview," *Mater. Struct.*, vol. 28, pp. 63–70, 1995.

[33] W. Fawaz, "Correcting and Preventing Concrete Corrosion," 2016.

[34] A. Pardo, M. C. Merino, A. E. Coy, F. Viejo, R. Arrabal, and E. Matykina, "Pitting corrosion behaviour of austenitic stainless steels - combining effects of Mn and Mo additions," *Corros. Sci.*, vol. 50, no. 6, pp. 1796–1806, 2008.

[35] A. Muwila, "The Effect of Manganese , Nitrogen and Molybdenum on the Corrosion Resistance of a Low Nickel (< 2 wt %) Austenitic Stainless Steel," 2006.

[36] M. Kaneko and H. S. Isaacs, "Effects of molybdenum on the pitting of ferritic- and austenitic-stainless steels in bromide and chloride solutions," *Corros. Sci.*, vol. 44, no. 8, pp. 1825–1834, 2002.

[37] Denny Jones, *Principles and prevention of corrosion*. .

[38] A. J. Sedriks, *Corrosion of stainless steels*. 1979.

[39] A. Bautista, G. Blanco, and F. Velasco, "Corrosion behaviour of low-nickel austenitic stainless steels reinforcements: A comparative study in simulated pore solutions," *Cem. Concr. Res.*, vol. 36, no. 10, pp. 1922–1930, 2006.

[40] M. C. García-alonso, M. L. Escudero, J. M. Miranda, M. I. Vega, F. Capilla, and M. J. Correia, "Corrosion behaviour of new stainless steels reinforcing bars embedded in concrete," vol. 37, pp. 1463–1471, 2007.

[41] N. Berke, "The Use of Anodic polarization to Determine the effectiveness of Calcium Nitrite as an Anodic Inhibitor," 1986.

[42] S. Fajardo, D. M. Bastidas, M. Criado, and J. M. Bastidas, "Electrochemical study on the corrosion behaviour of a new low-nickel stainless steel in carbonated alkaline solution in

the presence of chlorides," *Electrochim. Acta*, vol. 129, 2014.

[43] S. Fajardo, D. M. Bastidas, M. Criado, M. Romero, and J. M. Bastidas, "Corrosion behaviour of a new low-nickel stainless steel in saturated calcium hydroxide solution," *Constr. Build. Mater.*, vol. 25, no. 11, pp. 4190–4196, 2011.

[44] N. J. Laycock and R. C. Newman, "Temperature dependence of pitting potentials for austenitic stainless steels above their critical pitting temperature," *Corros. Sci.*, vol. 40, no. 6, pp. 887–902, 1998.

[45] N. J. Laycock, M. H. Moayed, and R. C. Newman, "Metastable Pitting and the Critical Pitting Temperature," *J. Electrochem. Soc.*, vol. 145, no. 8, pp. 2622–2628, 1998.

[46] J. O. Park, S. Matsch, and H. Böhni, "Effects of Temperature and Chloride Concentration on Pit Initiation and Early Pit Growth of Stainless Steel," *J. Electrochem. Soc.*, vol. 149, no. 2, p. B34, 2002.

[47] X. Zhang and D. W. Shoesmith, "Influence of temperature on passive film properties on Ni-Cr-Mo Alloy C-2000," *Corros. Sci.*, vol. 76, pp. 424–431, 2013.

[48] P. Ernst and R. C. Newman, "Explanation of the effect of high chloride concentration on the critical pitting temperature of stainless steel," *Corros. Sci.*, vol. 49, no. 9, pp. 3705–3715, 2007.

[49] R. Brigham, "Temperature as a crevice corrosion criterion," *corrosion-NACE*, vol. 30, no. 11, pp. 396–398, 1974.

[50] J. . Dundas and A. . Bond, "Corrosion resistance of stainless steels in seawater," 1985.

[51] ASTM G48-11, "Standard test methods for pitting and crevice corrosion resistance of stainless steels and related alloys by use of ferric Chloride solution," *ASTM Int.*, pp. 1–10, 2003.

[52] E. H. and J. S. R. Baoian, S. Dean Jr., H. Hack, *Corrosion tests and Standards, Application and interpretation, 2nd edition*. 2010.

[53] ASM International Handbook, *Stainless steels*. 1994.

[54] B. Jegdić, D. M. Dražić, and J. P. Popić, "Open circuit potentials of metallic chromium and austenitic 304 stainless steel in aqueous sulphuric acid solution and the influence of chloride ions on them," *Corros. Sci.*, vol. 50, no. 5, pp. 1235–1244, 2008.

[55] B. Jegdić, D. M. Dražić, and J. P. Popić, "Corrosion potential of 304 stainless steel in

sulfuric acid," *J. Serbian Chem. Soc.*, vol. 71, no. 5, pp. 543–551, 2006.

[56] V. S. Rao and L. K. Singhal, "Electrochemical and Surface Analytical Approach to Passive Film on 200 Series Stainless Steels Formed in Sulfuric Acid," *ISIJ Int.*, vol. 49, no. 12, pp. 1902–1906, 2009.

[57] M. . Arikan, "Determination of Susceptibility To Intergranular corrosion of UNS 31803 Type Duplex Stainless steel By Electrochemical Reactivation Technique," 2008.

[58] M. A. Martorano, C. F. Tavares, and A. F. Padilha, "Predicting Delta Ferrite Content in Stainless Steel Castings," *ISIJ Int.*, vol. 52, no. 6, pp. 1054–1065, 2012.

[59] C. Hsieh and W. Wu, "Overview of Intermetallic Sigma (σ) Phase Precipitation in Stainless Steels," *ISRN Metall.*, vol. 2012, no. 4, pp. 1–16, 2012.

[60] A. F. Padilha and P. R. Rios, "Decomposition of Austenite in Austenitic Stainless Steels," *ISIJ Int.*, vol. 42, no. 4, pp. 325–327, 2002.

[61] P. Seemann, S. Kurz, and P. Gümpel, "Martensite formation in a new manganese alloyed metastable austenitic steel (AISI 200-series)," *J. Alloys Compd.*, vol. 577, pp. 649–653, 2013.

[62] A. Di Schino and J. M. Kenny, "Development of high nitrogen,low nickel, 18 % Cr austenitic stainless steels," *J. Mater. Sci.*, vol. 5, pp. 4803–4808, 2000.

[63] P. C. Pistorius and M. Toit, "Low-Nickel Austenitic Stainless Steels : Metallurgical Constraints," *Twelth Int. Ferroalloys Congr. Sustain. Futur.*, pp. 911–918, 2010.

[64] G. Vander Voort, "Metallography and Microstructures of Stainless steels and Maraging steels," *ASM Handb. Metallogr. Microstruct.*, vol. 9, pp. 670–700, 2004.

[65] Princeton Applied Research, "Electrochemistry and Corrosion:Overview and Techniques."

[66] O. Siebert, "Laboratory Electrochemical Test Methods," *Lab. Corros. Tests Stand. ASTM STP 866*, pp. 65–90, 1985.

[67] ASTM G61-86 (Reapproved 2014), "Standard Test Method for Conducting Cyclic Potentiodynamic Polarization Measurements for Localised Corrosion Susceptibility of Iron-,Nickel-,or Cobalt-Based Alloys," pp. 1–9, 2014.

[68] ASTM Norma G 150, "Standard Test Method for Electrochemical Critical Pitting Temperature Testing of Stainless Steels," *Astm G 150*, pp. 1–13, 2004.

[69] G. Barberi, S. Rosso, G. Milanese, and M. Warwick, *Basics of Corrosion Measurements*, vol. 12, no. 1. 2010.

[70] ASTM G102-89 (Reapproved 2010), "ASTM G102 - 89 Standard Practice for Calculation of Corrosion Rates and Related Information from Electrochemical Measurements," *ASTM Int.*, pp. 1–7, 2010.

[71] Nace TM0169/G31-12a, "Standard guide for laboratory immersion corrosion testing of metals," *ASTM Int.*, pp. 1–10, 2012.

[72] ASTM G46-94 (Reapproved 2013), "Standard Guide for Examination and Evaluation of Pitting Corrosion," pp. 1–8, 2005.

[73] "InfoMine," *Chart builder|Charts*. [Online]. Available: http://www.infomine.com. [Accessed: 19-Oct-2016].

Chapter 9: Appendices

Appendix A: Pitting scans

Cyclic polarisation-Duplicate scans: 3.56 wt.% NaCl-crevice free cell

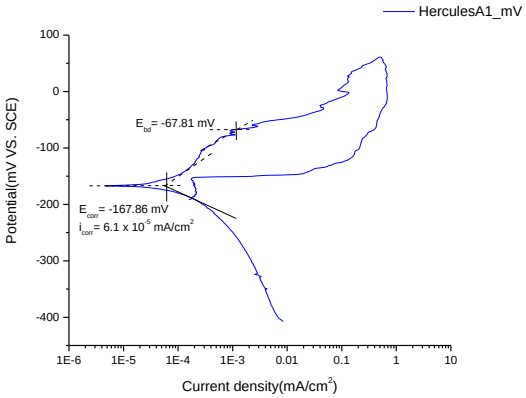

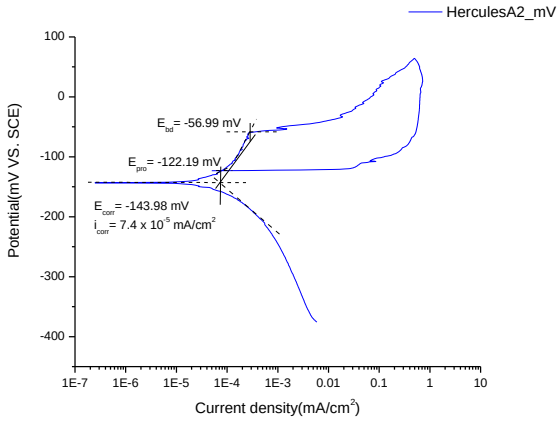

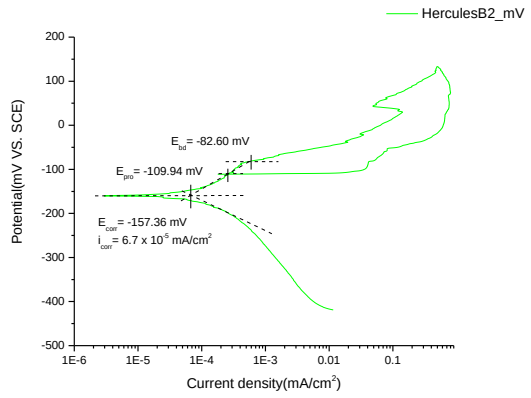

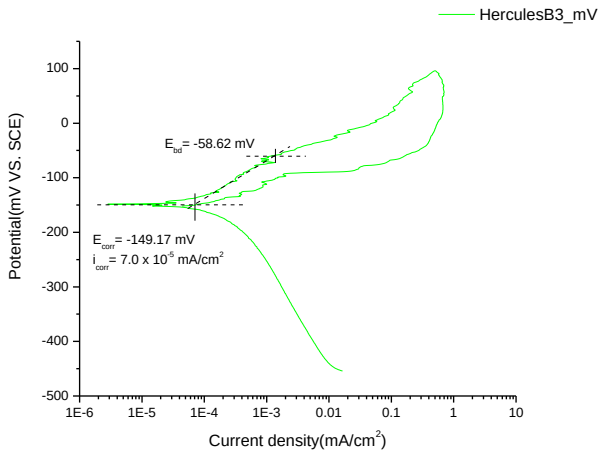

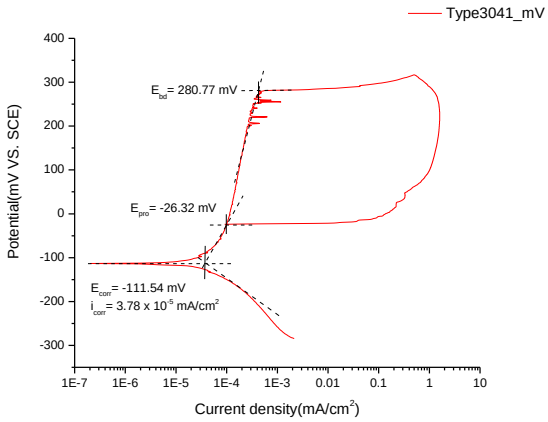

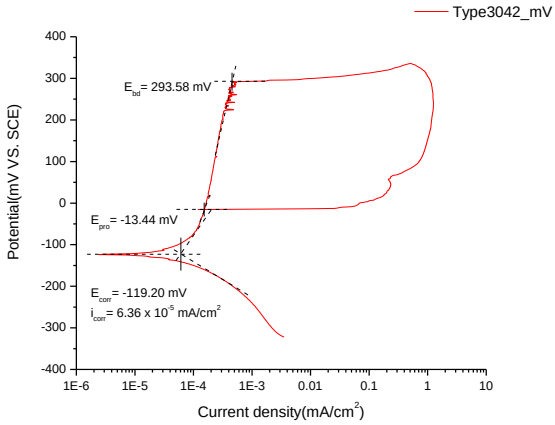

Cyclic polarisation Duplicate scans: 3.56 wt.% NaCl-crevice cell

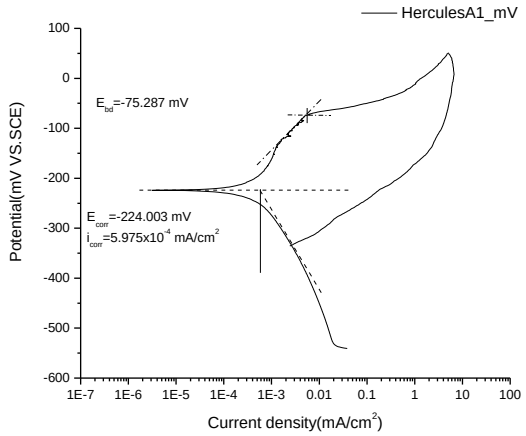

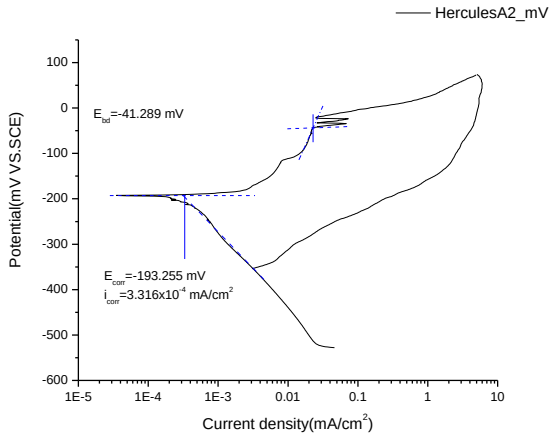

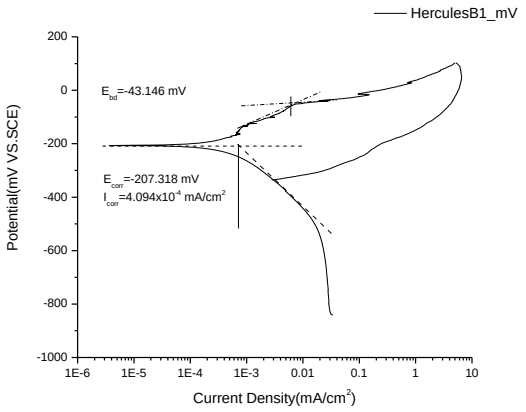

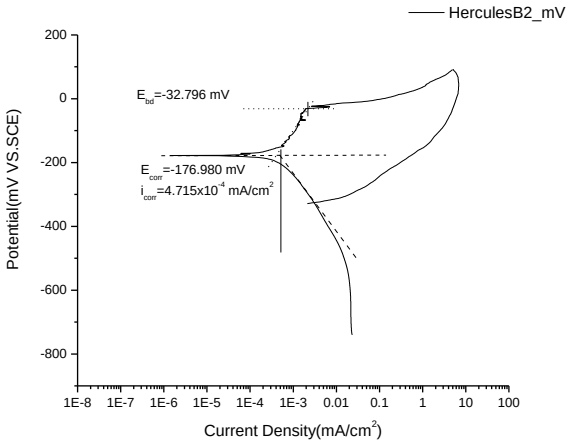

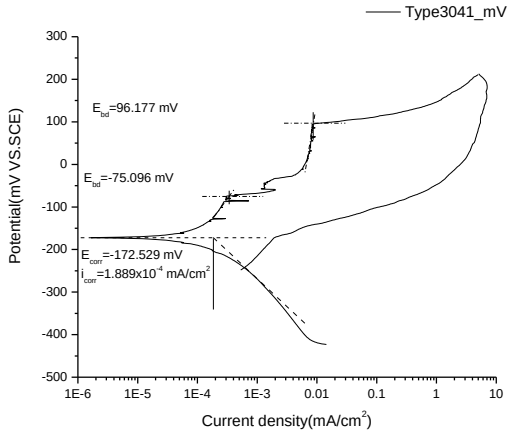

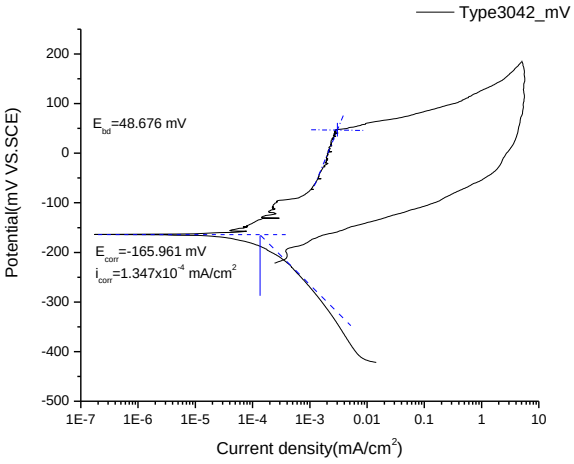

Cyclic Polarisation duplicate scans: 1 wt.% NaCl-Crevice cell

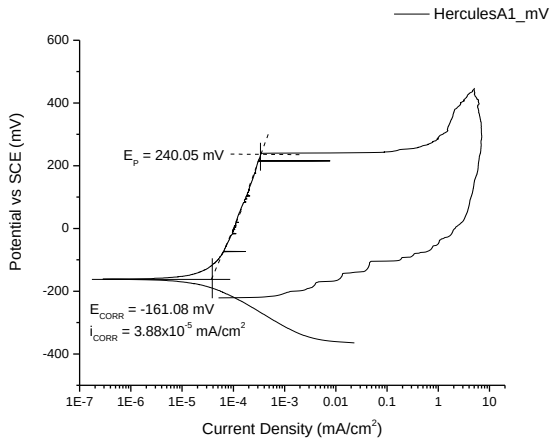

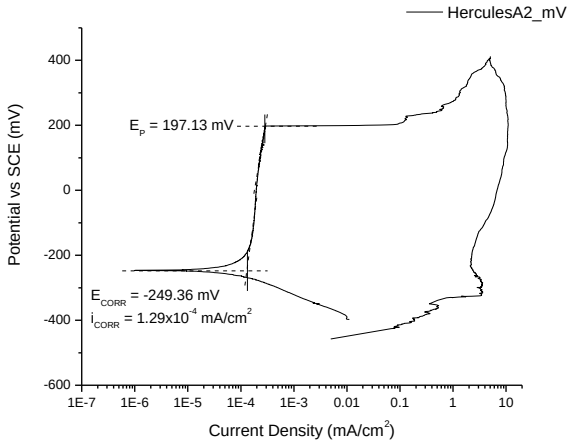

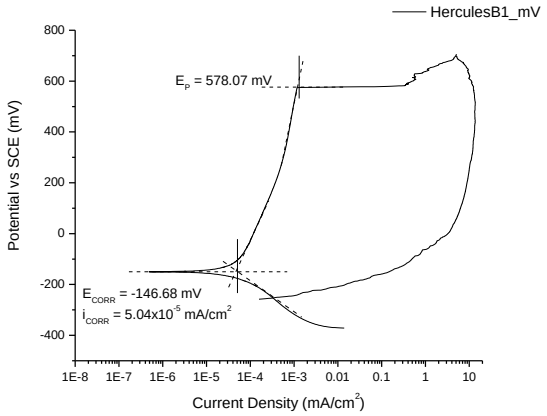

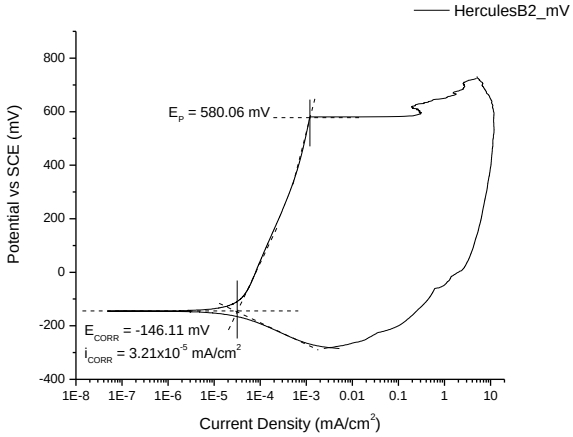

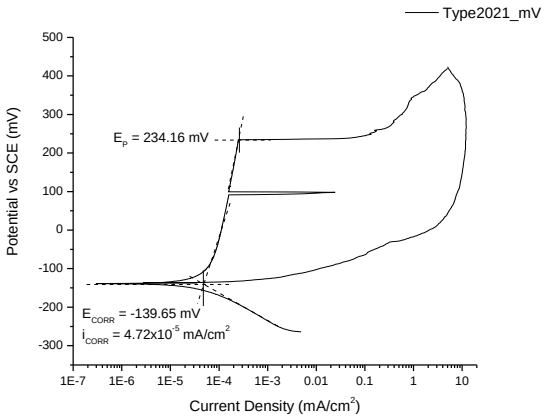

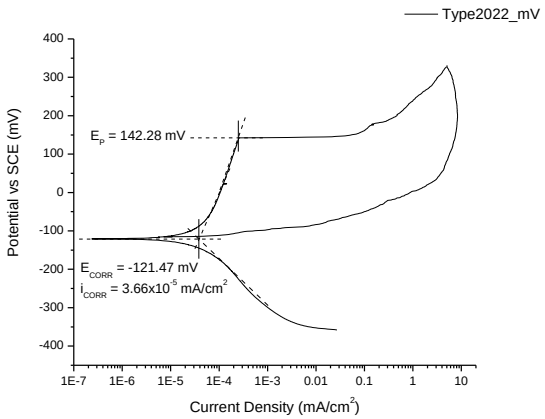

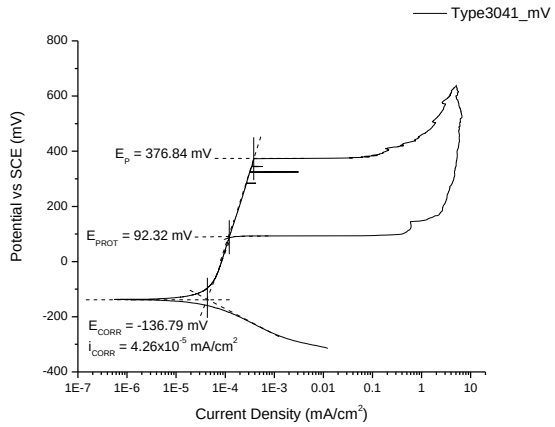

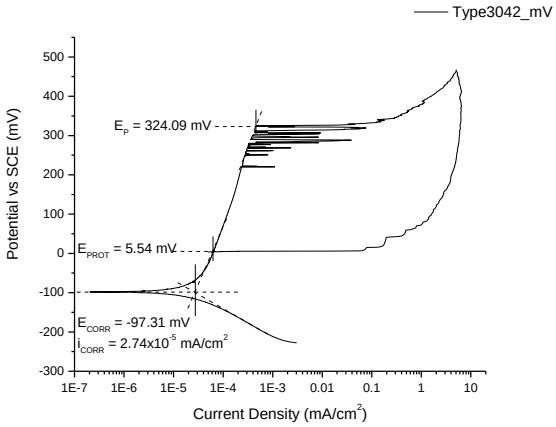

Cyclic polarisation duplicate scans: 5 wt.% H_2SO_4

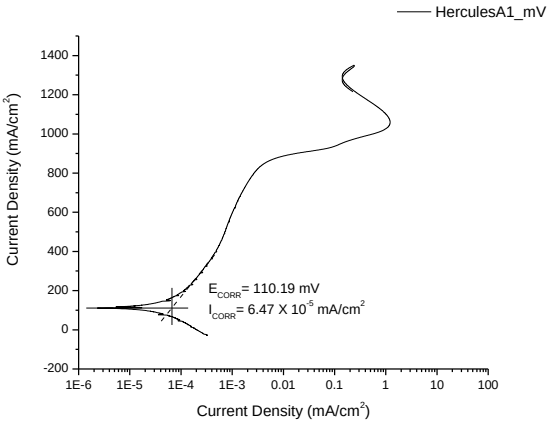

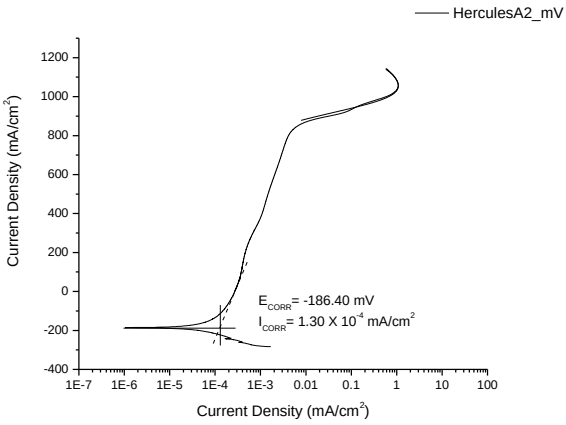

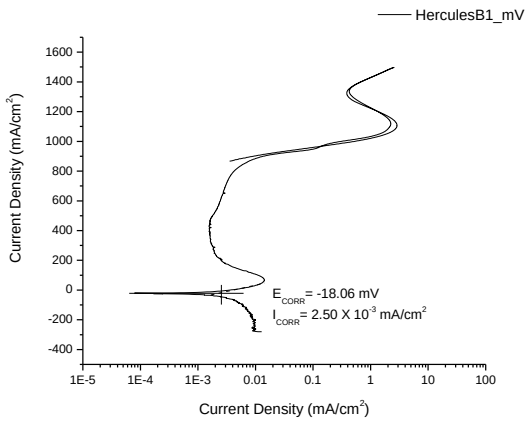

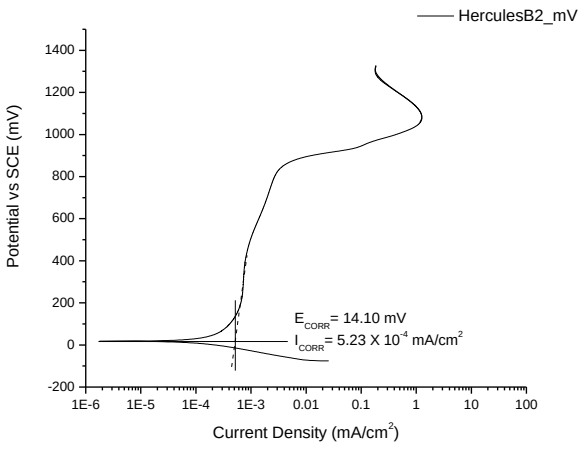

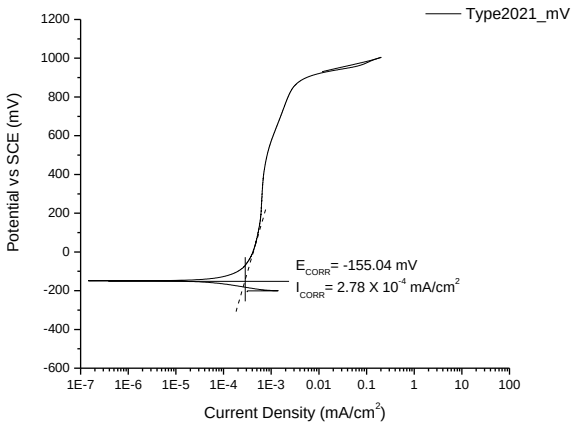
Type2021_mV
Potential vs SCE (mV)
Current Density (mA/cm2)
E_CORR = -155.04 mV
I_CORR = 2.78 X 10-4 mA/cm2

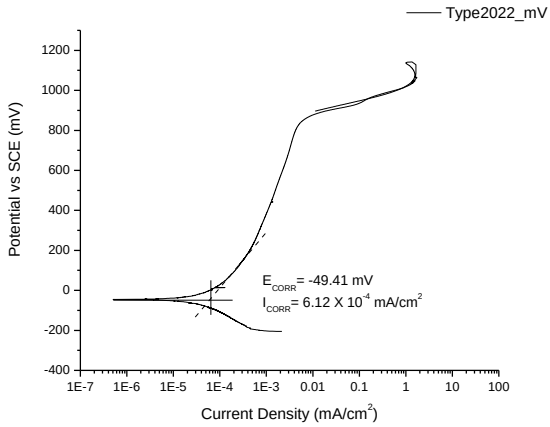
Type2022_mV
Potential vs SCE (mV)
Current Density (mA/cm2)
E_CORR = -49.41 mV
I_CORR = 6.12 X 10-4 mA/cm2

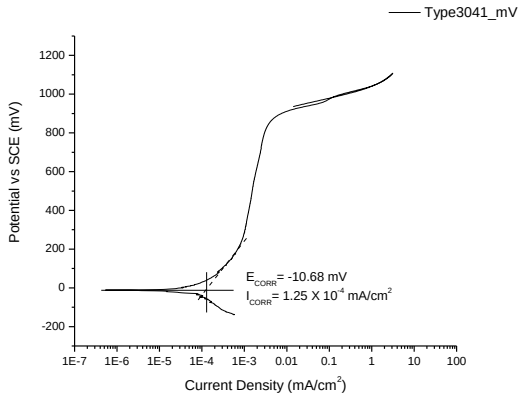
Type3041_mV
Potential vs SCE (mV)
Current Density (mA/cm2)
E_CORR = -10.68 mV
I_CORR = 1.25 X 10-4 mA/cm2

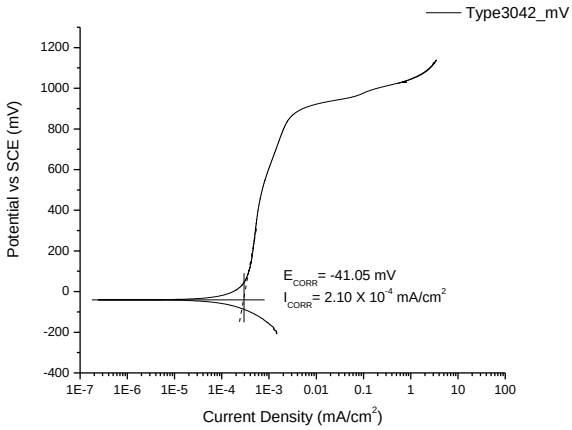
Type3042_mV
Potential vs SCE (mV)
Current Density (mA/cm2)
E_CORR = -41.05 mV
I_CORR = 2.10 X 10-4 mA/cm2

Appendix B: Hercules™ Data sheet

Compositional range of Test alloys

Grade	Typical chemical compositions, wt.%						
	C	Si	Mn	Cr	Ni	N	Mo
AISI 304	0.04-0.08	0.3-1.0	1.5 - 2.0	18-20	8-10	0.05-0.25	-
AISI 201	0.1-0.15	0.3-1.0	5.50-7.50	16-18	3.5-5.5	0.15-0.25	-
Hercules™ A	0.02-0.08	0.3-1.0	9.0-10.0	15-17	1.8-2.0	0.2-.030	-
Hercules™ B	0.02-0.08	0.3-1.0	9.0-10.0	15-17	1.8-2.0	0.2-0.30	0.5

Appendix C: Metal trend prices (2015-2016)

The price trend information is accessible from InfoMine website.[73]

Ni price in USD and SA Rand

Mo price in USD and SA Rands

Mn price in USD and SA Rands

Ferrochrome price in USD and Rands

Mo and Ni price trends over 6 months in USD

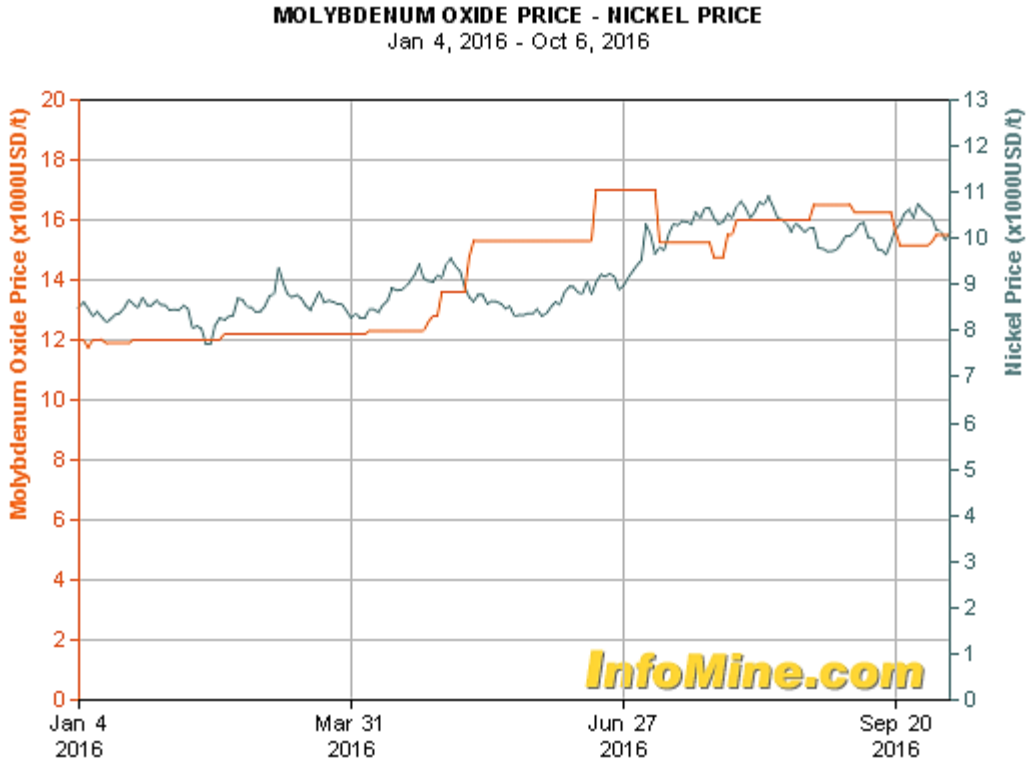

Ferrochrome-Mn-Mo-Ni price trends in SA Rands

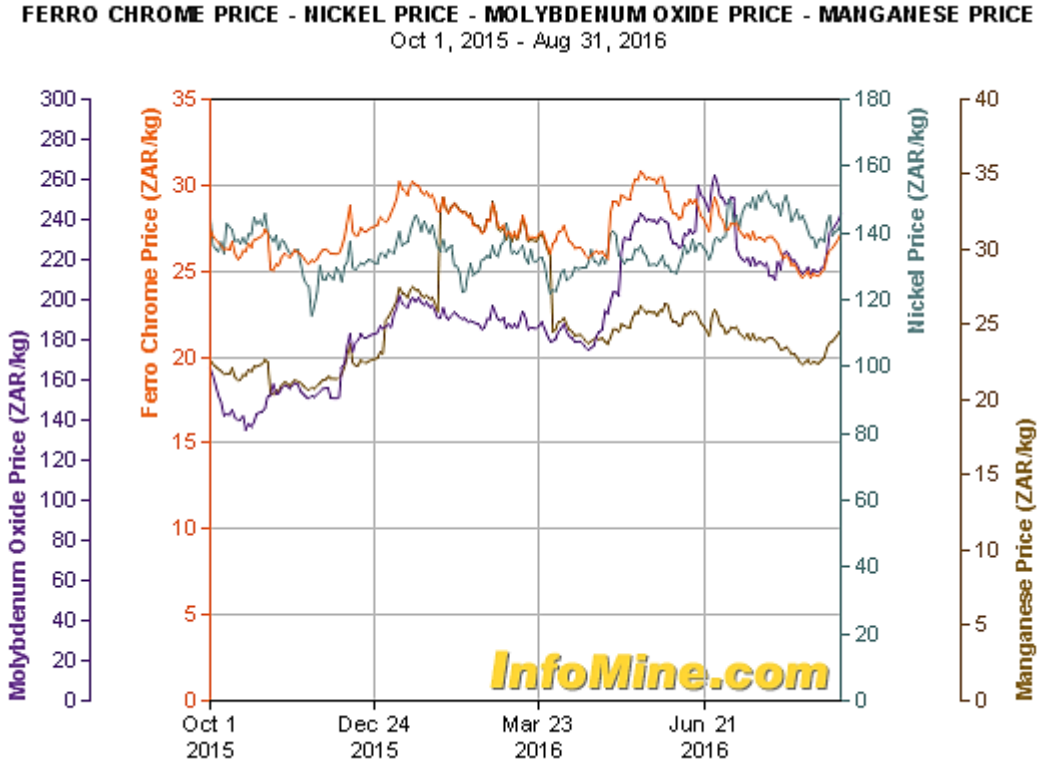

Chapter 10: EBE Faculty: Assessment of Ethics in Research Projects

Appendix Removed due to visible signatures

ADDENDUM 1:
Please append a copy of the research proposal here, as well as any interview schedules or questionnaires:

ADDENDUM 2: To be completed if you answered YES to Question 2:

It is assumed that you have read the UCT Code for Research involving Human Subjects (available at http://web.uct.ac.za/depts/educate/download/uctcodeforresearchinvolvinghumansubjects.pdf) in order to be able to answer the questions in this addendum.

2.1 Does the research discriminate against participation by individuals, or differentiate between participants, on the grounds of gender, race or ethnic group, age range, religion, income, handicap, illness or any similar classification?	YES	NO
2.2 Does the research require the participation of socially or physically vulnerable people (children, aged, disabled, etc) or legally restricted groups?	YES	NO
2.3 Will you not be able to secure the informed consent of all participants in the research? (In the case of children, will you not be able to obtain the consent of their guardians or parents?)	YES	NO
2.4 Will any confidential data be collected or will identifiable records of individuals be kept?	YES	NO
2.5 In reporting on this research is there any possibility that you will not be able to keep the identities of the individuals involved anonymous?	YES	NO
2.6 Are there any foreseeable risks of physical, psychological or social harm to participants that might occur in the course of the research?	YES	NO
2.7 Does the research include making payments or giving gifts to any participants?	YES	NO

If you have answered YES to any of these questions, please describe how you plan to address these issues (append to form):

ADDENDUM 3: To be completed if you answered YES to Question 3:

3.1 Is the community expected to make decisions for, during or based on the research?	YES	NO
3.2 At the end of the research will any economic or social process be terminated or left unsupported, or equipment or facilities used in the research be recovered from the participants or community?	YES	NO
3.3 Will any service be provided at a level below the generally accepted standards?	YES	NO

If you have answered YES to any of these questions, please describe how you plan to address these issues (append to form)

ADDENDUM 4: To be completed if you answered YES to Question 4

4.1 Is there any existing or potential conflict of interest between a research sponsor, academic supervisor, other researchers or participants?	YES	NO
4.2 Will information that reveals the identity of participants be supplied to a research sponsor, other than with the permission of the individuals?	YES	NO
4.3 Does the proposed research potentially conflict with the research of any other individual or group within the University?	YES	NO

If you have answered YES to any of these questions, please describe how you plan to address these issues(append to form)